**Implementation and Evaluation of Thermal Avoidance Strategies in Arid,
Cost-Constrained Climates Aimed at Improving Indoor Thermal Comfort:
A Case Study in Bhuj, India**

by

Johnathan J. Kongoletos

Bachelor of Science, Engineering
Massachusetts Institute of Technology, 2014

Submitted to the Department of Architecture
in Partial Fulfillment of the Requirements for the Degree of

Master of Science in Building Technology

at the

Massachusetts Institute of Technology

June 2018

Signature of Author…………………………………………………………………………………
Department of Architecture
May 24, 2018

Certified by…………………………………………………………………………………………
Leon Glicksman
Professor of Building Technology and Mechanical Engineering
Thesis Supervisor

Accepted by…………………………………………………………………………………………...
Sheila Kennedy
Professor of Architecture
Chair of the Department Committee on Graduate Students

Implementation and Evaluation of Thermal Avoidance Strategies in Arid,
Cost-Constrained Climates Aimed at Improving Indoor Thermal Comfort:
A Case Study in Bhuj, India

by

Johnathan J. Kongoletos

Submitted to the Department of Architecture
on May 24, 2018 in Partial Fulfillment of the
Requirements for the Degree of Master of Science in
Building Technology

Abstract

The use of air conditioning in the buildings sector has been rapidly increasing. The International Energy Agency projects that rising income and greater access to air conditioning equipment in many developing countries will increase CO_2-equivalent emissions, energy consumption, and urban heat island effects. India is a prime example of a region where new building trends, hot climatic conditions, increasing social aspirations, and rapid population growth is likely to spread the adoption of air conditioning. To reduce the need for air conditioning, the research team has worked to develop, implement, and evaluate methods to reduce temperatures within the built environment using largely passive means.

Building on the past work of Nelson and Gradillas, the thesis presents the results of long-term temperature monitoring within four homes in Bhuj, India. Results from the collective work have helped to inform future designs for the region, and resulted in an innovative roof concept. Using scale models, thermal simulations, and full-scale housing, results from the thesis explore new methods of implementing solutions for reduced solar heat gain, reduced heat absorption, and increased heat rejection. The research concludes by presenting early work on additional techniques and implications of using indigenous products to better thermal comfort conditions. Applicable outside of India, the techniques can be utilized in other regions and climates, as well as concurrently with active cooling systems to reduce energy consumption or extend existing capacity. Further work will seek to improve the design and adaptability of the system to different regions.

Thesis Supervisor: Leon Glicksman
Title: Professor of Building Technology and Mechanical Engineering

Acknowledgments

Table of Contents

List of Figures

List of Tables

Introduction

In areas such as India, heat waves can be deadly. The May 2015 Ahmedabad heat wave killed over 1,786 people in India alone (Ahmedabad Municipal Corporation, 2018) and five years before, a heat wave claimed an additional 1,344 deaths (Azhar, et al., 2014). As heat extremes become more common, this will lead to an increase in heat-attributable deaths, especially for vulnerable subsets of the population (European Environment Agency, 2016). The negative effects of frequent heat waves will be predominantly felt in hot/arid deserts and tropic regions where many developing nations are located (Nelson, 2017). In these countries, as incomes and living standards improve, the pursuit of thermal comfort in the built environment amid historic high temperatures and the consequent growth in air conditioning demand is a key driver of global electricity-demand demand growth (Bhalla, 2016). This growth will come with large costs and environmental implications.

Air conditioners are the go-to choice for keeping the built environment cool throughout many developed countries. This is due to a variety of factors, including the adoption of a universal building style, the urban heat island phenomenon, increased affluence of customers, and increased building heat gains, among others (Santamouris M. , 2007). However, the desire to keep buildings cool during hot days is not a new ambition. Vernacular architectural traditions, or those local building methods that have evolved over time for a given location, are able to meet the needs of a traditional lifestyle without the need for mechanized heating and cooling systems (Meir & Roaf, 2002). While vernacular architecture should be observed and taken into account during new construction, the social, cultural, economic, and regulatory aspects change over time, opening the door to modifications in building construction and obsolescence of concepts.

These types of changes are especially true in India, where the population is growing at 1.2% per year overall, and the population is urbanizing at a rate of 2.3% per year (US Central Intelligence Agency, 2018). It is estimated that 17.4% of India's urban residents live in housing 'unfit for human habitation,' also known as slums (Chandramouli, 2013). With the increasing population and urbanization rate, the demand for urban housing will increase in kind.

The following research focuses on evaluation and implementation of passive housing design as a means to improve interior conditions and livability, and decrease heat-related mortality in resource-constrained regions. The utilization of passive means, including heat avoidance strategies, allows for both reduced energy demand in homes with active cooling, as well as reduces the need for air conditioning equipment for families without the resources to own and operate the equipment. This work is applicable outside of the arid and cost-constrained climate of India, as shown by included research work on first steps in improving housing conditions in Nepal. Through this extension, while much of the work targets low-income populations, it is equally applicable to both energy savings and up-front savings through mechanical equipment load reductions.

To study thermally passive design and heat avoidance strategies, the research team at the Massachusetts Institute of Technology ("MIT") has collaborated with The Hunnarshala Foundation ("Hunnarshala"), based in Bhuj, Gujarat, India. Bhuj is a challenging city to design for thermal comfort due to the dangerous heat waves that frequently exceed 45°C (Gradillas, 2015). The state of Gujarat has a higher than average urban population percentage (43%) and 6.5% of the population live in slums (Government of India Ministry of Housing and Urban Poverty Alleviation National Buildings Organization, 2015). In partial response to a recent earthquake in 2001, the local, state, and national governments have been working under the "Housing for All by 2022" program to subsidize the construction of housing in the region. Providing a financial grants or interest subsidies up to 230,000 Indian rupees ($3,375) per household, the government has been crucial in helping to spurn development of housing targeted towards those earning less than 200,000 Indian rupees ($2,935) per year (Office of the Prime Minister of India, 2015; Nelson, 2017). Hunnarshala has been using their expertise and the Housing for All funding to build safe and livable housing, under which the MIT has been collaborating to holistically design homes with thermal considerations included.

Hunnarshala began this collaboration and initial research with former MIT student Madeline Gradillas, who laid the groundwork in understanding social, cultural, and economic factors, building material selection, and undertook the initial efforts in measurement and establishment of baseline thermal performance (Gradillas, 2015). Emma Nelson then continued the research through the development of energy modeling software to look at the performance and configuration of radiant barriers (Nelson, 2017).

Past Research

To begin the research, Gradillas monitored seven case study buildings for thermal performance between late August 2014 and late March 2015. Using these data along with cost estimates, a series of hypotheses were offered to prepare future work, refine the proof of concept design, and continue the co-design process. Within these hypotheses, Gradillas recommended the following building characteristics:

- Protect windows, walls, and rooftop from heat gains due to direct solar radiation;
- Incorporate high thermal mass walls;
- Minimize daytime ventilation;
- Increase nighttime ventilation; and
- Incorporate a double-layer roof with radiant barrier.

Gradillas makes a critical conclusion in that there is no silver bullet to improving thermal comfort, and that thermal performance will only improve with an amalgamation of strategies (Gradillas, 2015). As such, presented conclusions are dependent on external factors including, but not limited to, weather conditions, social reactions, building geometry and materials, and surface coatings. This note is important in that it applies across the discipline, ranging between income ranges, cultural vernaculars, and climates.

For further research, Gradillas suggested research into the following areas:

- Ventilation schedules;
- Exterior insulation solutions;
- Variation of building geometries;
- Optimization of radiative cooling;
- Application and modulation of movable insulation panels;
- Double-layer roof assemblies with thermally massive elements; and
- Implementation and scalability to the end user.

Nelson continued the work of Gradillas through measurement of existing test chambers in Bhuj, measurement of homes built in Bhuj, and simulation work. Nelson also included an economic aspect in addressing the affordability of proposed roof designs, of which all were within the desired price points for low-income residents throughout India (Nelson, 2017). Using the available data and comparisons, Nelson offered a set of recommendations for building construction:

- Low heat capacitance roof materials;
- Added thermal insulation to traditional reinforced concrete roofing;
- A low emissivity ceiling surface;
- Wall insulation;
- Low absorptivity wall color; and
- Incorporation of ceiling temperature into choice of ceiling vs. standing fan.

Nelson offered the following suggestions for pathways for future work:

- Optimization of nighttime radiant cooling;
- Minimization of solar heat gains;
- Dissemination of thermally passive designs to local and other resource-constrained regions; and
- Adaption of housing designs to cold climates.

Scope of Research

This research continues the work of Gradillas and Nelson in assessing in-situ performance using scaled test chambers to focus on performance in arid, hot, and cost-constrained climates. In the process of doing so, this research includes laboratory performance data of surface optical properties and thermal conductivity of selected samples, as well as application of that data to energy modeling. This research is particularly unique in that it includes long-term measurement results from four homes built in Bhuj, India, and includes commentary on the social viewpoints on the evaluated homes. Additionally, where Gradillas and Nelson focused significant work on heat flows in, around, and out of a home, this research includes the prevention of heat from reaching the home, or thermal avoidance strategies.

The thesis is structured as follows: Chapter 2 (Local Experiments) looks at a component-based perspective to replacing elements within the structure, as well as the implementation of a subset of those components within scaled testing located at MIT in Cambridge, MA. Chapter 3 (Bhuj Test Chambers) illustrates the application of individual testing to the larger test chambers located in Bhuj, India, especially in regards to surface variations of the inclined roof with above-sheathing ventilation (referred to as a double layer with air gap roof design by Nelson). Chapter 4 (Bhuj Housing) presents conclusions of the long-term performance of the monitored housing in India, as well as suggestions for further work and improvements. Chapter 5 (Nepal) extends some of the lessons learned from both the local experiments and long-term monitoring to application in Nepal, a colder climate with similar cultural and seismic considerations. Chapter 6 (Conclusions) then summarizes the results and findings of this research, as well as provides direction for further work in this field.

Local Experiments

In order to establish fundamental values for materials, as well as perform fast-turnover iterative testing, the team used a combination of laboratory and scale testing to determine what impact, if any, proposed ideas may have in Bhuj test chambers and homes.

Construction

In an effort to mimic the testing chambers from Bhuj, the MIT-based team designed and built a series of concrete testing chambers in June 2017 on the roof of MIT. These chambers were intended to provide the team with the ability to quickly change building construction elements and to increase the rate at which design changes are tested within a system.

The structures were built to a 1:4 linear scale from the housing in Bhuj. This scaling was chosen based on the available resources and matched the thickness of the wall in Bhuj to the scaled thickness of the concrete at MIT (2 ¼"). The structures were built on top of an RCC slab roof, placed so that the weight of each chamber was sitting on a column below. The weight of each chamber was distributed across the rubberized roof coating by a supporting 4' by 4' frame composed of 2" x 4" timbers with four interior lateral joists equally spaced within the frame and braced to prevent twisting of the members. Each frame was then sandwiched between ½" plywood and secured with screws. The base flooring of the chamber then used 4" thick aerated concrete blocks (k = 0.221 W/m*K, ρ = 589 kg / m³), upon which the concrete brick walls were placed (k = 0.952 W/m*K, ρ = 2081 kg / m³) and secured using silicone caulk (GE5000 Silicone Clear Sealant) to reduce air filtration while allowing for hassle-free disassembly. Silicone caulk was also used in a more conventional fashion on the interior of the chamber to further reduce infiltration. All of the 690 concrete bricks for the three chambers were sourced from a single pallet and visually matched each other. Figure 1 shows these materials prior to construction, with Figure 2 showing construction while underway.

Figure 1: Materials Used for test chamber construction

Figure 2: Test chambers midway through construction

The top of the chamber was then covered in ¾" plywood. The plywood was painted black (Behr Premium Plus Paint Exterior Flat Paint and Primer 4050 Matte Black) on both sides and the top surface was covered in a plastic layer to provide a water barrier. Another layer of concrete brick (2 ¼" thick) was then placed on top of the chamber for thermal massing dimensionally matched to the homes in Bhuj.

The structures were all oriented with the facades facing a major cardinal direction and were spaced to prevent shading between the chambers and from the surrounding parapet wall. Overall, the dimensions of the interior space are 43" x 43" x 19 ½".

Figure 3: Dry-fit assembly prior to addition of waterproofing

Further, as Figure 2 and Figure 3 show, a space of one 3 ¾" x 7 ¾" brick was left out of the east and west walls to allow for ventilation of the interior of the space. These openings were placed at the same height to diminish natural ventilation and ensure control over the chamber airflow. Each chamber was fitted with two consumer-grade CPU fans (BXQINLENX 5010 Dc12v), each moving 9.5 CFM of air and in a push-pull configuration to ensure a controlled air flow. Each fan was placed in an extruded polystyrene spacer and were protected with small backdraft shields to inhibit large wind-induced airflow. The fans were powered by a 12 VDC adapter which was connected to a UL-listed outdoor garden timer. Each of the fans was then wired in parallel so that each fan would see the same voltage at any given time.

The fan sizing was derived from a conservation of energy approach for the air volume inside the chamber. In this approach, the thermal mass of the structure containing the control volume is removed from the equation by confining the control volume to the air only, where the heat is stored by the air volume and can exchange through the boundaries of the control volume only through air ventilation from the outside, convection across the surfaces of the mass surrounding the volume, and heat can be generated inside the chamber. This is can represented in equation form as shown below.

$$Mc_v \frac{dT_{in}}{dt} + \dot{m}c_p(T_{out} - T_{in}) + hA(T_{surface} - T_{in}) + q'' = 0$$

Where

M = mass of the air inside the chamber

c_v = specific heat capacity of air at constant volume

T_{in} = air temperature inside the chamber

$\dot{m}$ = mass flow rate of air

c_p = specific heat capacity of air at constant pressure

T_{out} = outside air temperature

h = convective heat transfer coefficient

A = convective area within chamber (walls, ceiling, and floor)

$T_{surface}$ = surface temperature of the inside building surfaces

q'' = heat generation rate

The conservation of energy approach assumes that the convective heat transfer coefficients are constant between the full size and scaled size chambers, and allows the temperature to be non-dimensionalized based on the difference between inside and outside air temperatures. Below, the hA term has also been redistributed.

$$\frac{\rho \forall c_v}{hA} \frac{d}{dt}\left(\frac{T_{in}}{T_{in} - T_{out}}\right) + \frac{\dot{m}c_p}{hA} + \frac{T_{wall} - T_{in}}{T_{in} - T_{out}} + \frac{q''}{hA(T_{in} - T_{out})} = 0$$

Where

ρ = density of air inside the chamber (control volume)

$\forall$ = volume of air inside the chamber (control volume)

Using this scaling, $\frac{\dot{m}}{A}$ and $\frac{q''}{A}$ should remain constant between the full-size chamber and the scaled chamber. Where, $\dot{m}$ is the mass flow rate of air, q'' is the heat generation rate within the chamber, and A is the surface area within the chamber. The nature of the approach assumes that the convective heat transfer coefficients are constant between the full size and scaled size chambers. Evaluating $\frac{\dot{m}}{A}$ yields the following, which should remain constant between the two chambers.

$$\frac{\dot{m}}{A} = \frac{\rho \forall \cdot ACH}{A}$$

Where

ACH = the air change rate, in air changes per hour

Simplifying the above equation by dividing out constants (density) and replacing the $\frac{\forall}{A}$ term with length yields the following constant, which is a function of length (L) only.

$$(L \cdot ACH)_{full-size} = (L \cdot ACH)_{scale}$$

With the full-size chamber evaluated at an air change rate of 6 ACH (Nelson's simulation inputs), and the scale structures being ¼ the size of the full-size chamber, the air change rate of the scale structure should have been 24 ACH. Due to fan availability, the air change rate was rated to achieve an air change rate of 22.35 ACH (93%) for the final interior air volume of 25.5 ft³.

Instrumentation and Testing

Each chamber was instrumented with one Onset Computer Corporation HOBO UX120-006M, with four analog steel temperature sensors. Measurements were taken at 30 minute, synchronized increments. The four metering points were

- Air temperature (centered within the chamber),
- South wall temperature (center of steel casing was ½" from the inner wall of the chamber),
- West wall temperature (center of steel casing was ½" from the inner wall of the chamber), and
- Radiant temperature (centrally located in the plan of the chamber.

Figure 4: Metering and electrical components of testing chamber, prior to wire routing

22

The temperature data was complimented by a pre-existing Onset Computer Corporation HOBO U30 weather station installed 20 feet away and equipped with

- a solar radiation-protected temperature and relative humidity sensor (S-THB-M002, RS3-B),
- a solar radiation (Silicon Pyranometer) sensor (S-LIB-M003), and
- wind speed and direction sensors (S-WSB-M003, S-WDA-M003).

Figure 5: MIT Weather Station

Following an initial five-day period where the chambers were configured alike, the air temperatures of the chambers were found to vary in temperature by an average of 0.27 °C with a maximum difference of 1.01 °C at the moment when the ventilation fans turned on in the morning. The radiant temperatures varied by an average of 0.16 °C and the roof slab temperature varied by an average of 0.12 °C. The west wall sensor was not installed until after this initial period.

Starting in June 2017, the research team varied the construction of the chambers to determine the impact of the different building elements on the temperature profiles of the chambers. Using the garden timer, the small fans were operated from 7 PM to 9 AM daily for night ventilation. The timer was checked weekly to ensure that timing was correct.

Using the data from the chambers, the team checked all the data streams for consistency and quality controlled the data to look for and remove any issues with the metering. In one example, one of the sensors had become dislodged, and the time frame was cropped across all three chambers to compare the chambers on an equal field. After quality control, the team averaged the tests hour by hour over the testing period to create an 'average day'. This data is helpful to visualize the temperature trends, as well as determine relative performance. In each graph, the horizontal axis is the average of each hour in the dataset matching the hour displayed. The vertical axis is the corresponding temperature.
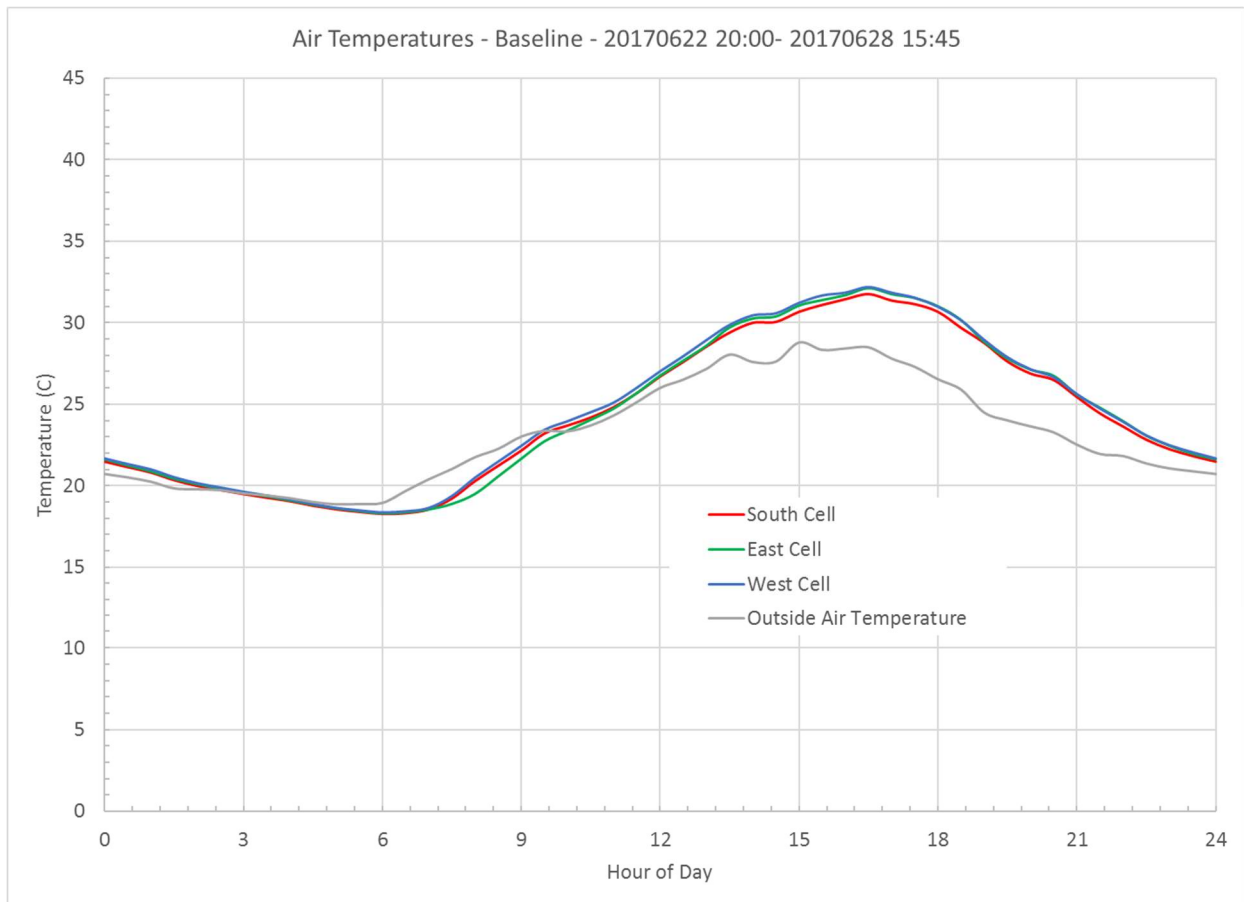
Figure 6: Air Temperature Average Day Plot for Baseline conditions, configured alike with 7 PM to 9 AM ventilation

The first alterations to the chambers from the baseline configuration (bare concrete walls and roof) a tested conversion between a stand-alone structure (like the second level housing in Bhuj) and a structure nested between two adjacent buildings (like the ground level housing in Bhuj). This was accomplished by adding exterior insulation (foil-faced 2" polyisoacyanurate, DOW Super TUFF-R™, R=2.29 m^2·K/W) (The Dow Chemical Company, 2018) to the north and south facades of the test chambers. The test was run for two weeks and the results are reproduced below in Table 1.

The first test, Test 1, was designed as a way to apply some of the conclusions presented in Emma Nelson's thesis and expand it to the ground level housing in Bhuj. Between the three chambers, one ("East") was used as a control for stand-alone housing, another ("South") was used as a base for row housing in the Ramdev Nagar community, and the third chamber ("West") was used to test the implication of surface coatings. Figure 7 shows the experimental setup with the right chamber ("West") having a painted walls and roof, while the left chamber ("South") remained unpainted with exterior insulation.

Figure 7: Test 1 Setup

Using the collected data, the following tables present the test conditions and results from various iterations in the building construction. Along the first column, 'Max' denotes the maximum temperature for the period, 'Min' the minimum temperature for the period, 'S.Dev' the standard deviation of the sample, and 'Peak Hour' the hour at which the maximum temperature was recorded. The rows on top are the chamber description, and the description of the alterations to the test chamber. The values, based on the 'average day', are provided as a method to compare the different tests. All temperature values are on the Celsius scale. The color-coding is based on the values of the cells, where red is a warmer temperature, and blue is a cooler temperature, and is compared to the point values

(I.e.: radiant) between the three chambers. In situations where the temperatures varied by only 0.1 °C (Test 1 Minimum values), the color coding was removed to avoid conclusions from insignificant differences.

Test 1		East Chamber				South Chamber				West Chamber			
6/28 - 7/12		"Control" (2nd level housing) All sides exposed No Paint				Base ground level housing North & South Exterior Insulation No Paint				- - North & South Exterior Insulation East and West exterior walls painted white			
[°C]	OAT	Radiant	Air	Roof Slab	West Wall	Radiant	Air	Roof Slab	West Wall	Radiant	Air	Roof Slab	West Wall
Max	29.2	34.9	35.9	38.5	40.6	33.4	34.2	36.9	39.1	32.9	33.5	37.6	34.0
Min	19.7	19.5	19.4	17.6	18.9	19.5	19.5	17.7	18.9	19.5	19.5	17.7	18.9
Peak Hour	15	15.5	15.5	15	17.5	16.5	15.5	15	17.5	15.5	15.5	15	17

Table 1: Test 1 Setup and Results, using a 7 PM to 9 AM ventilation schedule

Table 1 confirms Nelson's simulation results in that the wall insulation decreased peak air temperatures by at least 1°C (Nelson, 2017). Painting the walls white was also able to reduce the air temperature during the day by roughly another 1°C, but neither addition had an impact on the nighttime air temperature, which can be attributed to the fan-induced ventilation that was present.

Overall, the North & South Exterior Insulation allows the chamber to stay cooler throughout the day since it decouples the north and south walls from the outside air temperature. The West chamber, with the addition of the white painted walls, allows the interior of the painted west wall to remain much cooler during the heat of the day, and contributes to a lower maximum daily temperature. The interior of the chamber remains 4.3 °C warmer that the outside air temperature, giving little thermal relief to the occupants inside.

Although the roof slab temperatures vary by over 1.7 °C, this variation is not believed to be a function of the surface, material composition, or assembly itself, as the temperatures varied by only 0.21 °C during the initial baseline period where all chambers were configured alike.

The impacts of the painted west wall can be seen on a plot of the 'Average Day' (Figure 8). In this plot, values from the sampling period are averaged together hour by hour and displayed on a single 24-hour timeline.
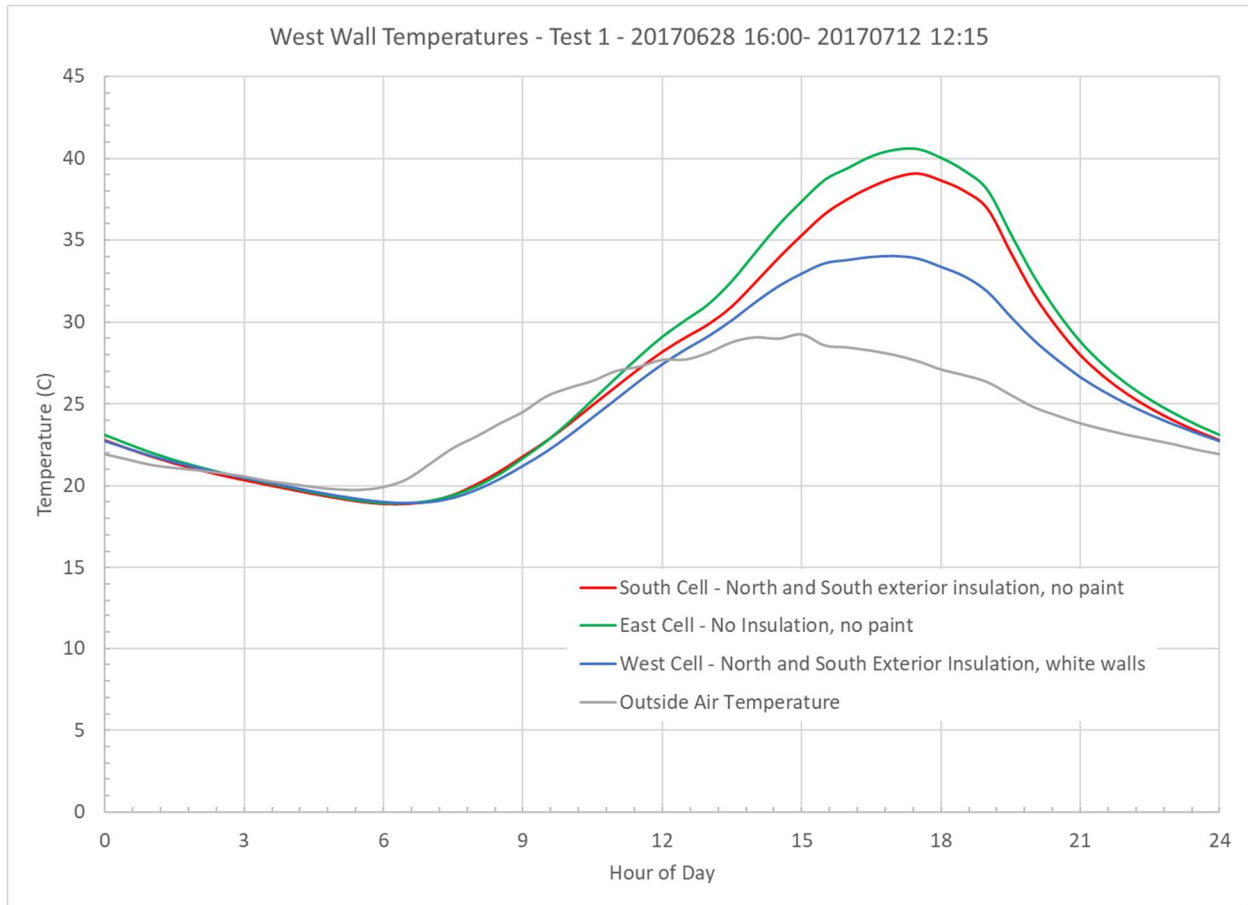
Figure 8: Test 1 Wall Temperatures 'Average Day', comparing white paint and insulation with 7 PM to 9 AM ventilation

Within the chamber, the West Wall sensor is placed in a hole that is perpendicular to the surface. The center point of the steel-encased sensor is then located about 15 mm inside the interior surface of the wall. Within the wall section, the sensor is placed one foot from an interior corner, at ½ the interior height of the chamber, and centered within the concrete brick.

As the figure above illustrates, the west wall temperature sensor shows some of the decrease in internal air temperature as a result of the insulation on the north and south walls. While not directly impacting the west wall, the change in the west wall is due to the reduced heat flow through the north and south walls, and the resulting decrease in air and radiant temperatures.

The addition of the white paint to the east and west walls then reduces the wall temperature, which would be important when considering the radiant or operative temperature within the space. Overall, using the data from Table 1, the peak air temperature reduces by 2.4 °C. This data is graphically represented below in Figure 9, which helps to elaborate on the table data by showing how the thermal contribution from the modifications depend on the positioning within the structure and the relationship to the sun's position. Rising in the east, the sun first strikes the east walls, where the implication is apparent due to the deviation of the West cell (white painted east wall) from the other two cells (bare concrete walls). The impact of the North and South exterior insulation is shown as the sun moves

27

towards the south and South Cell (with insulation on the south wall) begins to deviate from the bare structure (East Cell).
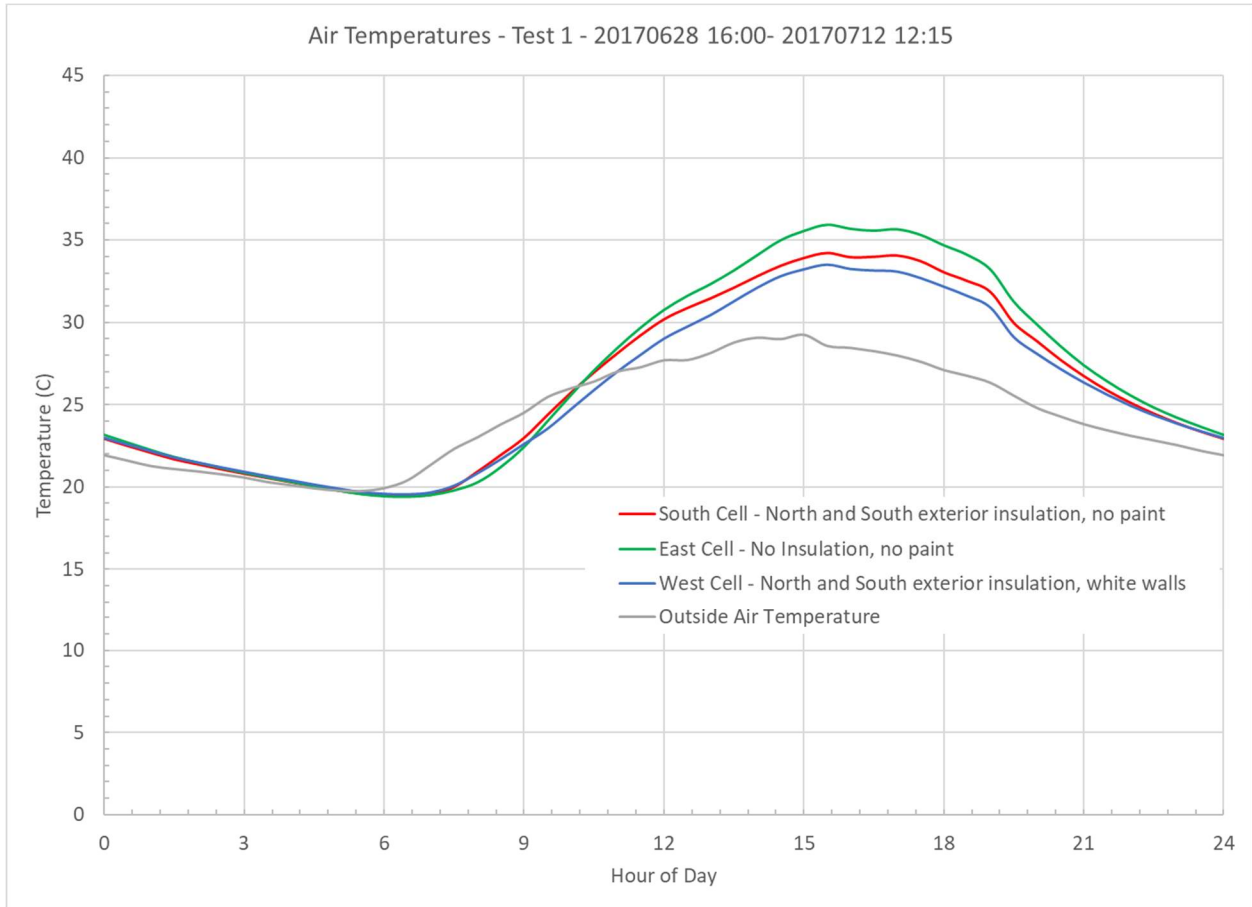
Figure 9: Test 1 Air Temperatures 'Average Day', comparing white paint and insulation with 7 PM to 9 AM ventilation

Test 2: White Paint and Overhangs

Test 2 is similar to Test 1, but in this case, all three chambers had 2" polyisocyanurate exterior insulation on the North and South facades designed to mimic the ground level housing in Bhuj, India. In Test 2, a 12" white-painted overhang was installed on the East and West face of the East Chamber to test the impact of solar insolation compared to the chamber with roof and walls painted white.

Figure 10: Test 2 Overhang Setup

Test 2		East Chamber				South Chamber				West Chamber			
7/12 – 7/21		Overhang on East and West faces North & South Exterior Insulation Roof and non-insulated walls painted white				- - North & South Exterior Insulation No Paint				- - North & South Exterior Insulation Roof and non-insulated walls painted white			
[°C]	OAT	Radiant	Air	Roof Slab	West Wall	Radiant	Air	Roof Slab	West Wall	Radiant	Air	Roof Slab	West Wall
Max	34.1	32.0	32.5	33.2	35.2	37.0	38.3	46.3	41.7	32.9	33.6	33.6	36.5
Min	22.4	22.3	22.2	19.8	22.2	23.1	23.0	20.2	22.2	22.6	22.6	19.5	21.8
Peak Hour	14.5	17	16.5	15	16	16.5	16.5	14.5	16.5	17	16.5	15.5	16

Table 2: Test 2 Setup and Results

While the overhangs did help contribute to a reduction of nearly 1 °C in the max air, max radiant, and max West wall temperatures, the overhangs also prevented the West wall from cooling down during the night, presumably due to the inhibition of radiative cooling to the sky.

The addition of the white painted roof surface also helped postpone the peak temperatures in the East and West chambers. Although slight, a later peak temperature implies that the building performance is more coupled with the thermal mass, and that the overall temperature curve is dampened as a result. This is corroborated with the plot of the Average Day, Figure 11, where a sharp deviation in mid-morning suggests the implication of significant contributions from overhead solar radiation. Thus, most of the reduction in air temperature is due to the addition of the white painted roof.
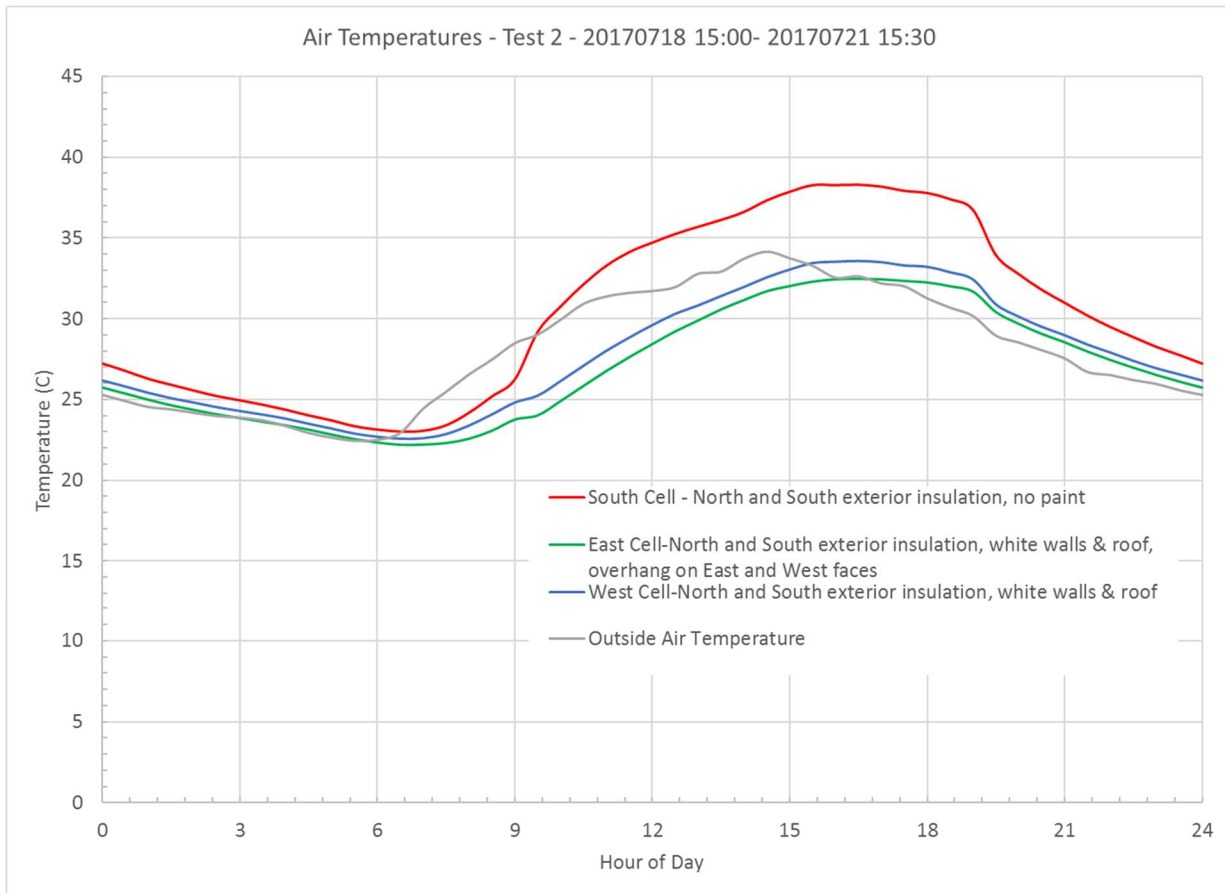
Figure 11: Test 2 Air Temperatures 'Average Day', comparing white paint and overhangs with 7 PM to 9 AM ventilation

Test 3 is then an extension of Test 2, where 90% coverage shade nets (Coolaroo Heavy Shade Fabric 302245, tan color) were installed over the roof at a height of 20 inches over the roof face (80 scale inches), and on the east and west wall faces four inches off the wall surface. The structure of the frames were mounted onto the wooden base of the chamber and diagonally tensioned to prevent rotation and horizontal movement. The frame of the netting material matched the plan or elevation views, so as to be more translatable to a building environment where the buildings abut other structures, like Bhuj.

Figure 12: Test 3 experimental setup with shade nets installed

Test 3	East Chamber				South Chamber				West Chamber			
7/21 – 7/31	Shade net on East and West faces North & South Exterior Insulation Roof and non-insulated walls painted white				Shade net above roof North & South Exterior Insulation Roof and non-insulated walls painted white				- - North & South Exterior Insulation Roof and non-insulated walls painted white			
[°C] / OAT	Radiant	Air	Roof Slab	West Wall	Radiant	Air	Roof Slab	West Wall	Radiant	Air	Roof Slab	West Wall
Max 24.5	23.4	23.9	23.3	26.2	24.2	24.6	24.2	26.8	24.0	24.5	23.3	27.2
Min 17.7	17.2	17.1	15.2	17.1	17.4	17.4	16.0	16.5	17.2	17.3	15.0	16.6
Peak Hour 13.5	18	18	16	18	18	18	18	18	18	18	16	18

Table 3: Test 3 Setup and Results

Building on the results of Test 3, the shade net on the East and West faces allowed the interior space to remain cooler than ambient, but did not match the performance of the overhang. Additionally, as shown in Figure 13, installation of a vertical shade net restricted the cooling of the walls down during the night, increasing the radiant and operative temperatures as a result. The radiant temperature method used in these chambers did not show that impact however.
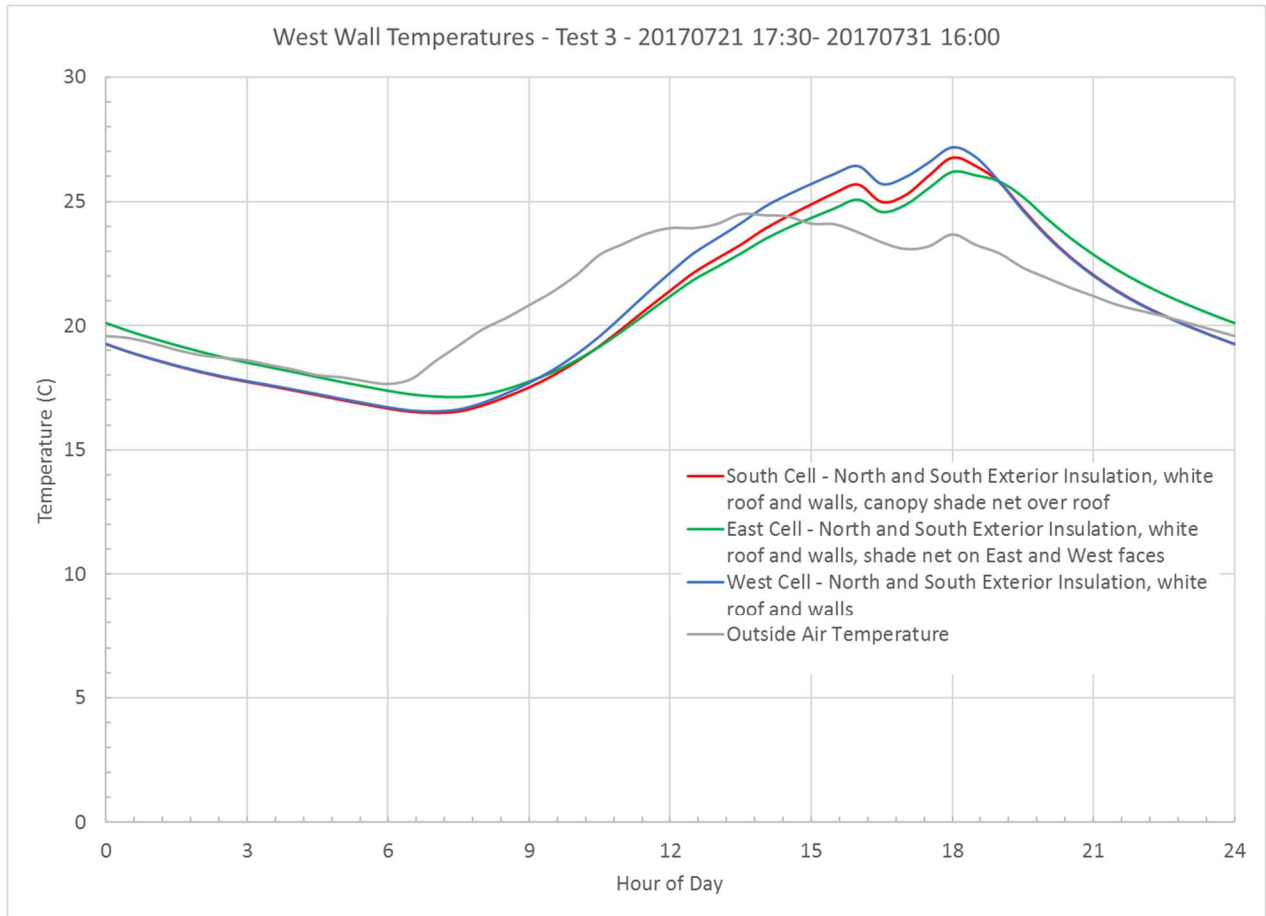
Figure 13: Test 3 West Wall Temperatures, comparing shade nets with 7 PM to 9 AM ventilation

The shade net above the roof, however, contributed negatively to would-be comfort inside of the chamber. Shown graphically in Figure 14, the addition of the canopy only helped reduce the interior air temperature by less than 1°C during a narrow portion of the day. Although not intentional, a plausible rationale for this negative performance at times would be due to the absorption of the sun's energy and re-radiation at longer wavelengths to the surface below. During the early morning, the overhead canopy can actually increase the heat incident on the roof as the shaded area of the sun's rays is more than the baseline case. Looking closely at Figure 12 supports this statement as the canopy is only shading the a small portion of the roof at 4 PM in the afternoon, when the photo was taken. An advertised UV blockage of 90% would then help to reinforce this hypothesis, since 90% of the sun's energy is being absorbed or reflected by the shade net.

Additionally, during the night, the shade net would then inhibit the re-radiation of thermal energy to the night sky. Where the blackbody temperature of the shade net is likely near air temperature, the blackbody temperature of the night sky can often be 20-30 °C cooler than outdoor ambient temperatures (Balcomb, 1992). Instead of the roof seeing 100% of the night sky, the roof would see 52.4% of the night sky with the shade net in the experimental position (Hottel, 1931). With radiation heat transfer being driven by temperature differences and view factors, the similar temperatures of the roof slab and the shade netting prevents any significant re-radiation of heat at night.
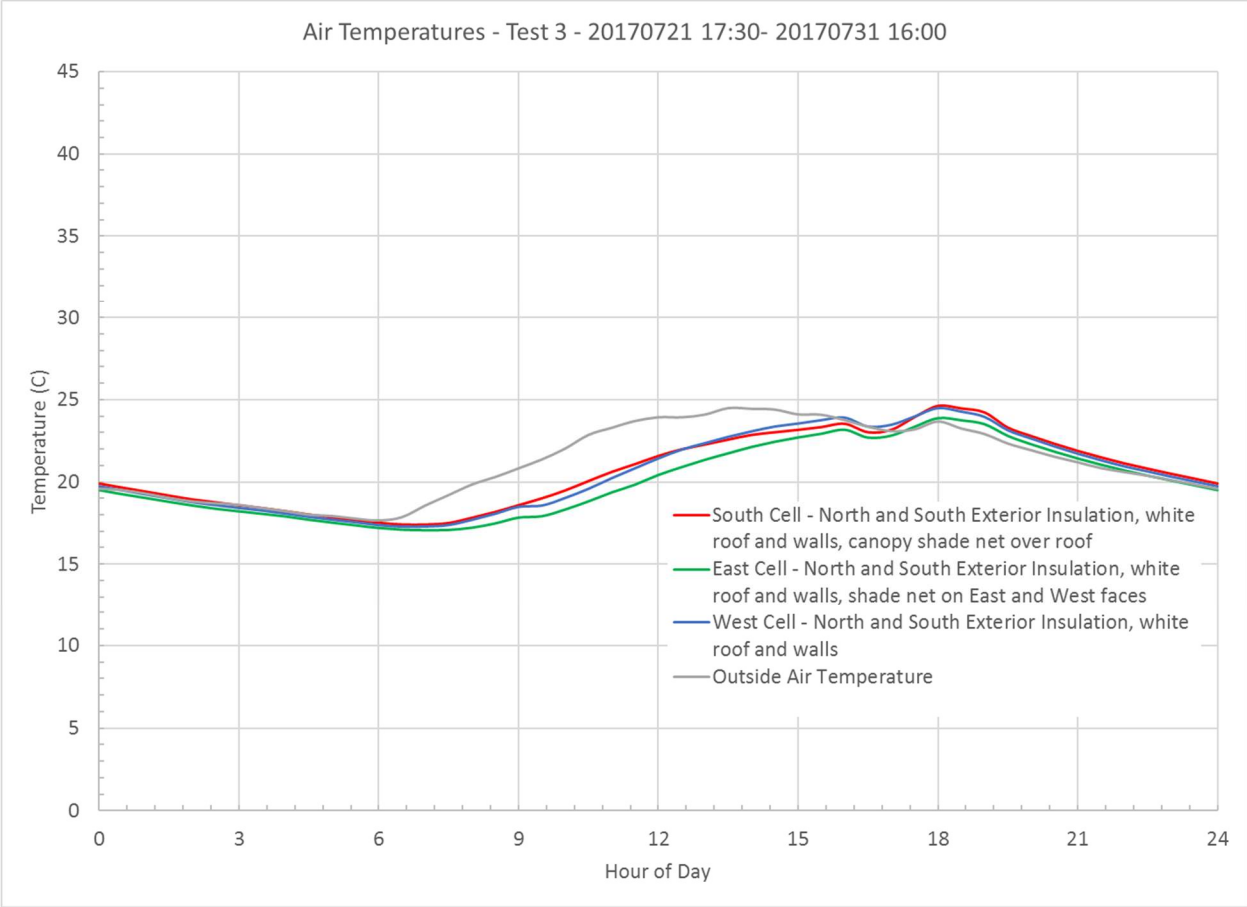
Figure 14: Test 3 Air Temperatures, comparing shade nets with 7 PM to 9 AM ventilation

Test 4 is designed to test the influence of the placement of insulation along the east and west walls, which are the exposed walls in the Bhuj case. The team used a 9/16" extruded polystyrene insulating sheathing (Owens Corning Foamular) as the insulation, which has an advertised thermal resistance of 0.53 °C·m²/W (Owens Corning Foam Insulation, LLC., 2015). The insulation was secured with masonry adhesive and the exterior layer was painted white to match the white-painted concrete brick. The team had expected that the exterior insulation would help decouple the thermal mass from the outdoor air temperature, and help moderate the thermal swings inside the chamber.

Figure 15: Test 4 with North and South foil-faced exterior insulation and East and West white-painted exterior insulation

The team used the third chamber to test the impact of interior insulation due to concerns over the weatherability of exterior insulation in a long-term setting. Conventionally, a mud-based plaster has been used in both India and Nepal as a surface treatment, but needs to be repaired frequently to ensure it remains weatherproof. Figure 16 shows an example of this mud-based plasterwork applied to the exterior of a home in Chitlang, Nepal. Due to the application and climatic conditions, this plasterwork has cracked and sloughed within three months of application.

Figure 16: Conventional mud-based exterior plasterwork in Chagam, Nepal showing cracking and sloughing

Test 4		East Chamber				South Chamber				West Chamber			
7/31 – 8/9		East & West Exterior Insulation North & South Exterior Insulation Roof and non-insulated walls painted white				East & West Interior Insulation North & South Exterior Insulation Roof and non-insulated walls painted white				- - North & South Exterior Insulation Roof and non-insulated walls painted white			
[°C]	OAT	Radiant	Air	Roof Slab	West Wall	Radiant	Air	Roof Slab	West Wall	Radiant	Air	Roof Slab	West Wall
Max	27.9	25.4	25.9	26.7	26.4	26.2	26.8	27.1	30.8	26.8	27.9	26.9	31.3
Min	19.0	19.3	19.1	16.9	19.7	19.0	18.9	16.7	17.6	19.0	19.0	16.6	18.3
Peak Hour	14	17.5	17.5	16.5	18.5	16.5	16.5	15	17	17	16.5	16.5	16.5

Table 4: Test 4 Setup and Results

The results confirmed the initial qualitative expectations that the exterior insulation would dampen out the fluctuations in temperature during the day. With the exterior insulation present, the chamber with exterior insulation added to the east and west walls helped to lower the maximum air temperature within the space by 2 °C and keep the interior temperature of the west wall nearly 5 °C cooler than the chamber without insulation. The Standard Deviation with the exterior insulation was also reduced by 25% from the chamber without insulation; given a quantitative illustration of the dampening of the daily temperature profile. However, a small increase in the minimum temperature of the chamber can also be observed, which may not be desirable when a home is nearly guaranteed to be occupied at night. Based on the data, the nighttime ventilation rate of 25 ACH was sufficient to reduce the inside air temperature to the values approaching outside conditions. Further opportunities are still present by reducing the nighttime temperature of the walls, a practice that could be accomplished by using standing fans within the chambers to improve convective coefficients along the surfaces. Regardless, all of the chambers helped to delay the peak air temperature of the outside environment by roughly three hours. With the peak inside temperatures less than the peak outside temperatures, all of the chambers are able to provide relief from the heat of the day, which will become more significant when the daily temperatures reach the 2017 Bhuj maximum temperature, 45.53 °C on April 13th, 2017.

The results also confirm that interior insulation on the east and west walls also provides a benefit by reducing the interior air temperature, although not as much as the exterior insulation. Figure 17 shows this data graphically. The inflection points in the temperature plots correspond to the timing of the fan, which turned on at 19:00 hours and off at 9:00 hours. Based on the plots, further optimization of the fan timing would help to reduce the inside temperature by allowing the chambers to retain the minimum temperature longer, also helping to lower the inside peak temperature.
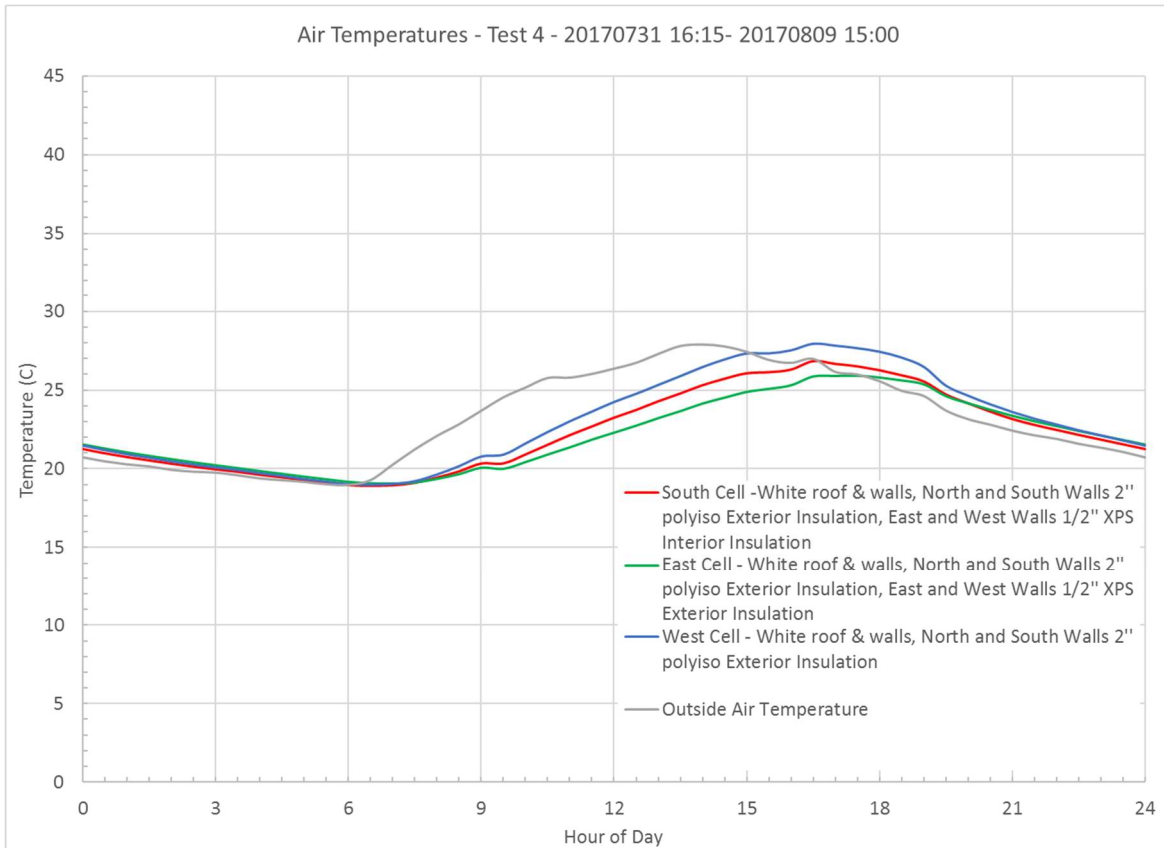
Figure 17: Test 4 Average Day Air Temperatures, comparing insulation positioning with 7 PM to 9 AM ventilation

While these gains are a significant step in the right direction, it should be noted that the roof had already been painted white from Test 2, so large solar gains had already been reduced from being absorbed at the roof.

Test 5 was designed to test the role and significance of placement of a radiant barrier comprised of an aluminum foil sheet. The team used the same black Behr exterior paint and applied it to the underside of the ceilings. For the South Chamber, the aluminum foil was stapled and glued in place using 3M Spray-Ment and applied such that the more polished side faced the interior of the chamber. For the West Chamber, the team used 1" x 2" nominal pine furring strips to offset the aluminum foil by 1 ½", and secured the aluminum foil such that the more polished side faced the newly-created cavity. The significance of the polishing is described later in the Optical Testing Section.

Figure 18: Test 5 experimental setup

The team used this opportunity to serve as a precursor to proposing a movement of the radiant barrier in the Bhuj test chambers, and a test bed for direct application to the ground level homes in Bhuj.

Test 5		East Chamber				South Chamber				West Chamber			
8/9 – 9/7		Black Ceiling - - North & South Exterior Insulation Roof and non-insulated walls painted white				Radiant Barrier Offset from Ceiling - - North & South Exterior Insulation Roof and non-insulated walls painted white				Radiant Barrier Directly applied to ceiling East & West Interior Insulation North & South Exterior Insulation Roof and non-insulated walls painted white			
[°C]	OAT	Radiant	Air	Roof Slab	West Wall	Radiant	Air	Roof Slab	West Wall	Radiant	Air	Roof Slab	West Wall
Max	26.1	26.1	26.7	25.7	29.7	26.3	27.0	26.9	29.8	26.3	27.1	26.2	30.6
Min	17.1	17.5	17.3	15.1	16.7	18.1	17.9	14.4	16.9	18.0	17.9	14.9	17.1
Peak Hour	15.5	17.5	17	16	17	17.5	17	16	17	17.5	17	16	17

Table 5: Test 5 Setup and Results

For this case, the team was dismayed to find that the radiant barrier had a negative impact on the performance of the chamber. Although the changes were modest, the application of the radiant barrier increased the maximum air temperature within the space, and led to an increase in the minimum nighttime temperatures of half a degree. Largely, looking at the plot of the data in Figure 19, most of the impact is due to an upwards shift of the minimum temperatures which is when the inside surfaces of the chamber are radiating to the ceiling. This radiation is largely blocked by the radiant barrier, and an idea that may be successful during the day is defeated by poor performance at night. Note that in Figure 19 the vertical scale has been changed from the other graphs of this series to give more resolution to the differences.
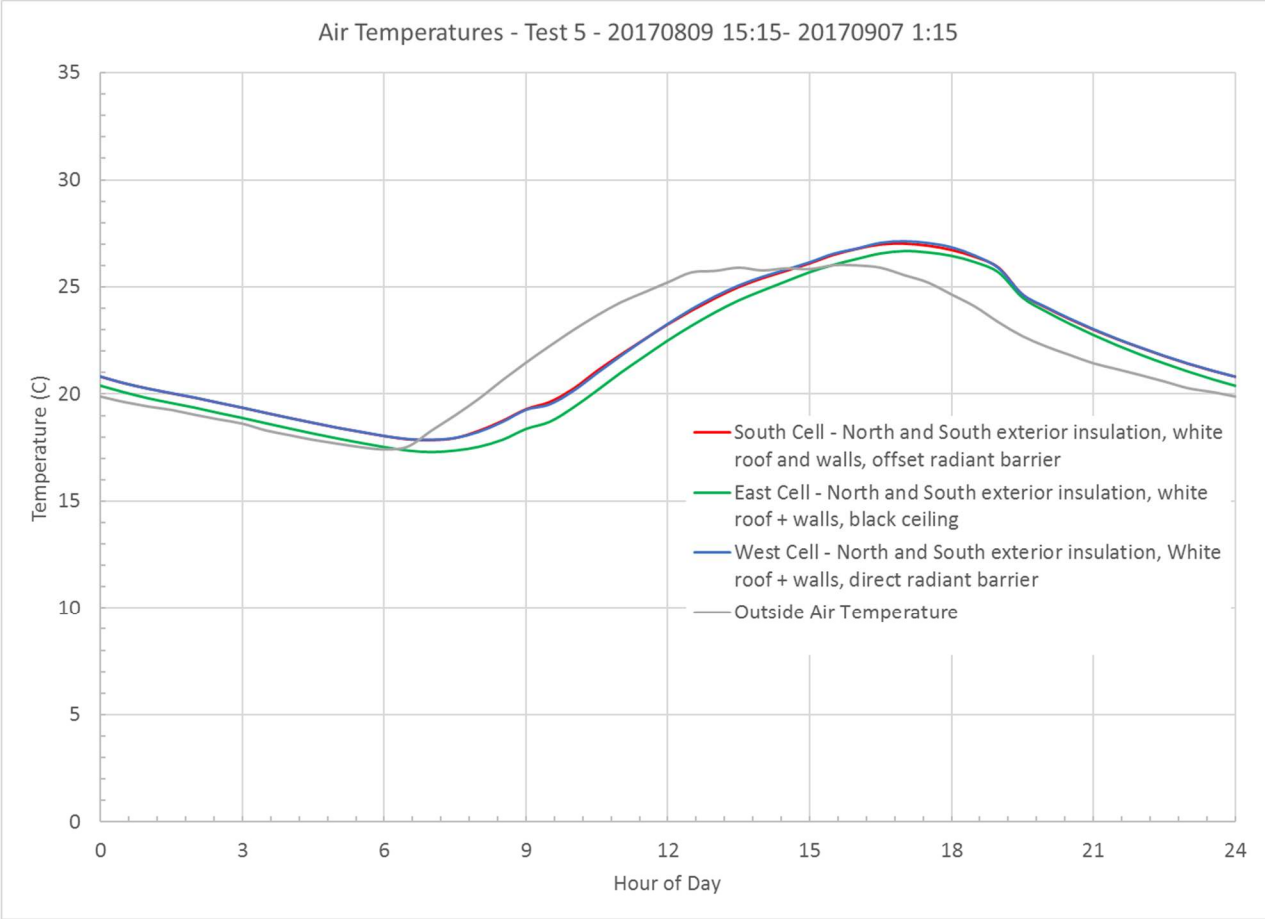
Figure 19: Test 5 Air Temperatures, comparing ceiling coatings with 7 PM to 9 AM ventilation

Pushing this idea further, it may be possible to test a scenario where the radiant barrier is present during the day, but removed or pulled out of the way at night, making it possible to change the radiant properties of the surface.

Test 6 retested some of the variations in a new arrangement for application into the ground level homes in Bhuj. Combining the radiant barrier ceiling elements with the interior insulation in the West Chamber, the test was a precursor to one run in Bhuj several weeks later. Largely, the difference between Test 5 and Test 6 is within the South Chamber, where the Radiant Barrier was relocated to direct application to the ceiling. Further, the Radiant Sensor was relocated from the radiant sphere to the East Wall to look at the impact of sun movements on each of the surfaces. The UX120-006M logger only has four channels, restricting the amount of data feeds without adding additional loggers.

Test 6		East Chamber				South Chamber				West Chamber			
10/30 – 11/8		Black Ceiling - - North & South Exterior Insulation Roof and non-insulated walls painted white				Radiant Barrier Directly applied to ceiling - - North & South Exterior Insulation Roof and non-insulated walls painted white				Radiant Barrier Directly applied to ceiling East & West Interior Insulation North & South Exterior Insulation Roof and non-insulated walls painted white			
[°C]	OAT	East Wall	Air	Roof Slab	West Wall	East Wall	Air	Roof Slab	West Wall	East Wall	Air	Roof Slab	West Wall
Max	16.3	14.6	14.1	13.5	15.7	14.4	14.0	14.0	15.0	12.4	12.9	13.6	12.8
Min	10.9	8.0	8.5	6.9	7.8	7.8	8.5	6.6	7.7	8.8	9.0	7.1	8.9
Peak Hour	15	15.5	16	15.5	16	15.5	16	15.5	16	17.5	16.5	15.5	18

Table 6: Test 6 Setup and Results

The results of Test 6 seemingly conflict with the results of Test 5, where the West Chamber is now cooler than the East Chamber. Before, it was vice versa. Test 6 was run nearly ten weeks after Test 5, where the hourly positioning of the sun had varied. The Average Day plot in Figure 20helps to add clarity to these numbers. Note that the scale has changed from the similar previous plots. The differences between the South and East Cell again follow the trends in Test 5, although the nearly linear offset between the radiant barrier and the black ceiling is no longer present. In Test 6, the added exterior insulation helps couple the east and west walls to the interior temperature, resulting in a similar dampening of the temperature plot as observed in Test 4. However, water infiltration or variation in sun positioning or hours of daylight may allow the chambers to remain colder than the outside air temperature.
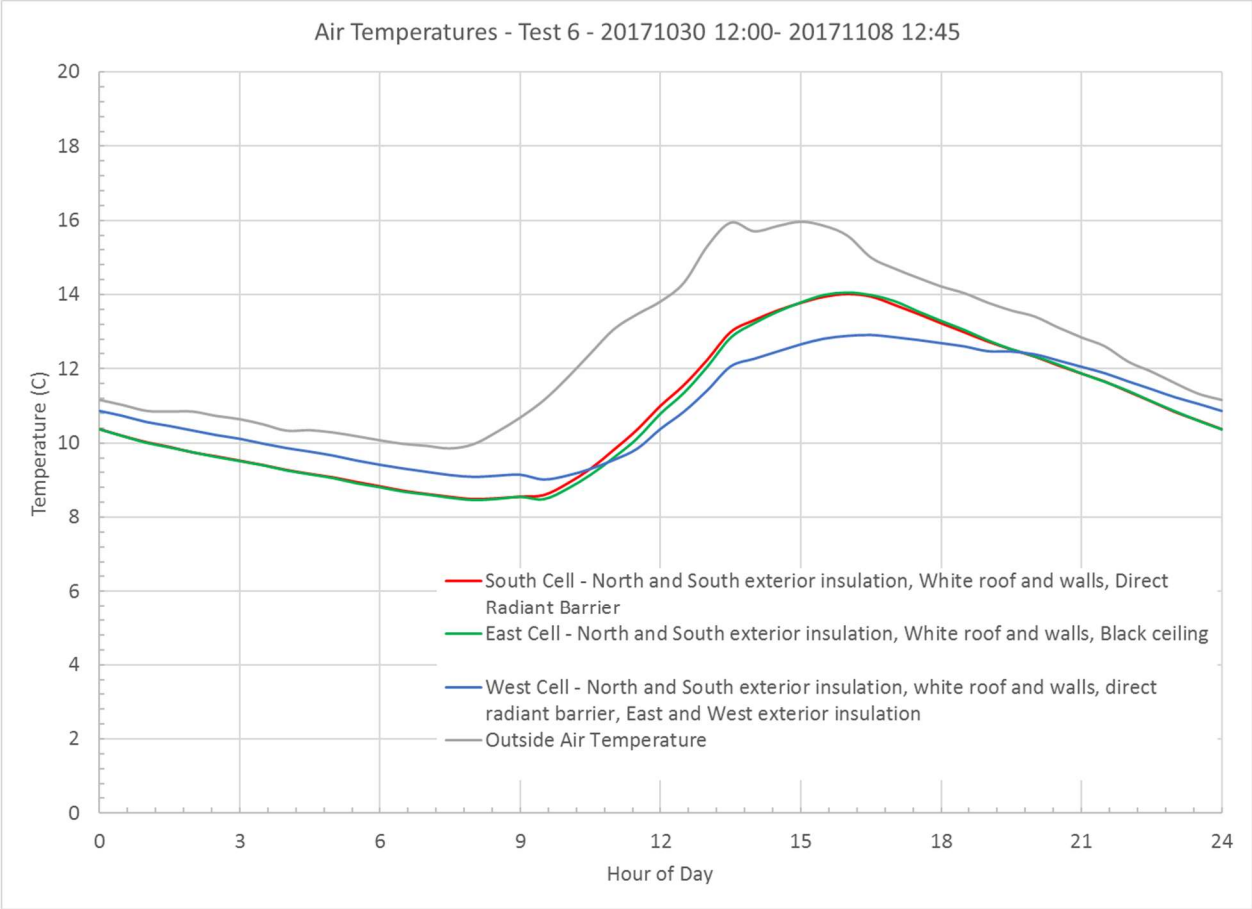
Figure 20: Test 6 Air Temperatures, comparing ceiling coatings and insulation with 7 PM to 9 AM ventilation

While direct conclusions are difficult to draw between different weather sampling periods, the test iterations sought to maintain a consistent baseline chamber setup after the chambers matched the setup seen in the Bhuj housing. This baseline, with the white roof and walls, north and south exterior insulation, and non-reflective ceiling, serves as the control throughout the experiments.

Building off that baseline, the testing iterations allowed the team to ascertain the variations caused by each additional modification to the chamber. The initial testing established the degree to which each modification leading up to the baseline helped to reduce interior temperatures. The results of those tests are represented in the stepped list below, where each indentation would incorporate the changes from the higher-level modifications. This approach allows the values to be additive, meaning that the modification from each indentation can be added to establish the total amount of peak temperature change. The values in parentheses then represent the total change from the bare structure, without any modifications.

North and south exterior insulation: 1.7°C decrease in peak air temperature from base structure (-1.7°C compared to bare structure).

    White Wall Paint: 0.7 °C decrease in peak air temperature from North and South exterior insulation (-2.4°C compared to bare structure)

        White Roof Paint: 4.0°C decrease in peak air temperature from White Wall Paint (-6.4°C compared to bare structure).

            Overhang to the east and west faces: 0.9 °C decrease in peak air temperature from White Roof Paint (-7.3°C compared to bare structure).

                Interior insulation on east and west faces: 1.1°C decrease in peak air temperature from White Roof Paint (-7.5°C compared to bare structure).

                Exterior insulation on east and west faces: 2.0°C decrease in peak air temperature from White Roof Paint (-8.4°C compared to bare structure).

                Direct radiant barrier: 0.4°C increase in peak air temperature from White Roof Paint (-6.0°C compared to bare structure).

                Offset radiant barrier: 0.3°C increase in peak air temperature from White Roof Paint (-6.1°C compared to bare structure).

                Shade netting, overhead: 0.1°C increase in peak air temperature from White Roof Paint (-6.3°C compared to bare structure).

                Shade netting, façade: 0.6 °C decrease in peak air temperature from White Roof Paint (-7.0°C compared to bare structure).

Based on the results collected from the scale chambers, the most promising immediate steps to reduce peak temperatures, balancing social concerns and experimental results, are the application of white paint to the roof and exterior of exposed walls, exterior insulation on exposed walls, and scheduling of night ventilation. Although not explicitly tested, the optimization of window fan operation through parallel monitoring of indoor and outdoor conditions will yield better results than the arbitrary timing selected for the above chambers. Further research will also seek to quantify the application of a radiant barrier to a low-mass roof, which should have improved performance over the high-mass (concrete) roofing. Overall, without the air fan optimization, the tested improvements will reduce the peak air temperature by 6.7 °C from other row homes, and 8.4°C from bare stand-alone structures.

Moving forward, further research can look into the interactive effects of the shading approaches in the presence of the best performing chamber above.

In addition to thermal monitoring in the MIT-based scale chambers, the research team conducted a series of tests to determine the optical surface properties of several building samples from India. Specifically, the team was looking to determine the absorptivity and emissivity values for a handful of these building materials. The team tested the following building materials:

- Indian-sourced aluminum foil;
- Indian-sourced galvanized corrugated metal sheet;
- Indian-sourced 4 mm thick aluminized bubble wrap;
- Indian-sourced 6 mm thick aluminized bubble wrap; and
- US-sourced aluminum deposited Mylar.

To test these materials across both solar and room temperature regions, the team used a Surface Optics Corporation SOC 400-T reflectometer, a directional input hemispherical output reflectometer, for the samples between 400 and 1,900 nm (Surface Optics Corporation, 2004), and the Fourier Transform Infrared reflectance of the samples between 400 and 2,400 nm (Persky & Szczesniak, 2008).

The SOC400T utilizes a silicon carbide spectral source which is focused on a sample or calibration surface, compared to a 'chopper' reference, and then reflected through a concentrator to a detector. A conceptual drawing is shown below, reproduced from Persky and Szczesniak. Using this technique, Persky and Szczesniak used a fused silica reference to calculate the estimated reflectance precision to be 0.003 at low reflectance levels, and 0.007 at higher reflectance levels.
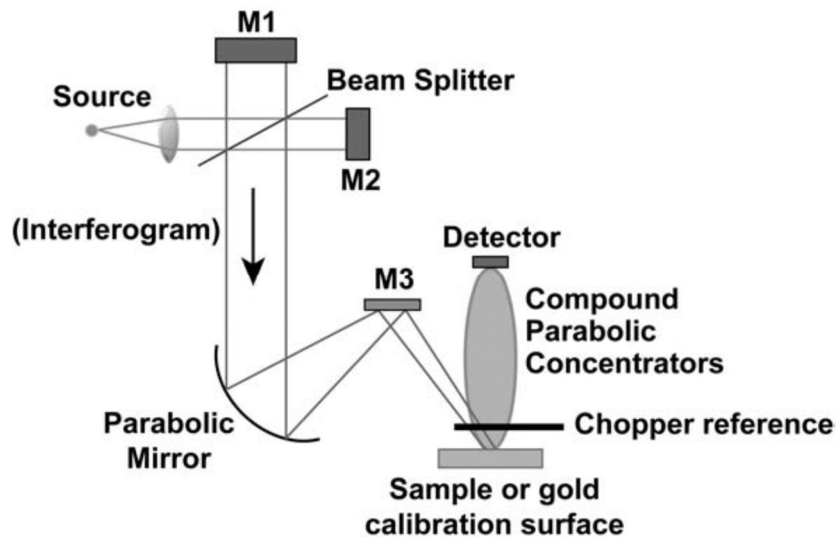
Figure 21: Conceptual Drawing of SOC400T directional input-hemispherical output reflectometer (Persky & Szczesniak, 2008)

Throughout the testing, the reflectometer was referenced intermittently against a piece of 75% Specralon® (a highly diffuse reflectance reference material) to confirm that the value matched the initial values, did not drift during the sampling process, and also provide a means to utilize the methods from Persky and Szczesniak. The results of these repeated sampling are shown below, in Figure 22. Throughout much of the short wavelength spectrum, the 75% Spectralon® reference sample measurements exhibit little change, with the exception of the wavelengths bands of 995-1074 nm and 1210-1387 nm. These bands of interference may correlate with ambient temperatures around 15°C, or cooling system supply temperatures.
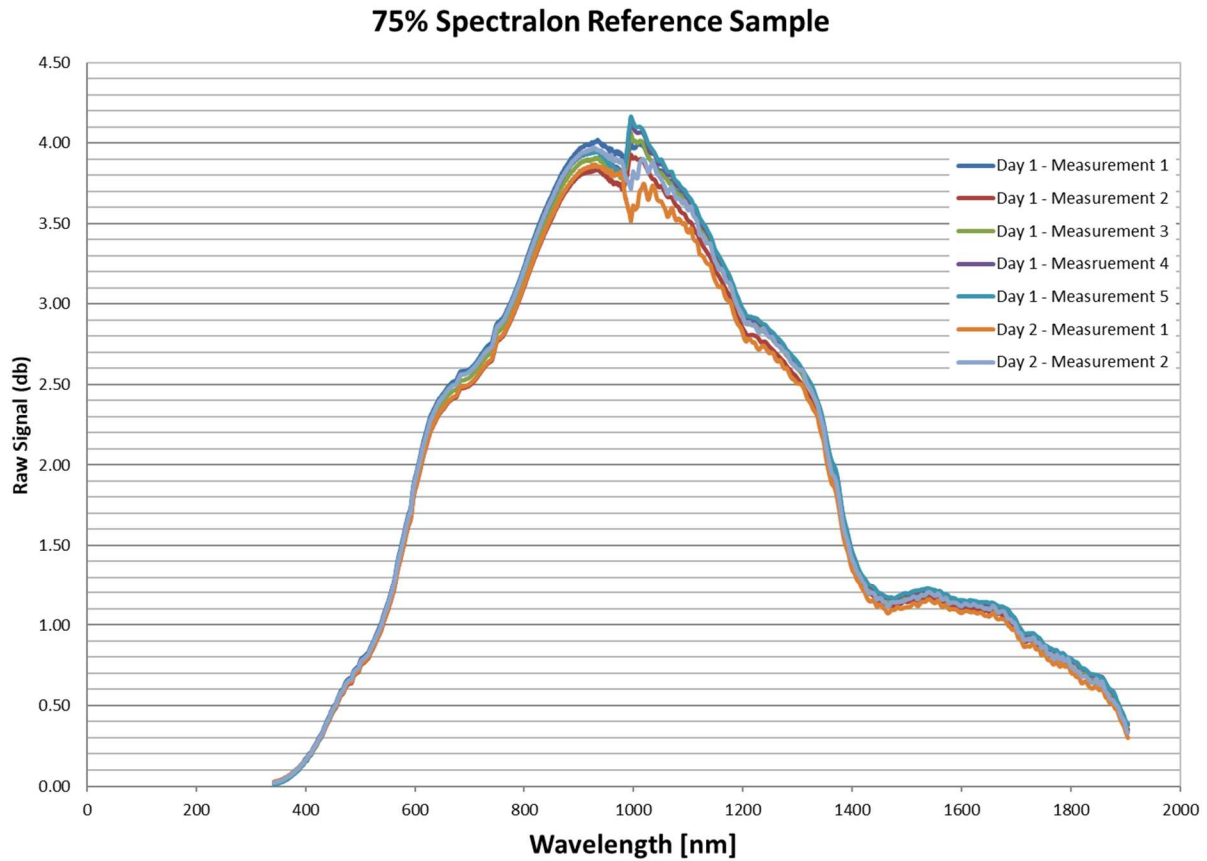
Figure 22: 75% Spectralon® Reference Sample repeatability tests

For the directional-hemispherical reflectivity measurements, the raw data delivered by the SOC 400T was initially adjusted based on a comparison to the manufacturer's specification for 75% Spectralon® and the raw measurement without a sample on the sampling surface. This adjustment is detailed below, reproduced from the SOC 400T User Guide (Surface Optics Corporation, 2008).

$$\rho_{calc,sample} = \rho_{meas,zero} + (\rho_{raw,sample} - \rho_{meas,zero}) \cdot \frac{\rho_{inf,75\% \; Spectralon \; manf} - \rho_{zero}}{\rho_{meas,75\% \; Spectralon \; sample} - \rho_{meas,zero}}$$

Where the terms are below, with the range of values when applicable.

$\rho_{calc,sample}$ = the calculated reflectivity of the sample

$\rho_{raw,sample}$ = the raw value for the reflectivity of the sample

$\rho_{meas,zero}$ = the measured reflectivity without a sample present (0-0.2)

$\rho_{inf,75\% \; Spectralon \; manf}$ = the reflectivity of the 75% Spectralon as inferred from the vendor calibration standard (0.725-0.79) (Labsphere, Inc., 2017)

ρ_{zero} = the accepted reflectivity without a sample present (assumed to be zero)

$\rho_{meas,75\% \; Spectralon \; sample}$ = the measured reflectivity of the 75% Spectralon® (0-4.3)

Applying the above relationship to the sample data, the team computed the reflectivity of the sample based on the 75% Spectralon® samples for each of the 768 samples between 342.6 nm and 1904.1 nm, at 1.6 nm increments. The resultant values are plotted below, where the horizontal axis is the wavelength and the vertical axis is the calculated reflectivity.
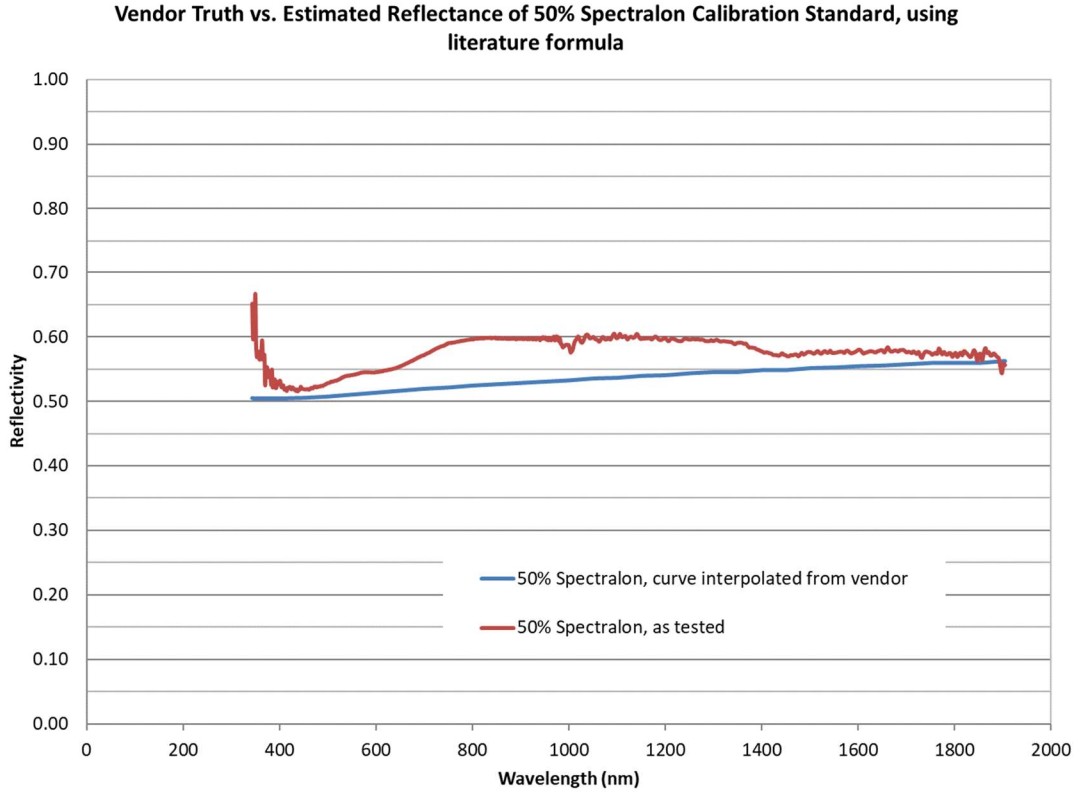
Figure 23: Vendor Truth vs Estimated Reflectance of 50% Spectralon® Calibration Standard, using literature formula

As Figure 23 helps illustrate, using the literature value produces a significant (7 percentage points) deviation between the vendor truth and the calculated values. This difference is largely due to the non-zero signal from the zero sample measurements, which near a raw signal value of 0.24 from the 704 nm to 984 nm range. With the help of an optical scientist, who for security concerns cannot be mentioned by name or affiliation, the above equation can be simplified when using a non-transmissive sample. Thereby, rewriting and rearranging the above equation yield the equation below. Note that the equation below applies the assumption that ρ_{zero}, or the accepted non-sample reflectivity, is equal to zero.

$$\rho_{calc,sample} = \rho_{inf,75\% \ Spectralon \ manf} \cdot \frac{\rho_{raw,sample} - \rho_{meas,zero}}{\rho_{meas,75\% \ Spectralon \ sample} - \rho_{meas,zero}}$$

Where the terms are below, with the range of values when applicable.

$\rho_{calc,sample}$ = the calculated reflectivity of the sample

$\rho_{raw,sample}$ = the raw value for the reflectivity of the sample

$\rho_{meas,zero}$ = the measured reflectivity without a sample present (0-0.2)

$\rho_{inf,75\% \ Spectralon \ manf}$ = the reflectivity of the 75% Spectralon as inferred from the vendor calibration standard (0.725-0.79) (Labsphere, Inc., 2017)

$\rho_{meas,75\% \ Spectralon \ sample}$ = the measured reflectivity of the 75% Spectralon® (0-4.3)

47

Applying the above equation to the 50% Spectralon® sample, the results are in closer agreement with the accepted values from the 50% Spectralon® vendor. Figure 24, below, illustrates the agreement with the accepted values, based on the 75% Spectralon® sample. In this figure, the wavelength is graphed on the horizontal axis and the reflectivity on the vertical axis. The two plots represent the vendor-advertised values, and the as-tested values.

Throughout the breadth of the measurement spectrum, the measured values agree well with the vendor truth. However, the values at the periphery of the measurement range begin to show the limitations of the approach at wavelengths lower than 415 nm and greater than 1891 nm. Within the electromagnetic frequency range, acceptable values can be derived from the purple color of the visible regime to the short-wavelength infrared. Most importantly for this research, this acceptable range includes the 501.5 nm value, which is the peak solar energy wavelength.

Vendor Truth vs. Estimated Reflectance of 50% Spectralon Calibration Standard, using literature formula
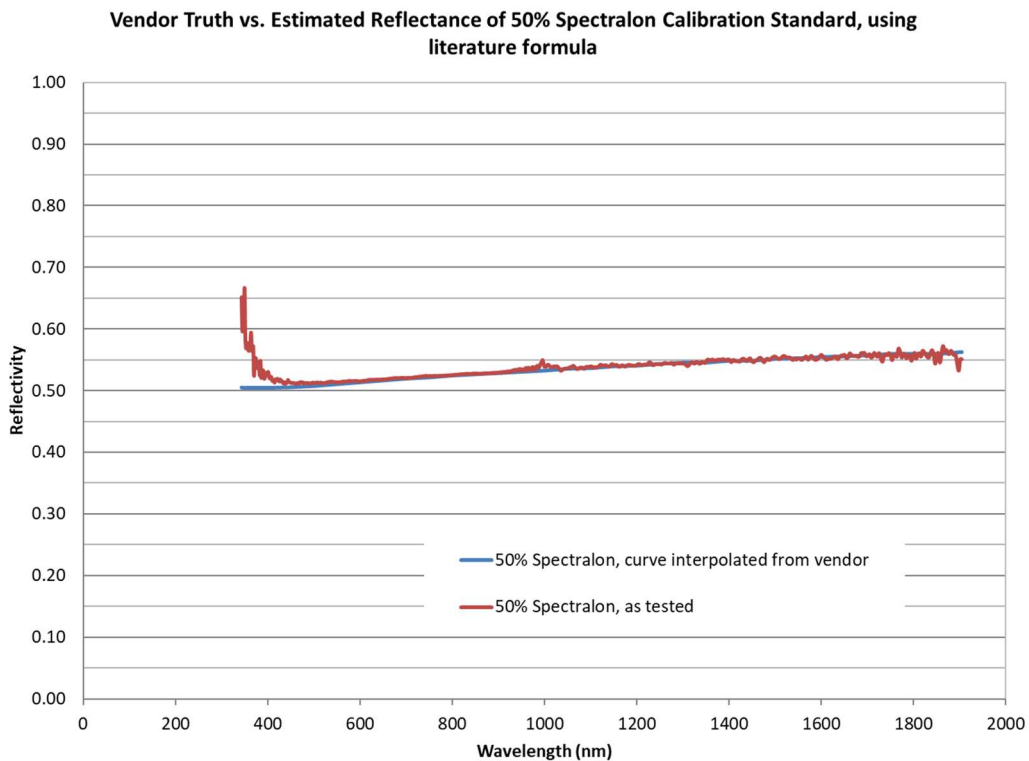
Figure 24: Vendor Truth vs Estimated Reflectance of 50% Spectralon® Calibration Standard, using simplified formula

Using the second equation leading to Figure 24, the team compiled the remaining results in the following graph, Figure 25. Within the graph, a vertical dotted line was drawn at the 501.5 nm wavelength to indicate the peak solar wavelength values. This wavelength is the most likely to be published in literature listing values for solar reflectivity.

48
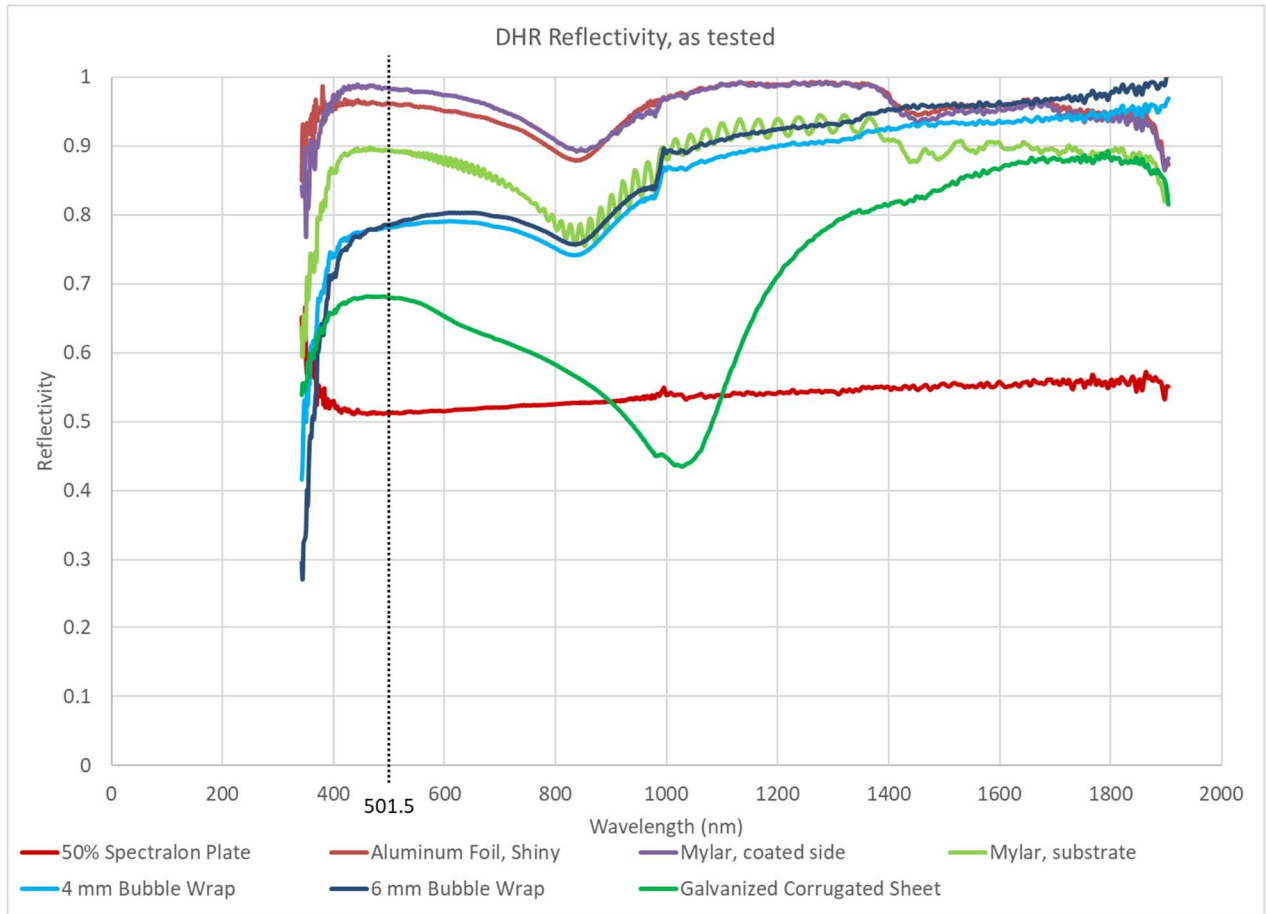
Figure 25: DHR Reflectivity Results

While reflectivity was measured through the DHR methodology, it is more meaningful to think in terms of absorptivity values in order to reference to literature and to apply to building simulations. To convert the reflectivity measurements taken from the instrument with the absorptivity values referenced in literature, the samples were assumed to be non-transmissive. Using Kirchoff's law and accepting the assumption, the reflectivity is related to the absorptivity by the relation below.

$$1 = \rho + a$$

Where ρ is the reflectivity and a is the absorptivity. Using this relation, the team reproduced Figure 25 in terms of the absorptivity, as shown in Figure 26.
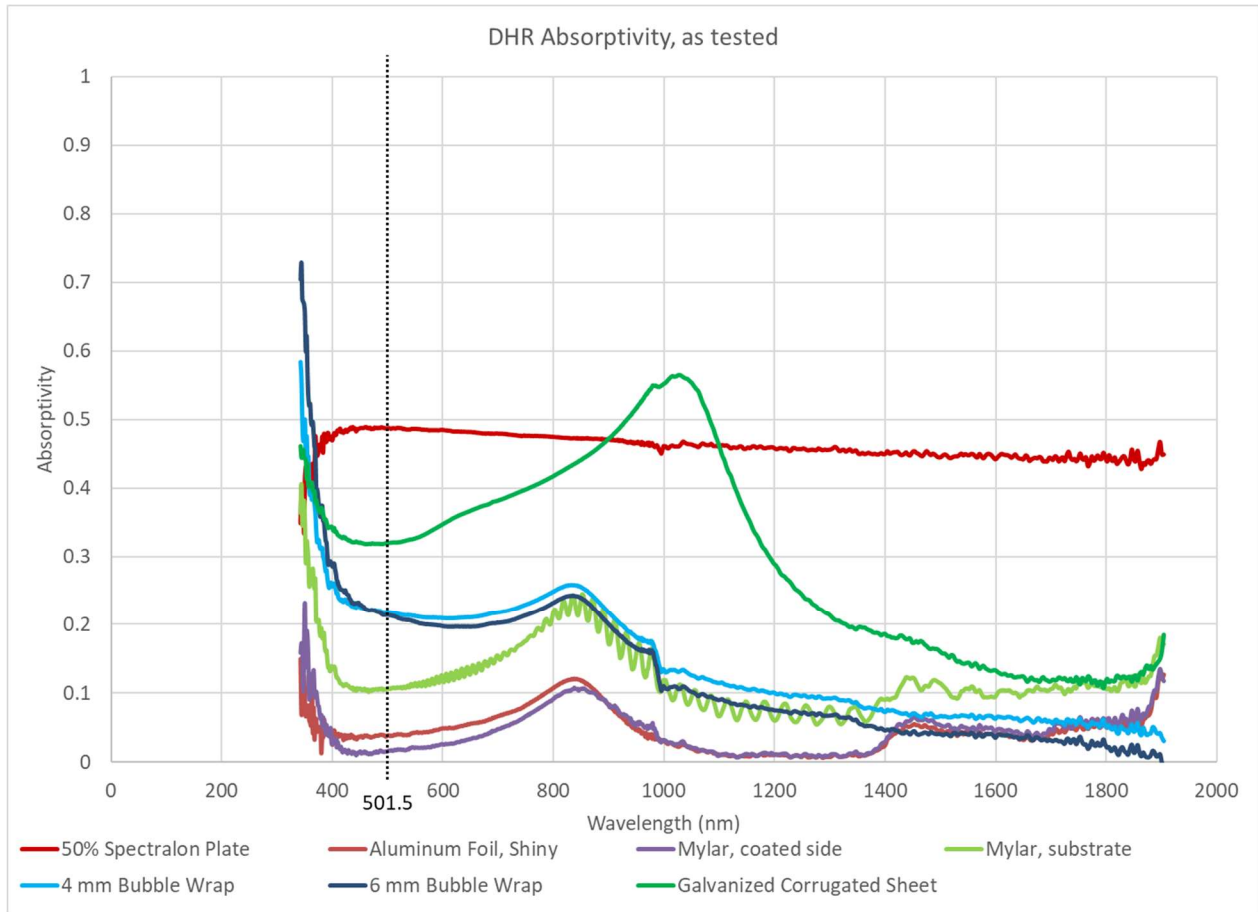
Figure 26: DHR Absorptivity Results

The materials and values of absorptivity at the wavelengths corresponding to receiving radiation from solar energy (5780 K, 501.5 nm) are shown below in Table 7. The corresponding peak wavelength was calculated using Wien's displacement law (Rohsenow & Hartnett, 1973). For the values presented below, the Aluminized Bubble Wrap was assumed to be equivalent to the 0.15 value presented by Kreith, but different from the 0.04 value presented by Modest. Among the three grades Modest presented for Mylar, the absorptivity was assumed to be equivalent to the two thinner grades, 0.00025" and 0.001" thick. A caliper to measure the thickness of the Mylar base layer was not accessible to such precision. Additionally, the absorptivity values were rounded down in the number of significant figures to match the decimal places available from the literature.

Material	Absorptivity at 501.5nm	Accepted Values [1,2,3]	Difference [%]
50% Spectralon®	0.487 (n=1)	0.492	1
Aluminum foil, shiny side	0.04 ± 0.02 (n=2)	0.04	2
Aluminized Bubble Wrap 4 mm thick	0.22 ± 0.07 (n=6)	0.15	45
Aluminized Bubble Wrap 6 mm thick	0.21 ± 0.06 (n=6)	0.15	43
Mylar, coated side	0.02 (n=1)	0.10	83
Mylar, substrate	0.11 ± 0.02 (n=2)	0.17	37
Galvanized Iron ("Tin sheet")	0.32 ± 0.02 (n=44)	0.65	51

Table 7: Tested values of absorptivity for material receiving radiation from solar energy (5780K)

Assuming the system is at steady state, and that the emissivity is approximately equal to the absorptivity at the stated temperature, the tested values have a mixed agreement with the published literature values. Both the 50% Spectralon® sample and the Aluminum foil have good agreement, with less than a 2% error to accepted values. The Mylar substrate and 6 mm thick aluminized bubble wrap have variance from the accepted values, with near 50% difference from accepted values. The coated side of the Mylar, which is assumed to be a vacuum deposited Aluminum, does not agree well, with a 80%+ difference value.

Variations are to be expected between field samples and laboratory measurements. Oxidation and weathering of surfaces can change the surface optical properties of materials, just as sunlight bleaches clothes hung to dry or fades exposed, non-UV stabilized plastics. This is especially true of the Indian-sourced galvanized iron which may have a different composition than the Western literature measurements. The variations in the aluminized bubble wrap values from the literature value can be explained by an over-reaching approximation to the aluminum foil values listed by Kreith. The aluminized bubble wrap also has a thin protective plastic coating which may change the absorptivity or transmissivity properties of the surface. The tested Mylar was also a consumer grade Mylar sheet, which may have had low quality control or a different formulation from the official Dupont Mylar formula mentioned in the literature.

---

[1] (Labsphere, Inc., 2017)

[2] (Kreith & Kreider, 1978)

[3] (Modest, 2013)

Where the DHR method described above was suitable for use within the visible and near-infrared spectrum, Fourier Transform Infrared Reflectance (FTIR) is another methodology that can be useful for extending the range of reflectance values above the 1,891 nm useful maximum wavelength of DHR. FTIR extends over the 2,000 nm to 25,000 nm range. This is especially important because it includes the 9,670 nm area, which is the peak thermal wavelength near room temperature conditions (299.53 K, 25°C). The SOC400T was again used for the FTIR measurements and was set to scan a spectral range of 2,000 to 25,000 nm four times, scanning the sample sixteen times per run. Within the FTIR settings, no operator adjustment of the values needed to be done, as the reflectivity readings were given directly from the machine outputs.

The SOC400T was calibrated with a reference zero setting (no sample on the port) similar to the DHR settings, but also used an Infragold NIR-MIR reflectance specimen (calendar year 2007 production run). The Infragold standard was expected to yield a flat reflectance curve with a reflectance value of 0.95 over the entire band, as shown on the left of Figure 27. Where the original curve may be hard to read, the horizontal axis is the wavelength in micrometers, ranging from 0 to 22 microns (22,000 nm) in increments of 2 microns (2,000 nm). The vertical axis is the 10° Hemispherical Reflectance (%) expressed from 75 to 100. (Labsphere, A HALMAN Company, 2010) The right side shows the as-tested values, on the same scale.
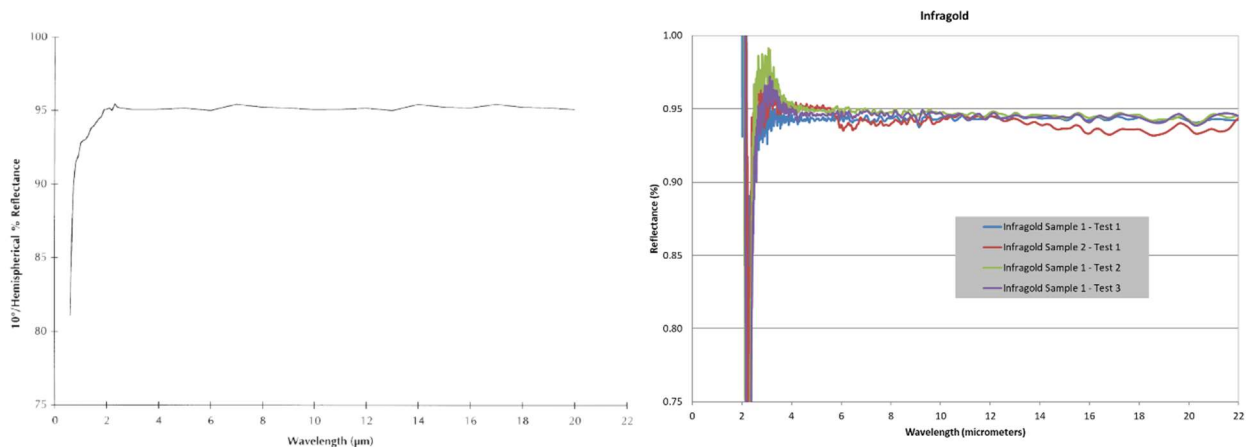
Figure 27: Infragold reflectivity comparison between vendor truth (left) and as-tested values (right)

As the plot shows, the tested values agree well with the Infragold sample across a large band (4.2 microns to 22 microns), but deviate lower than 4.2 microns. Accepting this correlation as a validation of the testing setup, the team measured the same building samples as were measured in the DHR, producing the reflectivity values as shown in Figure 28. Similar to the limitations imposed on the DHR results, a similar approach should be applied to the FTIR results, where the extreme ranges are less trustworthy than values closer to the center of the range.
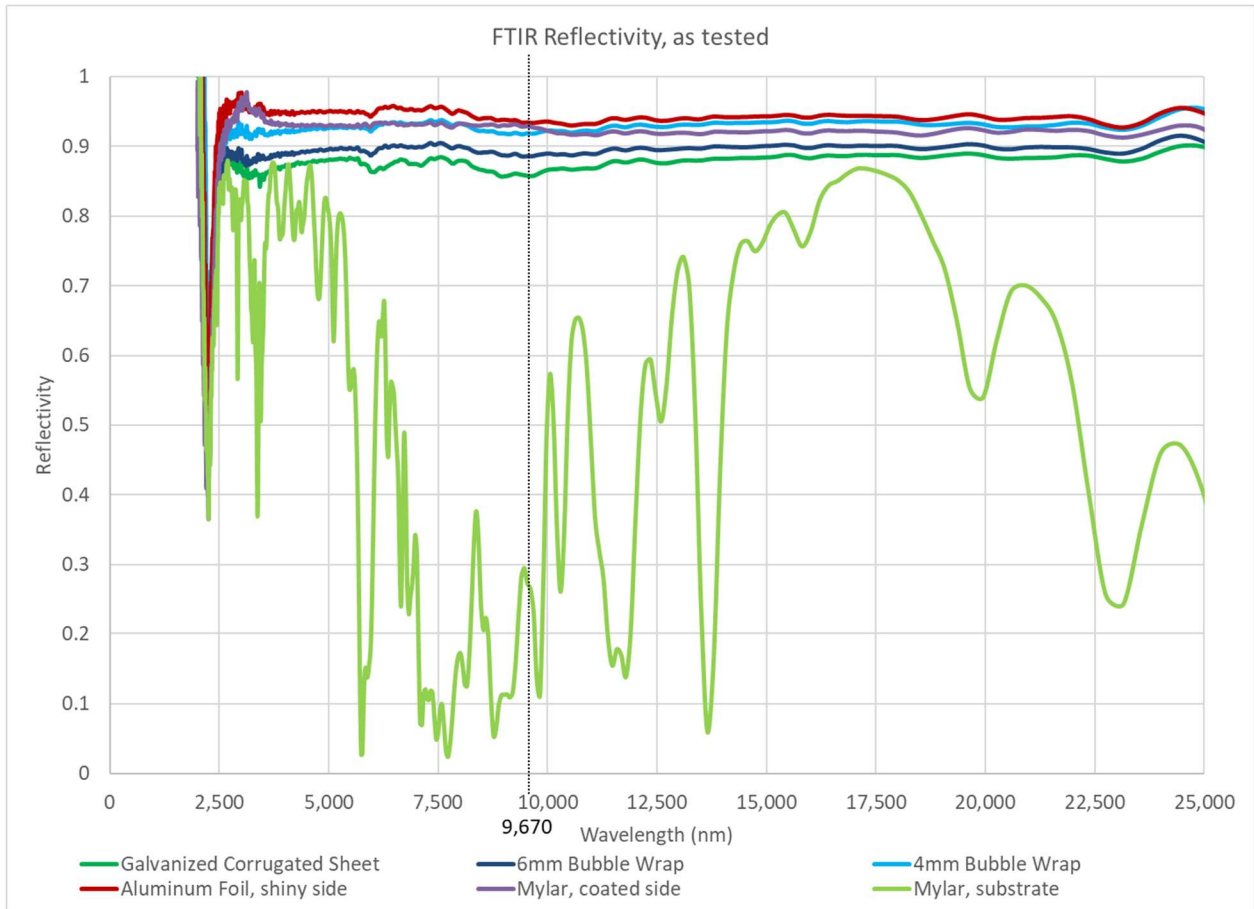
Figure 28: FTIR Reflectivity Results

Subsequently, similar to the DHR approach, the team applied the Kirchoff's Law, assuming that the transmissivity was zero. This allowed the team to produce the absorptivity values as shown in Figure 29, showing the absorptivity values as function of the wavelength within the infrared spectrum.
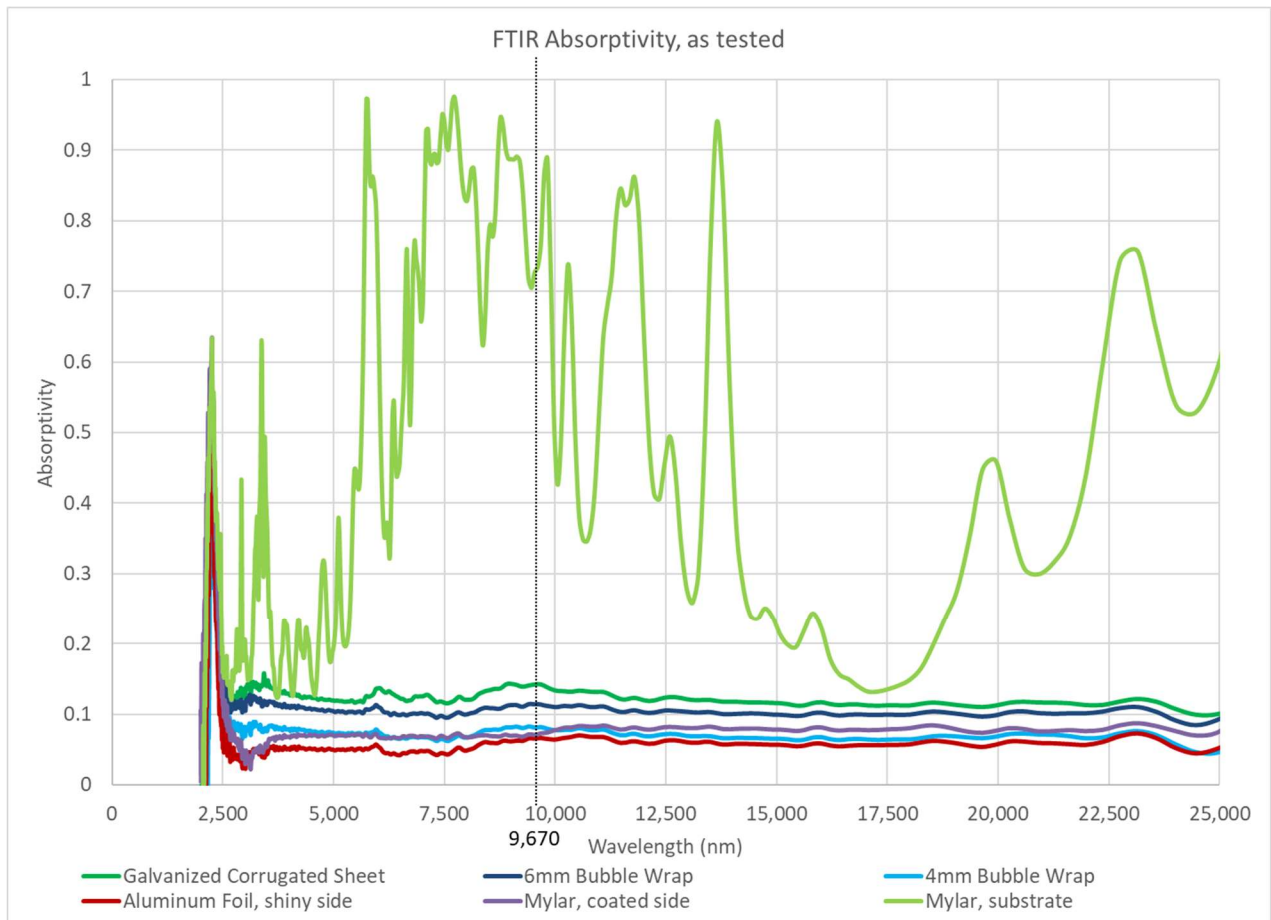
Figure 29: FTIR Absorptivity Results

Material	Absorptivity at 9,670 nm (300 K)	Accepted Values [4],[5],[6]	Difference [%]
Aluminum foil, shiny side	0.07 ± 0.05 (n=7)	0.05	40
Aluminized Bubble Wrap 4 mm thick	0.08 ± 0.05 (n=11)	0.05	62
Aluminized Bubble Wrap 6 mm thick	0.11 ± 0.03 (n=8)	0.05	127
Mylar, coated side	0.07 ± 0.04 (n=5)	0.025	192
Mylar, substrate	0.77 ± 0.01 (n=5)	0.63 - 0.81	22 - 5
Galvanized Iron ("Tin sheet")	0.14 ± 0.11 (n=12)	0.13	9

Table 8: Tested values of absorptivity for material receiving radiation from solar energy (~300K)

---

[4] (Labsphere, Inc., 2017)

[5] (Kreith & Kreider, 1978)

[6] (Modest, 2013)

While on first glance the errors are much higher with FTIR, most of the values overlap with the accepted values when including the confidence bound. Further, the largest differences are seen when the absorptivity values are low. The practical effect on the net heat flow is modest as the absolute difference is lower between the as-tested and accepted values. A notable exception to these low absorptivities is the vacuum-deposited aluminum on Mylar at 293 K, which is highly dependent on the thickness of the Mylar, a value which is unknown. The accepted values are between the 0.63 and 0.81 listed for the 0.025 mm and 0.75 mm thick Mylar at 293 K, respectively.

Bringing together Table 7 and Table 8 allows the team to derive the absorptivity to emissivity ratio, commonly expressed as α/ε or $\alpha_S/\varepsilon_{IR}$, which is especially useful for exterior exposed elements within a building. Implied within the two terminologies are that the absorptivity (α_S) is within the solar range, and that the emissivity (ε_{IR}) is within the infrared range. This allows the ratio to be very useful when trying to restrict heat from being absorbed during the day (low solar absorptivity) and release heat to the cool environment at night (high infrared emissivity), a core characteristic of materials best suited for environments like Bhuj, India. Application of these materials are limited though, as environmentally induced degradation from oxidation or UV exposure may inhibit long-term use.

Material	501.5 nm (Solar Range)		9,670 nm (Infrared Range)	
	Absorptivity	Accepted Values	Absorptivity	Accepted Values
50% Spectralon®	0.487 (n=1)	0.492	--	--
Aluminum foil, shiny side	0.04 ± 0.02 (n=2)	0.04	0.07 ± 0.05 (n=7)	0.05
Aluminized Bubble Wrap 4 mm thick	0.22 ± 0.07 (n=6)	0.15	0.08 ± 0.05 (n=11)	0.05
Aluminized Bubble Wrap 6 mm thick	0.21 ± 0.06 (n=6)	0.15	0.11 ± 0.03 (n=8)	0.05
Mylar, coated side	0.02 (n=1)	0.10	0.07 ± 0.04 (n=5)	0.025
Mylar, substrate	0.11 ± 0.02 (n=2)	0.17	0.77 ± 0.01 (n=5)	0.63 - 0.81
Galvanized Iron ("Tin sheet")	0.32 ± 0.02 (n=44)	0.65	0.14 ± 0.11 (n=12)	0.13

Table 9: Tested values of material absorptivities

For derivation of the $\alpha_S/\varepsilon_{IR}$ ratio, the emissivity within the infrared range must be assumed to be equal to the absorptivity within the infrared range. This assumption is valid for all steady-state cases where the incident wavelength spectrum is near equal to the emitted wavelength spectrum. This assumption can typically be extended to conditions where the two surfaces are close in absolute temperature.

| | Absorptivity_Solar / Emissivity_Infrared | | |
Material	As-tested	Accepted Values	Difference [%]
Aluminum foil, shiny side	0.57	0.40	43
Aluminized Bubble Wrap 4 mm thick	2.75	3	8
Aluminized Bubble Wrap 6 mm thick	1.91	3	36
Mylar, coated side	0.59	4	93
Mylar, substrate	0.14	0.27 – 0.21	47 - 32
Galvanized Iron ("Tin sheet")	2.29	5	54

Table 10: Absorptivity-to-emissivity ratios for tested samples

Table 10 alone suggests that aluminum foil will be a beneficial choice for a roof coating. However, both the absorptivity and emissivity values are sufficiently close to zero that the heat transfer through radiation will already be impeded. A better choice could be the Mylar substrate, which absorbs near 11% and emits nears 77% of blackbody potentials. However, Mylar is one explicit material that experiences severe degradation in the presence of UV light, as abstracted by Kreith.

Setup

   In addition to scale and optical testing, the research team conduced one-dimensional thermal conductivity testing on various samples sourced from both India and the United States. These measurements allowed the team to test and validate assumptions on several materials that are used within the building construction, and to apply these measurements to the simulation models. To make these measurements, the team used a Netzsch Heat Flow Meter (HFM) 436/3/1 Lambda v3.04 to place a sample in a steady-state condition between two different temperatures and then derive the thermal conductivity. The HFM 436 series is advertised to measure Thermal resistances between 0.05 and 8.0 m²K/W with ±1% to 3% accuracy, and 0.25% repeatability (NETZSCH-Gerätebau GmbH, 2014).

   Inside the Netzsch HFM 436/3/1, the machine has an integrated Peltier system to establish the thermal temperature gradient, and a thickness gauge to determine the thickness of the sample. The system also has integrated heat flux transducers to determine when steady state conditions have been met, and when a reading can be taken for the representative thermal conductivity. It is important to note that the HFM can only sample in a single dimension, and so all the materials tested had uniform construction through the central area of interest, defined by the 10cm x 10cm center of the 30cm x 30cm sample area. An illustration and schematic of the system is shown below, in Figure 30.
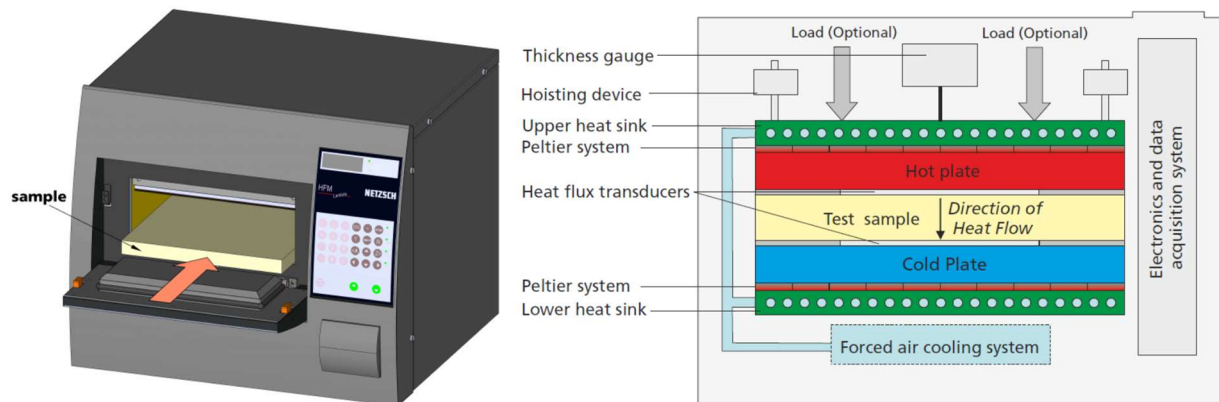
Figure 30: NETZSCH HFM 436/3/1 Lambda illustration and schematic (NETZSCH-Gerätebau GmbH, 2014)

Before starting testing, the machine was calibrated against a piece of insulation from the National Institute of Standards and Technology (NIST). This piece of insulation is made from one inch thick Standard Reference Material 1450d, Fibrous Glass Board, and has a calculated thermal conductivity of 0.031 W/(m·K) at 280K (Zarr & Leigh, Standard Reference Material 1450d, Fibrous Glass Board, for Thermal Insulation Measurements, 2014). The thermal conductivity of the sample increases linearly at an approximate rate of 0.0011 W/(m·K) per each 10 K increase in temperature, and the thermal conductivity does not have significant variance with bulk density values within the 115 to 122 kg/m³ range (Zarr, Harris, Roller, & Leigh, 2011). Periodic retesting of the calibration sample using the calibrated values has produced thermal conductivity values ranging from 0.0325 W/(m·K) at a mean temperature of 287 K to 0.0345 W/(m·K) at a mean temperature of 315 K, with a stated accuracy of ±5%. Based on NIST Special Publication 260-173, these values are about equal to the extrapolated values of 0.0317 W/(m·K) and 0.0348 W/(m·K) at the as-tested temperatures, without including the stated accuracy range. Figure 31, below, illustrates the as-tested values and the NIST Special Publication 260-173 values plotted as a function of temperature, and shows the close agreement between the two lines of best fit.
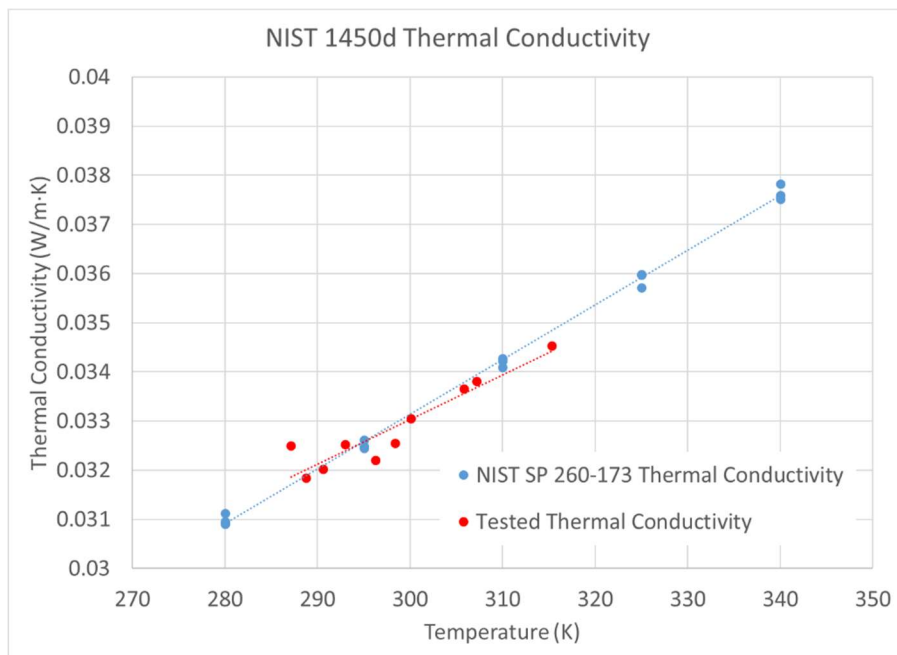
Figure 31: NIST 1450d Thermal Conductivity

To further ensure that the calibration sample remained constant throughout the duration of testing, the sample has been maintained with marginal thickness plastic wrap to maintain the as-tested humidity values within the sample. The sample has then been stored away from sources of physical damage. However, possible sources of the difference between the NIST values and the as-tested values may be related to the amount of physical samples (NIST utilized 450 testing panels where only 1 panel was tested with this work), or to the variance in the HFM machine itself. Nonetheless, the values are within the acceptability range given the instrument.

The team then used the calibrated HFM to compare against the published insulation properties of Owens Corning FOAMULAR Insulation. The HFM measured values ranging from 0.0296 W/(m·K) at 289 K to 0.0325 W/(m·K) at 315 K, compared to the 0.029 W/(m·K) published in the Owens Corning Technical Bulletin without reference to temperature (Owens Corning Foam Insulation, LLC., 2011). The 5% accuracy published by the instrument would allow values below an as-tested thermal conductivity of 0.0305 W/(m·K) to considered within acceptable ranges. This would include half of the as-tested values and suggest good agreement with the published values. Variations between the printed bulletin and the as-tested values may be due to sample bias, past storage and delivery methods, lack of bulletin specificity, and variations within the manufacturing process.

Figure 32 shows the experimental data compared to the published values. Note that the vertical axis is of a different scale than Figure 31.
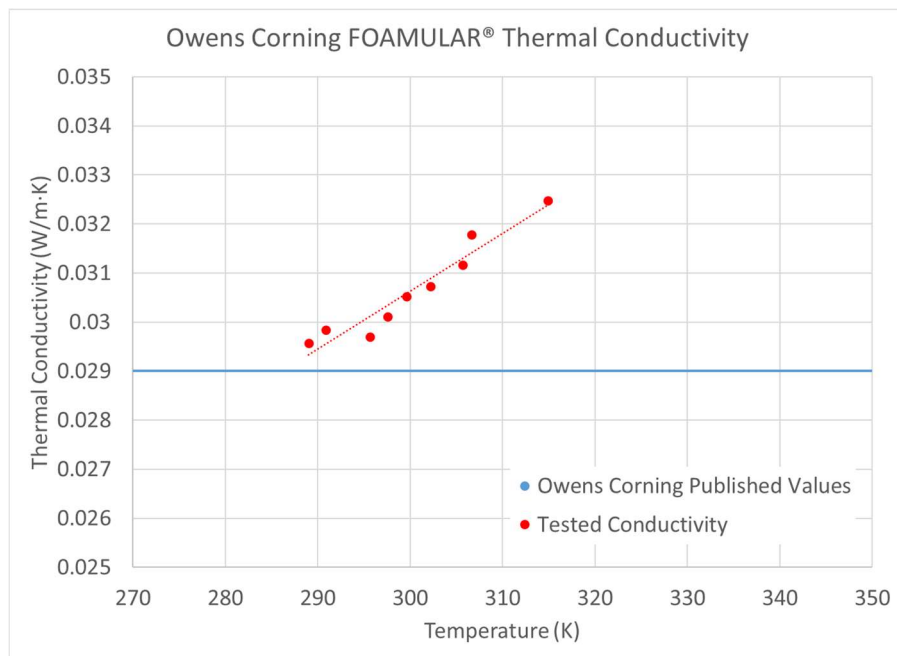
Figure 32: Owens Corning FOAMULAR® Thermal Conductivity

With validation complete, the team tested several Indian-sourced and Nepali-sourced for thermal conductivity. Of particular interest to application in Nepal, where building insulation is not included in the vernacular or modern architecture, were fiber mats and rug-like materials, where the team found 1.86 cm thick woven straw mats being used for mattresses and an occasional floor rug or runner. These mats, shown on the right of Figure 33, are woven by hand within the villages using dry straw and were not typically considered marketable.

Figure 33: Nepali-sourced straw mats during production (left), and 1' x 1' finished product (right)

Using the HFM, the straw mats had a tested conductivity an average thermal conductivity of 0.0556 W/(m·K), based on 10 samples. The thermal conductivity varied linearly with temperature, starting at 0.0532 W/(m·K) at 290 K to 0.0589 W/(m·K) at 312 K. This was tested when the heated plate was on top and the chilled plate on the bottom. Reversing the plates to have the heated plate on bottom and chilled plate on bottom resulted in a marginal increase in average thermal conductivity of 0.0012 W/(m·K).

This category of thermal conductivity ranges is approximately equal to that of Perlite board insulation (0.052 W/(m·K)), 100 to 600 mm thick Attic glass fiber insulation (0.052 to 0.055 W/(m·K)), or pulpboard (0.07 W/(m·K)) (The American Society of Heating, Refrigerating and Air-Conditioning Engineers, 2018). Drawing conclusions from these other values helps reinforce that the Nepali-sourced straw mats are good thermal insulators and that these types of materials would be prime candidates for local use as insulation materials. However, the dry porous straw also presents a fire, mold, and pest risk that must be taken into account if used in a building application.

One method of mitigating this risk is through the application of a plaster to the interior surface. This would help prevent a fire from igniting the insulation, and would also help prevent bugs from eating or making a home of the insulation. To test the implication of applying plaster to the surface of the straw mat, the straw mat was hung on a vertical surface such that the primary weave ran horizontally (90° rotation from Figure 33 right) and a 2:1 mixture of DAP® Plaster of Paris to room temperature tap water was mixed and applied by hand to the surface. It was smoothed via a masonry trowel, let to set

for 6 hours, and placed in a heated drying chamber at 30°C for 48 hours. Principally, part of this effort was to determine how easily the plaster adhered to the weave of the straw mat. Due to the coarse surface of the straw mat, the plaster adhered readily and did not roll or flake off.

The sample was then removed from the vertical surface and tested within the HFM machine. With the 0.46 cm thick plaster, the sample thickness had increased 0.46 cm and the thermal conductivity of the material had increased to an average value of 0.1141 W/(m·K) at 303 K, based on nine tests ranging from 0.0705 W/(m·K) at 291 K to 0.1345 W/(m·K) at 315 K. Perhaps more importantly, the overall R-value, a measure of how well a material assembly resists thermal conduction, decreased from an average value of 0.3364 (m²·K)/W of the straw mat alone, to 0.2113 (m²·K)/W with the plaster. This decrease in R-value, and increase in conductivity, can be attributed to the loss of contact resistance between the upper (warm) plate within the HFM and the straw mat sample. While discouraging at first, this change is encouraging in that it highlights that the method of affixing the straw mat is a pivotal part of the insulation process. Additional layering of the straw mats, perhaps with a cross-grain approach to each other, may help to improve the overall thermal R-value and is worthy of additional research. Further, while the HFM can only test the thermal conductivity of the sample between two opposing plates on parallel planes, more work will be needed to assess the in-situ performance when the grain of the straw mat is aligned with or transverse to airflow patterns.

In addition to the Nepal-sourced straw mat, the team sourced a coconut fiber mattress from India. While not easily available in Bhuj, these mattresses are importable from neighboring cities. Within these mats, the coconut fibers are pressed in a 2 cm thick mat, cut to size, and shipped to market. Additionally, the exterior appears to be sealed via adhesive, steam, or heat, as it exhibits some short-term beading to water droplets. Within a building environment, these mats can be used to seal walls and can be placed above a false or drop ceiling to provide resistance to heat transfer. The team tested a sample of this material via the HFM to determine an average thermal conductivity of 0.0472 W/(m·K) at 298K, on par with low-density (8 kg/m³) glass fiber batt insulation (The American Society of Heating, Refrigerating and Air-Conditioning Engineers, 2018). The thermal conductivity of the sample increased linearly at a rate of 0.003 W/(m·K) per 10 degree K rise, and is valid across the tested range of 289 K to 312 K.

Figure 34: Coconut Fiber Mattress

Compared to the straw mats, the coconut fiber mattresses are assumed to be even more susceptible to flaring up during a fire due to the thin fibers and loose construction. The team was concerned about the flammability of the mat beforehand and tested the assumption by taking a match to a small sample. Figure 35 shows selected frames of the combustion process, where the fibers flash into combustion within seconds of receiving a small flame. While the small test is not a perfect parallel for placement within a home, the team does not believe that the coconut fiber mattress material is a safe insulation material without additional fire prevention measures.

Figure 35: Selected Frames from Coconut Fiber Mattress Ignition; left to right: 0 sec., 2 sec., 4 sec., 9 sec., 18 sec.

Additionally, the natural fibers would provide potential housing for pests, leaving a surface covering and additional pest-control measures vital for use of this material in a structure. To help alleviate these issues, the team applied a 0.36 cm thick plaster coat to the surface of the coconut fiber mattress, dried the sample in the same manner as the straw mat, and retested the thermal conductivity of the entire sample. The thermal conductivity increased from 0.0472 W/(m·K)to 0.0616 W/(m·K), and the thermal resistivity decreased from 0.4117 (m²·K)/W to 0.3822 (m²·K)/W. Since the surface of the coconut fiber mat was planar prior to the plaster addition, the deterioration of the contact resistance had less of an impact. Overall, the addition of the plaster did not substantially change the resistivity of the material.

62

The team also sourced an Indian-made basket weave Jute rug from a U.S. vendor, and cut the sample to size to test the thermal conductivity. The Jute rug was also observed within a handful of the homes in Bhuj, and the U.S. sourced version was measured within the HFM to have an average thermal conductivity of 0.0734 W/(m·K) at 0.003 W/(m·K) per 10 degree K rise, and is valid across the 289 K to 313 K temperatures tested. An image of the Indian-made basket weave Jute rug is shown below with a one foot ruler for scale (Figure 36). Subsequently, 0.24 cm thick plaster was applied to the same sample, set to dry in the same manner as the other samples, and tested within the HFM. The thermal conductivity of the jute rug increased from 0.0734 W/(m·K) to 0.1380 W/(m·K), where the thermal resistivity decreased from 0.2546 (m²·K)/W to 0.1536 (m²·K)/W.

Similar to the straw mat, the basket weave jute rug also suffered from the deterioration of the contact resistance for the same reasons. Moving forward, fire, pest, and potential moisture issues are synonymous with all of natural fiber materials, including the Jute rug below.

Figure 36: U.S. sourced Indian made Jute basket weave rug with one foot ruler for scale

The thermal conductivity and resistivity values are summarized in the tables below.

Material (Origin)	Thermal Conductivity, without plaster	Thermal Conductivity, with plaster
Straw Mat (Nepal)	0.0556 W/(m·K)	0.1141 W/(m·K)
Coconut Fiber Mattress (India)	0.0472 W/(m·K)	0.0616 W/(m·K)
Jute Rug (India)	0.0734 W/(m·K)	0.1380 W/(m·K)

Table 11: Natural Fiber Materials Summary

Material (Origin)	Thermal Resistivity, without plaster	Thermal Resistivity, with plaster	Thickness	
			Material	Plaster
Straw Mat (Nepal)	0.3364 (m²·K)/W	0.2113 (m²·K)/W	1.866 cm	0.462 cm
Coconut Fiber Mattress (India)	0.4117 (m²·K)/W	0.3822 (m²·K)/W	1.988 cm	0.359 cm
Jute Rug (India)	0.2546 (m²·K)/W	0.1536 (m²·K)/W	1.868 cm	0.244 cm

Table 12: Natural Fiber Materials Summary

Wrapping up the natural fibers, the team had tested samples of the building supplies used in the small-scale testing chambers at MIT. In particular, the team tested the values of the 4" aerated concrete blocks that make up the base of the chamber, and the traditional concrete bricks that made up the walls of the test chambers. For both the thermal conductivity tests and the thermal chambers, the team used samples from within a single pallet each, reducing the chance of variations in concrete mixtures imposing variability on the results.

A cut sample of the aerated concrete blocks was weighed and measured to have a density of 589 kg/m³, which was then measured as having an average thermal conductivity of 0.2209 W/(m·K), based on five samples. The results had a marginal slope and can be considered to have a near constant thermal conductivity across the tested range of 292 K to 315 K.

A randomly selected and air-dried sample from the pallet of concrete bricks was also weighed and measured to have a density of 2,081 kg/m³, and then measured to have an average thermal conductivity of 0.9155 W/(m·K), based on 10 samples. Similar to the aerated concrete, the results had a marginal slope and can be considered to have a near constant thermal conductivity across the tested range of 293 K to 315 K. Images of both the aerated concrete block and concrete brick are shown below, in Figure 37.
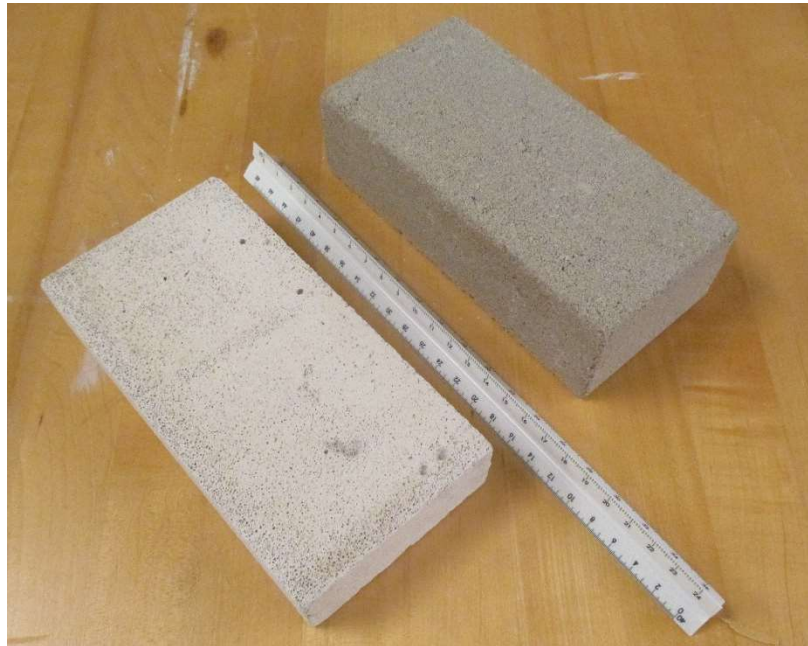
Figure 37: Concrete Samples; Aerated Concrete on Left, Standard Mixed Concrete on Right. One foot ruler for scale.

The two thermal conductivity values are summarized in the table below.

Material (Density [kg/m³])	Thermal Conductivity
Aerated Concrete Block (589)	0.2209 W/(m·K)
Concrete Brick (2,081)	0.9155 W/(m·K)

Table 13: Concrete Materials Summary

In measuring the concrete samples, and more aligned with another student's research to produce concrete panels, the team was confronted with surface irregularities in the concrete samples. To remove these irregularities, the team attempted to create a thermally conductive high viscosity gel using easily available and lower cost materials. The rationale behind this approach was an effort to make a conductive bridge between the testing plates and the sample, while using a marginal thickness material. The viscosity of the material would allow the surface irregularities of the concrete sample to be absorbed by the viscous gel, and excess viscous gel would be pushed outside of the sample area, but would be contained within a plastic sleeve to maintain cleanliness within the machine.

The first attempt was made using un-scented Vaseline® (Petroleum) Jelly. To test the material beforehand, a large quantity of the sample was placed in a plastic sleeve and placed in the HFM. With an initial height of nearly 2 cm, the HFM was used to compress the Vaseline® sample into a 0.502 cm thick plane, roughly 9" x 9". The initial testing proceeded as planned, producing an average thermal conductivity of 0.1265 W/(m·K) across mean temperature ranges of 292 K to 295 K. However, when the upper plate surpassed the 304.4 K (31.3° C), the viscosity of the sample decreased and the sample lost contact with the upper plate, preventing convergence of the remaining data points. While not expected, the Petroleum Jelly melted at some point above 31.3° C and below 34° C, the next set point. Beforehand, the team had expected the Vaseline® sample to melt at some point between 36 and 60° C, closer to human body temperature (International Programme on Chemical Safety, 2002).

Discovering that the pure Vaseline® sample was more insulative than anticipated, the team added General's Powdered Graphite to the Vaseline®, mixing until the solution appeared to be saturated and the graphite did not appear to become easily wetted by the petroleum jelly. These efforts were successful in achieving a modest increase in the thermal conductivity. The mixture rose to an average thermal conductivity of 0.1364 W/(m·K), an 8% increase over the pure petroleum jelly. Similar to the pure petroleum jelly, the graphite mixture began to exhibit decreased viscosity near 32° C, and testing did not continue at higher temperatures.

The team then switched to White Lithium Grease following the same rationale that led to the selection of the petroleum jelly. The team used Lucas® Oil Products White Lithium Grease with better success, measuring thermal conductivities across a 0.475 cm sample thickness. Using the HFM, the team tested the thermal conductivity of the sample at an average thermal conductivity of 0.1214 W/(m·K) between 292K and 304K. The lithium grease sample also had an average increase in thermal conductivity of 0.002 W/(m·K) per 10 K increase in temperature across the tested temperature range. No gross changes in viscosity were observed to hamper the testing.

The lithium grease had a conductivity about equal to the pure petroleum jelly, which is a good basis to improve upon. The team chose to use the lithium grease and a reconfigured thermocouple arrangement for the few selected samples, and shelved the work after the readings were obtained. In the long term though, the White Lithium Grease began to separate, with the fluid separation from the bulk grease product suspension. According to an inquiry into the manufacturer, this is a normal process that occurs with older products. The shelf life of the product is 1½ to 2 years, and the grease was placed

in the plastic sleeve and used for testing roughly one year after the date of manufacture. Separation was first noticed six months after it the grease had been placed in the plastic sleeve, or 1½ years after manufacture (Lucas Oil Products, Inc., 2018).

While Sander, et al. contribute to this discussion by noting that there "is no consensus…on what is a desirable characteristic for fluid separation" (Sander & McDaniel, 2007), the team will continue to test other greases and substances for further use as a long-term substance to fill surface irregularities.

The three thermal conductivity values are summarized in the table below.

Material	Thermal Conductivity
Vaseline / Petroleum Jelly	0.1265 W/(m·K)
Vaseline / Petroleum Jelly mixed with Graphite	0.1364 W/(m·K)
Lithium Grease	0.1214 W/(m·K)

Table 14: Thermal Interface Summary

The team also worked to experimentally determine the equivalent change in thermal conductivity resulting from the placement of an alternating radiant barrier system, as mentioned in the Nelson thesis. The core of the concept is based on an offset radiant barrier being placed under the ceiling during the day, helping to prevent thermal radiation from the hot roof from reaching the interior of the structure and making the occupants uncomfortable. During the night, the radiant barrier is moved out of the way to allow the interior of the structure to be radiatively exposed to the cool roof, and then to cool the interior of the structure. The figure below, reproduced from the Nelson thesis, illustrates the concept as applied to a structure.
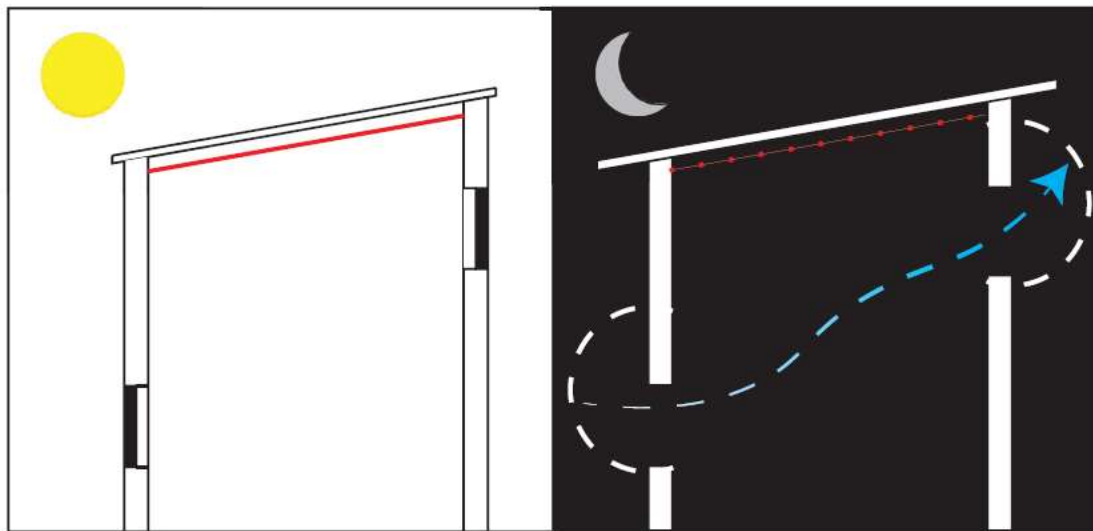
CGI Roof Alternating Radiant Barrier

Figure 38: Alternating Radiant Barrier concept, reproduced from Nelson

To test this system on a small scale, the team built a set of louvers within a fame that would fill the horizontal space within the HFM. All of the timber elements were made from ¼" x 1½" straight grain poplar. These louvers were then covered with Nashua Tape Multi-Purpose HVAC Foil Tape to become the radiant barrier. The finished, as-tested sample is shown below, in Figure 39.
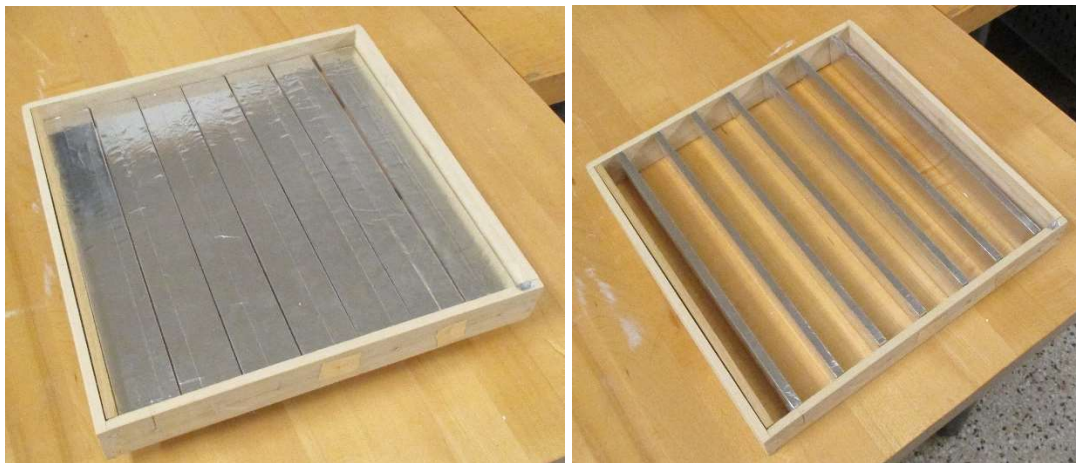
Figure 39: Alternating Radiant Barrier Test Sample, Left: Closed during Day, Right: Open at Night

To determine the heat transfer during both day and night, the team alternated which plate would be the warmer plate. During the day, it would be expected that the upper plate would be warmer than the lower plate, and during the day, the reverse would be expected. While intended to operate such that the louvers would be closed during the day and open at night, the team tested both operation methods to be aware of the impact of the system in opposite situations, such as colder climates or forgotten switching. In total, this produced a set of five tests for each setup. Within the HFM, both plates are a dull black color, where a black-body thermal radiation approximation would be appropriate given the absence of contradictory information. Convection was not inhibited by the setup, and so must be factored in when applying the concept to practice. For all test, the convection coefficient will vary with a larger test setup and without a boundary condition from the lower plate.

With the louvers closed, and the upper plate warmer than the lower plate (day orientation), the average thermal conductivity was 0.0436 W/(m·K) across five samples, ranging from 292 K to 309 K, and with a slope of 0.003 W/(m·K) per 10 K rise in temperature.

With the louvers closed, and the upper plate cooler than the lower plate (night orientation), the average thermal conductivity was 0.0604 W/(m·K) across five samples, ranging from 294 K to 309 K, and with a negligible slope across the tested temperature range.

With the louvers open, and the upper plate warmer than the lower plate (day orientation), the average thermal conductivity was 0.3556 W/(m·K) across five samples, ranging from 294 K to 308 K, and with no clear slope across the tested temperature range.

With the louvers closed, and the upper plate cooler than the lower plate (night orientation), the average thermal conductivity was 0.4116 W/(m·K) across five samples, ranging from 294 K to 309 K, and with a slope of 0.016 W/(m·K) per 10 K rise in temperature.

The table below summarizes the above thermal conductivity values by the louver position and plate temperature relationship.

Upper Plate / Louvers	Warmer	Cooler
Closed	0.0436 W/(m·K)	0.0604 W/(m·K)
Open	0.3556 W/(m·K)	0.4116 W/(m·K)

Table 15: Alternating Radiant Barrier Summary

As Table 15 helps show, the closed louver state inhibits the heat transfer by an order of magnitude as compared to the open louver state. When the upper plate is warmer, convective flows should be reduced, thereby making the value more indicative of the changes in radiation heat transfer only. When the upper plate is cooler, convection will play a larger role, as witnessed by the larger thermal conductivity values. Even in the closed state, the internal convective flows increase the heat transfer.

These results are encouraging for three reasons. First, the thermal conductivity test helps to validate that this approach is a plausible metric for having a selective insulation system, which would allow more control over heat flows throughout the year. This is particularly important when homeowners in warm climates may be below their thermal comfort, and wish to maintain some heat within the structure. Second, the test indicates that even if the alternating system failed to switch between the open and closed states, there is still a direction bias in the heat transfer. However, the system still remains biased towards an insulating surface. Third, related to the first reason, the system can also be deployed in colder climates, where heat would want to be retained during the night, and welcomed throughout the day. In a colder climate, the louver schedule would flip from the Figure 38 direction.

Conclusion

While this chapter largely presents data from smaller scale testing, the individual contributions of the various components is directly applicable to larger issues. Beginning with the scale testing, the contribution of various surface coatings, materials, solar position, and ventilation were discussed en route to scale testing in Bhuj. The scale testing performed at MIT helps illustrate that there are simple passive elements within building construction that can drastically reduce interior peak air temperatures from a bare structure. Using materials that have low absorptivity values, e.g. white paint, and insulating surfaces to prevent heat intrusion from the facades exposed to large amounts of heat can reduce the peak temperature by up to 6.4 °C. Additional means, such as additional exterior insulation on the east and west façades, can help reduce the peak air temperature by another 2.0 °C, resulting in a total of 8.4 °C decreased peak interior air temperature from the bare structures.

Further, the testing demonstrated that some applications of conventional heat avoidance strategies may have detrimental impacts if not properly implemented. In the case of the always present solar shade, the solar shade restricted passive cooling during the night, and thereby helped to increase the peak temperature during the day. Likewise, some materials that show great promise as thermal insulators can pose significant risks to the occupants in other ways. A crucial example of this is the flammability test of the coconut fiber.

Bhuj Test Chamber Experiments

Purpose and Construction

Beginning in November 2014, Madeline Gradillas built and instrumented five test chambers in Bhuj, India on a small farm referred to as Paraspar. These chambers were designed "to validate, prove, or disprove design decisions" through full-size prototypes, and to advance "the understanding of local construction materials and techniques" through implementation. These test chambers measure 2.4 m wide by 2.4 m deep by approximately 2.4 m high, and the walls are constructed of locally-quarried 23 cm thick sandstone blocks. Each chamber is oriented to the four cardinal directions, having one 0.75 m wide by 0.5 m high screened opening on the north and south facing walls. Each opening has an outer-hinged solid panel that can be manually operated. These openings are offset vertically by 1.5 m to enhance buoyancy-driven ventilation when possible (Gradillas, 2015).

Within the site, the chambers are spaced sufficiently far apart that neighboring shadows will not reach another chamber. While not present in the 2015 Gradillas thesis, a border security wall was built during the period of this thesis which neighbors chambers 1 and 2, and can be seen in Figure 40 below.

Figure 40: Paraspar Site Plan, image courtesy of Google Earth

As part of work from Gradillas (2015) and Nelson (2017), chambers 1, 2, and 5 began with a nearly-horizontal single pitch corrugated metal roofing, and chambers 3 and 4 had a horizontal 4" concrete slab roof. Chambers 3 and 5 are shown below, viewing from the northwest and southwest corner, respectively.

Figure 41: Test chambers 3 (left) and 5 (right), in Paraspar, Bhuj, India

This chapter contains the results of both experimental and, where applicable, simulated results for test chambers located in Bhuj, India. The simulated results are supplied to help validate the experimental results and extrapolate the impacts to the entire year. The team used EnergyPlus[7] via the Archsim[8] plugin for Rhinoceros[9]/Grasshopper[10] to model the chambers using the Indian Society of Heating Refrigerating & Air-conditioning Engineers (ISHRAE) energy plus weather (*.epw) file[11] for Bhuj-Rudramata, India, a location 5 km from the test chambers. The straw insulation mentioned in the chapter's text was modeled with conductivity 0.07 W/m·K (The American Society of Heating, Refrigerating and Air-Conditioning Engineers, 2018).

To establish the simulation, the team built up the geometry using known values from the building plans and field measurements, as well as physical properties from textbooks (Incropera, Dewitt, Bergman, & Lavine, 2011) and ASHRAE (The American Society of Heating, Refrigerating and Air-Conditioning Engineers, 2018). Additional values are modified to match tested values from field measurements, and the application of these values are mentioned where applicable.

---

[7] Version 8.4.0
[8] As part of DIVA 4 from Solemma.
[9] Version 5 SR14 64-bit, v5.14.522.8390 05/22/2017, Robert McNeel and Associates
[10] Version August-27,2014, Build 0.9.0076, Robert McNeel and Associates
[11] Retrieved from White Box Technologies, 28 March 2018, ISHRAE WMO#426340. Lat 23.250, Long 69.667, Elev 80

Based on the past research by Gradillas and Nelson, the team understood that nighttime ventilation of the chambers would be necessary to improve comfort during the heat of the day. Nelson quotes Santamouris and Kolokotsa by stating that night ventilation may help the Bhuj structures by reducing peak indoor temperatures by up to 3 °C (Santamouris & Kolokosta, 2013). However, much of these claimed improvements rely on heat avoidance strategies already being put in place. Lechner, in Heating, Cooling, Lighting, illustrates the importance of these principles by defining avoidance as the first tier towards achieving thermal comfort. Incorporating this within basic building design, Lechner defines heat avoidance as "the appropriate use of shading, orientation, color, vegetation, insulation, daylight, and the control of internal heat sources." (Lechner, 2001) One of the most common techniques of heat avoidance is through reducing the solar absorptivity of the surface, or painting the outside surfaces white.

In Bhuj, many of the homeowners are already moving towards this strategy for their walls. Using a lime-based whitewash, they are applying the lime to the walls and achieving significant benefits. As Nelson's 2017 thesis shows on page 115 for a nearby home, the application of two layers of lime-wash on the south facing façade was able to reduce the interior wall temperature by roughly 2 °C as compared to gray paint. The test chambers, however, were either fully insulated on the walls, or fully exposed with the bare sandstone, suggesting that a better comparison could be made.

To help with the direct comparisons, in October of 2017, the Hunnarshala team applied white paint to the walls of Chamber 1, as shown in Figure 42. The structure of the walls are composed of 23 cm thick locally quarried sandstone and the interior left the sandstone block exposed. Within Chamber 1, the roof was made of a single layer of corrugated galvanized iron sheeting. No significant ventilation was possible through the structure, as there were no substantial gaps in the façade or roof, and the window shutters remained closed for the duration of the testing.

Figure 42: Chamber 1 before (left) and after being painted (right). Photos courtesy of Pradip Rangani, Hunnarshala.

During these tests, the team installed three meters, gathering four sampling points. The team placed all of the sensors along the middle line of the chamber, using one Onset UX90-003 at a height of 0.5 m, one Onset UX90-003 at 1.75m and one Onset U23-002 2x External Temperature logger measuring both the temperature of the tin sheet, and the surface temperature of the dirt floor. These points were then compared with a solar radiation shielded (Onset RS3-B) temperature and humidity meter (Onset U23-002), installed at a height of 2m and located 5m away from the chamber and any shading object. All readings were taken at 15 minute synchronized intervals.

Test 1: Baseline

The first week served as a self-calibration period to gain an understanding of how the structure performed thermally. The structure represents the basic economy housing that would be built in the region and these values would be a baseline against which the team could compare suggested improvements. The resulting average day temperatures are displayed numerically (Table 16) and graphically (Figure 43) below. Conditional formatting has been applied to the maximum and minimum values to highlight the warmest (red) and coldest (blue) periods.

Test 1: 10/4/2017 – 10/10/2017		Outside Air Temperature	Ground	Air 0.5 m	Air 1.75 m	Ceiling
Tin Sheet, Bare Structure	Max [°C]	39.23	33.49	34.90	35.96	50.52
	Min [°C]	23.04	29.32	28.75	28.52	23.44
	Peak Hour	14.5	19.5	18	17.5	14

Table 16: Chamber 1 Test 1 setup and results

74
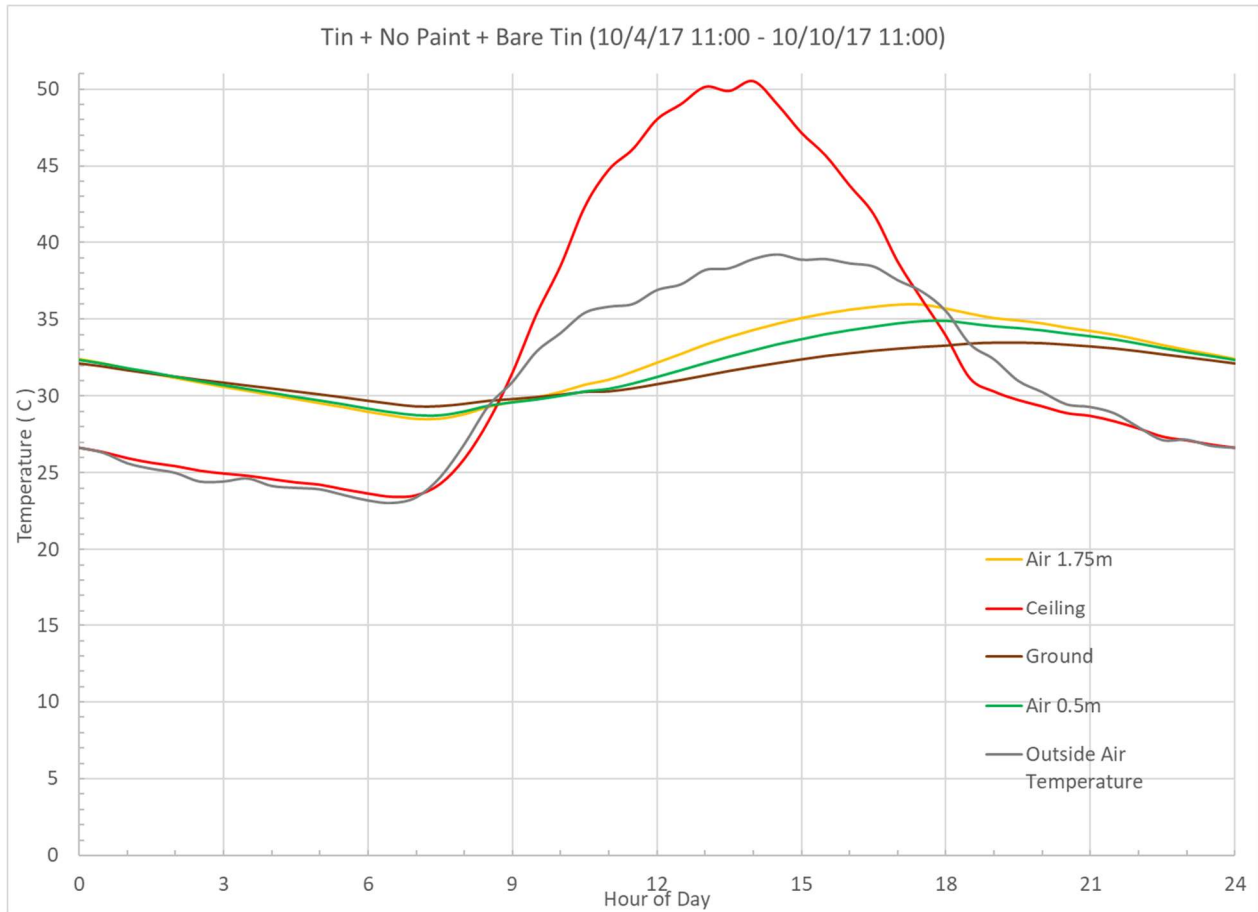
Figure 43: Chamber 1 Test 1 Average Day Plot

In Figure 43, the coloring of the lines is akin to an American traffic light, where the uppermost point (the ceiling) is colored red, and the lower (air temperatures) are amber and green. The ground is brown and the outside air temperature grey. Based on the collected data from October, the tin sheet reaches 11°C warmer than the ambient temperature during the heat of the day, and becomes about the ambient temperature at night. This data verifies Nelson's claim that the single layer tin sheet can easily reach 50°C (Nelson, 2017). Further, during the hottest months (March-May), this difference is likely to increase.

With the windows closed 24/7, the structure provides shelter from the midday heat largely through the thermal mass, but that same thermal mass keeps the structure 5°C warmer through the night. Typically, the use of night ventilation will help with keeping the internal temperature lower, but was not employed in this chamber.

The second test for Chamber 1 was designed to evaluate the influence of a white exterior paint, or a thorough lime-wash coating, on the thermal response of the building. The changes in surface coatings are visible in Figure 42, and the results are shown in Table 17 and Figure 44, below.

Test 2: 10/10/2017 – 10/22/2017		Outside Air Temperature	Ground	Air 0.5 m	Air 1.75 m	Ceiling
Tin Sheet, White Painted Walls, Bare Tin	Max [°C]	39.50	31.18	32.08	32.67	48.29
	Min [°C]	21.77	27.57	26.85	26.59	21.69
	Peak Hour	14.5	19	18	18	13

Table 17: Chamber 1 Test 2 setup and results
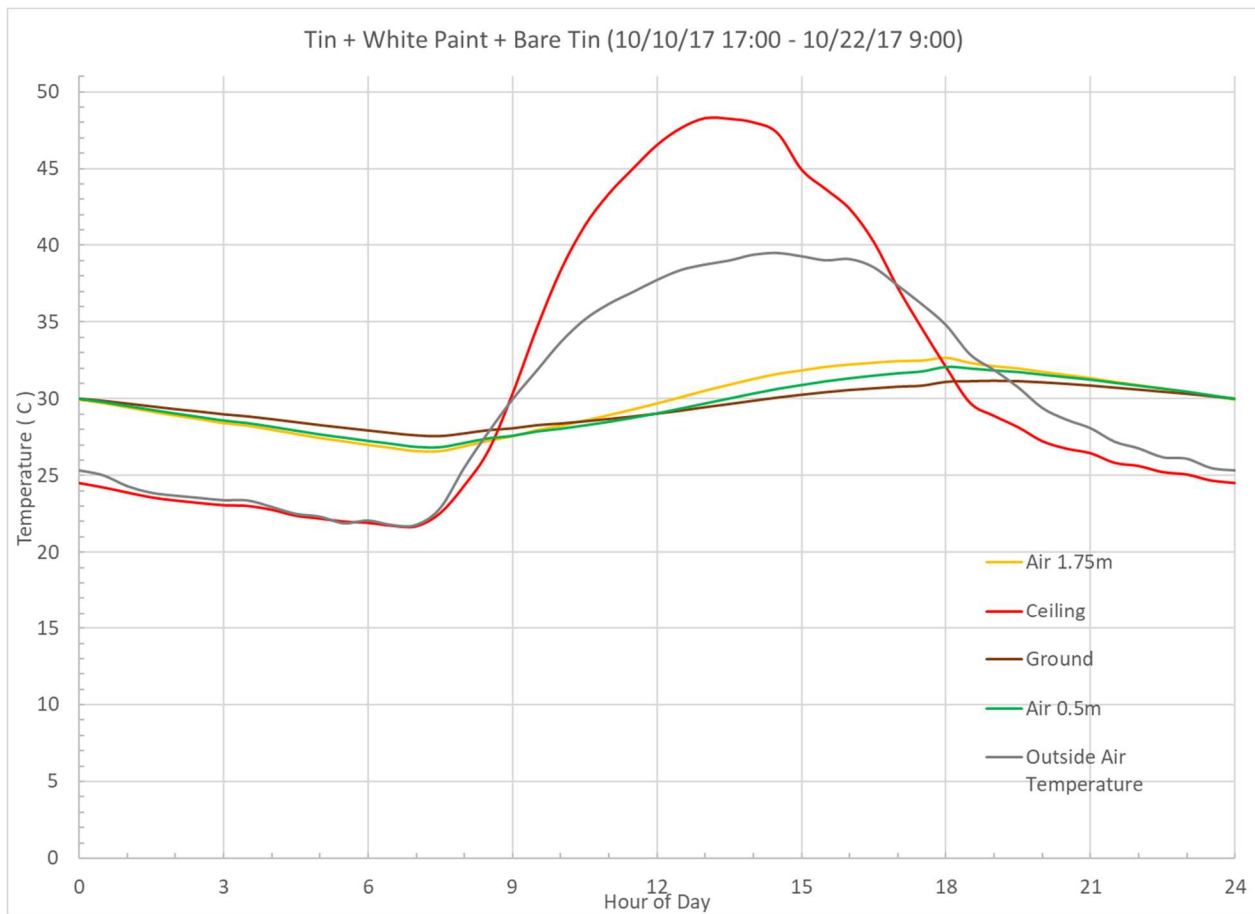
Figure 44: Chamber 1 Test 2 Average Day Plot

From the testing, the team observed that the maximum air temperatures for all values decreased when compared to the outside air temperatures. The maximum temperatures typically decreased by 2 to 2.5 °C, and the minimum temperatures decreased by about 1 °C when accounting for a difference in the daily low temperatures. While the peak temperatures did move closer to the peak temperature of the day, the ceiling temperature was cooler throughout the day, reducing the implied radiant temperature as well. Further, the spread of temperatures within the structure throughout the

day remains tighter with the white walls than without. As mentioned in Nelson's 2017 thesis, this spread is important as air movement within the structure has the potential to exacerbate moving heat from the ceiling into the air volume (Nelson, 2017).

Test 3: Aluminized undercoating on tin roof

The third test for Chamber 1 retested some of the work in the Nelson thesis, with an intent to experimentally apply Nelson's simulation and validate the conclusions. In this test, a radiant barrier (household aluminum foil) was glued to the bottom of the corrugated sheet, and the rest of the structure remained the same as Test 2.

Test 3: 10/23/2017 – 10/29/2017		Outside Air Temperature	Ground	Air 0.5 m	Air 1.75 m	Ceiling
Tin Sheet, White Painted Walls, Aluminized Tin	Max [°C]	37.28	29.43	30.29	30.76	45.61
	Min [°C]	20.35	26.89	25.73	25.43	21.65
	Peak Hour	14	19.5	18	18	13.5

Table 18: Chamber 1 Test 3 setup and results

Compared to Test 2, the adition of the interior aluminized coating on the interior of the Test 3 roof shows a modest reduction in peak ceiling temperature when compared to the peak outside air temperature. During the night the addition of the aluminized coating keeps the minimum temperature about equal to Test 2, despite Test 3 having cooler outside temperatures than Test 2.
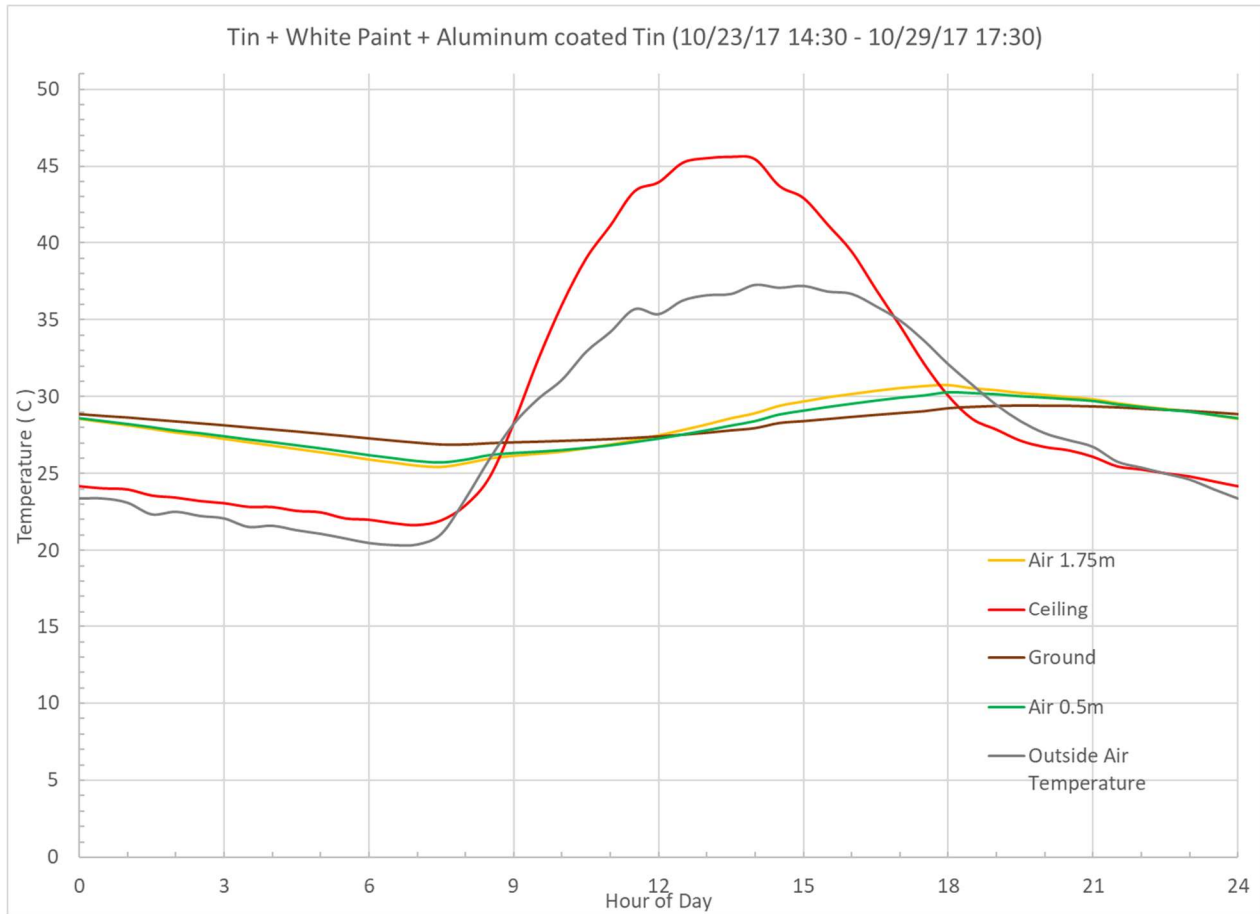
Figure 45: Chamber 1 Test 3 Average Day Plot

The results alone do not support any major change in air temperatures throughout the day, but imply that the air temperature will be modestly warmer at night with the aluminized coating in place. Diving into the potential drivers of this behavior more, the thickness of the added aluminum layer is marginal and the overall macroscopic form has not changed, suggesting that there are no major changes in the driving conditions of conduction or convection. This then leaves radiation as the modified heat transfer mechanism.

Within Nelson's 2017 thesis, Nelson concluded that 'a radiant barrier should be placed on the ceiling exposed to the room interior', and that this modification could help reduce the operative temperature by 4°C (Nelson, 2017). However, the experimental data does not unilaterally confirm this hypothesis. Looking into this further, the team used Energy Plus along with an RCC roof structure to compare the impacts of aluminizing the interior surface. While not a direct parallel to the corrugated roofing, Energy Plus was better able to simulate structures with thicker RCC roofing than thinner corrugated sheets.

In this simulation setup, the only variation between the two simulations was the thermal absorptivity values for the interior of the RCC slab. The baseline structure, with the concrete exposed, was simulated with a thermal emittance of 0.9, and the aluminized interior structure was simulated with

a thermal emittance of 0.071, matching the experimental values produced in Local Experiments. Both surfaces were applied as constants, unchanging with time. The structure walls remained as 23 cm thick sandstone blocks without any surface treatment or coverings. There were no internal gains, and the structures were ventilated with 6 air changes an hour from 7 PM to 7 AM. The ISHRAE Bhuj weather file was used to compute hourly building performance for the duration of a year.

To analyze the data, each month was analyzed individually in terms of an average day. Using this monthly approach allowed the team to look at the implication of the yearly weather and solar patterns on the thermal performance of the building. Matching the Nelson approach, air and operative temperature were used as the principal metrics for comparison. The months of April, June, and December are shown below as a function of the hour of the day, and were chosen to be representative of the summer non-monsoon season, the summer monsoon season, and the winter season.

The comparative results for the simulation are shown below, in Table 19, where a positive number is highlighted in red and is a condition where the aluminized surface is warmer than the non-aluminized surface, and blue represents a condition where the aluminized surface is cooler than the non-aluminized surface. All temperature values are in degrees Celsius.

[°C]	April		June		December	
Hour	Air Temp.	Operative Temp.	Air Temp.	Operative Temp.	Air Temp.	Operative Temp.
0	0.07	0.44	0.04	0.31	0.08	0.59
1	0.06	0.46	0.04	0.34	0.08	0.61
2	0.05	0.47	0.03	0.35	0.07	0.62
3	0.04	0.48	0.02	0.35	0.07	0.62
4	0.03	0.49	0.01	0.35	0.06	0.63
5	0.02	0.49	0.01	0.34	0.05	0.63
6	0.02	0.49	0.01	0.34	0.04	0.63
7	-0.10	0.43	-0.06	0.30	0.03	0.62
8	-0.12	0.41	-0.07	0.28	-0.14	0.54
9	-0.12	0.39	-0.07	0.26	-0.17	0.51
10	-0.12	0.33	-0.07	0.21	-0.18	0.47
11	-0.14	0.24	-0.07	0.15	-0.19	0.41
12	-0.06	0.19	0.00	0.11	-0.18	0.34
13	0.07	0.14	0.08	0.07	-0.06	0.31
14	0.13	0.07	0.08	-0.01	0.03	0.28
15	0.11	-0.02	0.06	-0.08	0.08	0.24
16	0.09	-0.07	0.05	-0.12	0.10	0.22
17	0.08	-0.07	0.04	-0.12	0.08	0.23
18	0.06	-0.02	0.03	-0.08	0.05	0.26
19	0.06	0.07	0.03	0.00	0.07	0.35
20	0.07	0.18	0.04	0.10	0.08	0.43
21	0.08	0.28	0.05	0.18	0.09	0.49
22	0.09	0.36	0.05	0.24	0.10	0.54
23	0.08	0.40	0.05	0.28	0.09	0.57
24	0.07	0.44	0.04	0.31	0.08	0.59

Table 19: Simulated Improvement from Aluminized Interior Ceiling

The conclusions drawn from the simulation data are similar to those drawn from the experimental results. The addition of the aluminized ceiling interior produces no significant changes in interior air temperature. When matching the simulated December to the test results from late October, the addition of the aluminized ceiling interior produce slightly warmer nighttime temperatures. While not drawn from the experimental results directly, it also produces modestly cooler temperatures in the morning and early afternoon. Critically, the operative temperatures determined from the simulation are warmer in the wintertime, presumably as the exposure of the roof to the solar gains are less intense due to the lower elevation of the sun. In the summer, this increase is reduced, but still present during the late evening and early morning hours. However, operative temperatures are lower by 0.1 °C during the hours of the day when the outdoor heat is at its highest, agreeing with the direction of the influence suggested by Nelson.

At this time, it should be noted that the operative values rendered by the simulation are indicative of an unoccupied chamber. When the chamber is occupied, the presence of the aluminized ceiling will absorb less and reflect more thermal radiation from the occupant, making the occupant feel warmer. For a single person, these impacts are on the order of 1 to 2% of the radiative exposed surface area, and the direction of this impact can be desirable during the winter, but non-desirable when entertaining with many people present.

Relating this back to the Nelson conclusion, the conclusion as stated pertains to the use of double layer roofing or an air gap, also known as roofing with Above-Sheathing Ventilation, and not the corrugated sheet or RCC slab roofing tested and modeled above. The Nelson conclusion is refined more in Chamber 2, where the placement of the aluminized coating is varied to determine thermal implications with a goal of potential productization.

In October of 2017, Chamber 2, formerly with a tin sheet roof, was refitted with the same double roof system that was installed in the Ramdev Nagar homes and detailed in Nelson's thesis. Also referred to as above-sheathing ventilation, the double roof system is comprised of an inner layer made of mud rolls, and an outer layer made up of Mangalore tile. The mud rolls are made by taking mud-covered coarse fabric and rolling it around a wooden centerpiece. The result is a product for the interior layer which has both insulation and thermal mass. Both Nelson and Gradillas describe the process in greater detail, as well as define the tested conductivity of the finished product at 0.117 W/m·K.

The Mangalore tiles are a form of vertically and horizontally interlocking tiles that are also referred to as French or Marseille tiles in different global regions with slight differences, although all have a similar form.
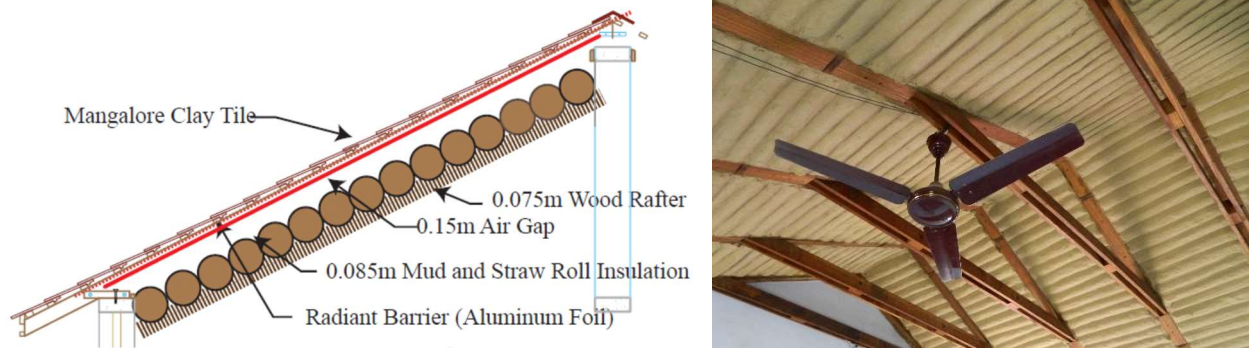
Figure 46: Left: Mangalore Tile double layer roof (illustration from Nelson), Right: view of finished mud rolls from interior

During a visit to Bhuj, the team noticed that there was daylight visible where the tiles overlapped, as shown on the left side of Figure 47. Currently, the roof system has an aluminum foil radiant barrier glued to cardboard and placed in the air cavity between the two layers. The right side of Figure 47 illustrates this application of the aluminum foil to the cardboard within the roofing system, as viewed from the eave looking into the cavity.

Figure 47: Left: Overlap of Mangalore tiles showing unfilled space (credit Vadim Kuklov), Right: Radiant barrier as applied in Ramdev Nagar homes, January 2017

In the current configuration, the team believed that the radiant barrier inhibits the flow of air through the air cavity by removing the potential for two-directional flow through the cavity and air flow through the outer layer. The team thought that the spacing could be put to use to increase the ventilation through the air cavity by relocating the radiant barrier to the underside of the tiles directly, whereby the spacing would be preserved and the cardboard would be removed. While the roof has been in place in a home for greater than a year, the test chamber was reconfigured with a Mangalore tile roof with 28° pitch, to match the homes and test the placement of the radiative barrier. Figure 48 below shows the radiative barrier placed directly on the tile (left), and applied to an intermediate cardboard layer (right).

Figure 48: Directly applied radiant barrier (left) and radiant barrier applied to cardboard (right)

Since the team only used one chamber to conduct this test. The chamber walls were painted white to reduce the influence of sun on the walls and crossflow between the two sides of the roof system was reduced by placing a rafter between the two sides and cementing the roof to the rafter, effectively dividing the cavity in half between the two sides. The air cavity was left open to permit flow through the cavity, and both the eave and ridge used wood boards to serve as wind shields. Both shields were painted white to minimize the thermal impact.

Figure 49: Mangalore Tile Roof, Test Chamber 2

The team used Onset HOBO U23 external temperature sensors to record the data from three spots within the air cavity (Eave, Middle, and Ridge), as well as the internal temperature of the ceiling. Figure 50 illustrates these placements for the side of the chamber with directly-applied radiant barrier. Since the chamber itself was not divided in half, the air temperature sensors had a reduced value in comparing the impact of the radiative barrier placement.

The sensors were labeled according to their position, where 'Indirect' refers to the radiant barrier applied to the intermediate cardboard layer, and 'Direct' refers to the placement of the radiant barrier on the tile directly. All of the sensors were set to record on 15 minute synchronized intervals and were compared with the Outside Air Temperature at the site, also synchronized to the same intervals.
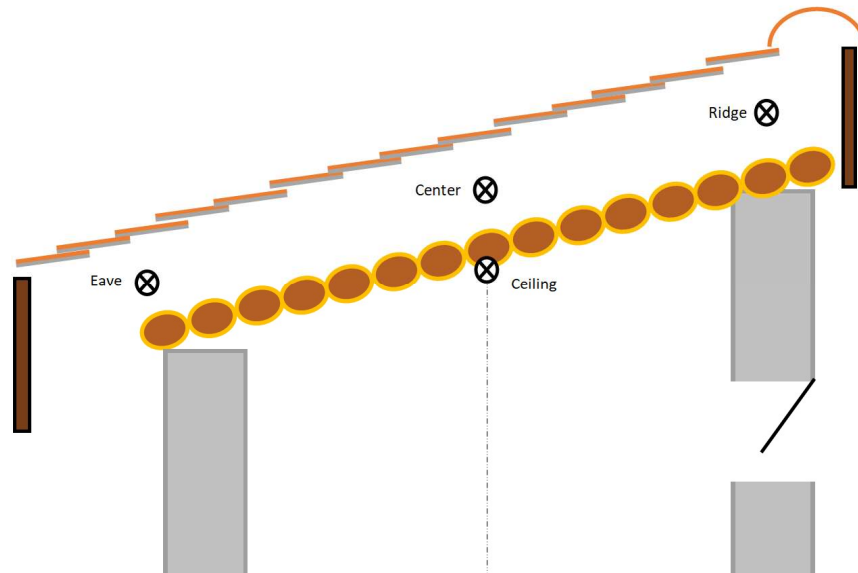
Figure 50: Chamber 2 Sensor Placements, shown for the side with Directly-Applied Radiant Barrier

[°C]	Outside Air Temperature	Indirectly Applied Radiant Barrier				Directly Applied Radiant Barrier			
		Ceiling	Eave	Center	Ridge	Ceiling	Eave	Center	Ridge
Max	28.29	23.65	27.13	24.61	27.22	24.64	29.7	28.85	28.69
Min	14.26	17.54	14.13	16.58	15.97	17.03	13.13	13.95	14.85
Peak Hour	15.75	19.00	15.50	16.50	15.25	17.50	15.50	15.25	15.25

Table 20: Chamber 2: Indirect vs. Direct Radiant Barrier (November 2017)

Table 20 shows the results of the testing. During this time, the team also retested the impact of night ventilation, and the results above span both the periods of night ventilation and the periods of no ventilation. From the tests, the hypothesis that the directly applied radiant barrier would help reduce the peak air temperature did not prove true. Based on the results, the directly applied radiant barrier raised the temperature of the air cavity and the ceiling by 1°C. Further, the directly applied radiant barrier allowed the air cavity to exceed the outside air temperature, which was not the case with the indirectly applied radiant barrier.

At night, the directly applied radiant barrier allowed the roof system to cool down between 0.5°C and 3.5°C more than the indirect application. While this is positive news, the homeowners have been most vocal about the daily maximum temperatures, which is when heat stress is most likely to onset. The indirectly applied radiant barrier has an additional benefit in that it helps to delay the peak temperature of the ceiling by 90 minutes, meaning that the indirectly applied radiant barrier provides more protection from the heat at the peak temperature of the day. The indirect application also creates an additional air cavity, which will increase the overall thermal resistivity of the ceiling

Based on these results, the team does not suggest placing the radiant barrier directly on the Mangalore roof tiles. The team does continue to suggest the integration of the radiant barrier, as both Nelson and Gradillas have reaffirmed the importance of the radiant barrier within the roof with Above-Sheathing Ventilation.

Wall Color and Ventilation Impacts

The team used the reconfiguration of the chamber as an opportunity to evaluate the impact of the wall color and of night ventilation in setting without homeowners present. Although short, the team used the two days prior to the walls being painted to establish a baseline and then alternated the presence of night ventilation to better understand the thermal performance within the chamber. Air temperature sensors (Onset HOBO UX120-003M) loggers were placed in the centerline of the chamber at 0.5m and 1.75 m heights, and set to record on the same 15 minute, synchronized intervals as the outside air temperature (OAT). The setup of these tests and the results are presented below, in Table 21.

[°C]	Mangalore Tile with natural-colored walls			Mangalore Tile with white-painted walls			Mangalore Tile with white-painted walls		
	11/11 – 11/13			11/13 – 11/21, 11/29 – 12/8			11/21 – 11/29, 12/8 – 12/15		
	Day: Closed & Night: Open			Day: Closed & Night: Open			Day: Closed & Night: Closed		
	OAT	Air: 0.5 m	Air: 1.75 m	OAT	Air: 0.5 m	Air: 1.75 m	OAT	Air: 0.5 m	Air: 1.75 m
Max	33.27	30.13	31.04	27.73	23.28	23.63	28.95	23.43	23.59
Min	17.8	24.51	24.51	15.15	16.25	17.35	13.31	18.91	18.46
Peak Hour	15.25	19.00	19.00	15.25	19.00	19.00	15.75	20.50	20.25

Table 21: Chamber 2 wall color and ventilation comparison

Based on the results from the table above. The white painted walls helped reduce the maximum air temperatures by between 1.4 and 1.9 °C relative to the peak outside air temperature, and reduce the minimum temperatures by between 4.5 and 5.6 °C relative to the minimum outside air temperature, as compared to the natural sandstone exterior. While there was no numerical impact on the timing of the peak temperature, the white-painted walls allow the night ventilation to keep the inside air temperature about 2°C warmer than the outside air temperature, where the natural-colored walls hurt the overall thermal performance by retaining heat throughout the night. Figure 51 shows the graphical results from the air temperature sensors before and after the walls were painted white.
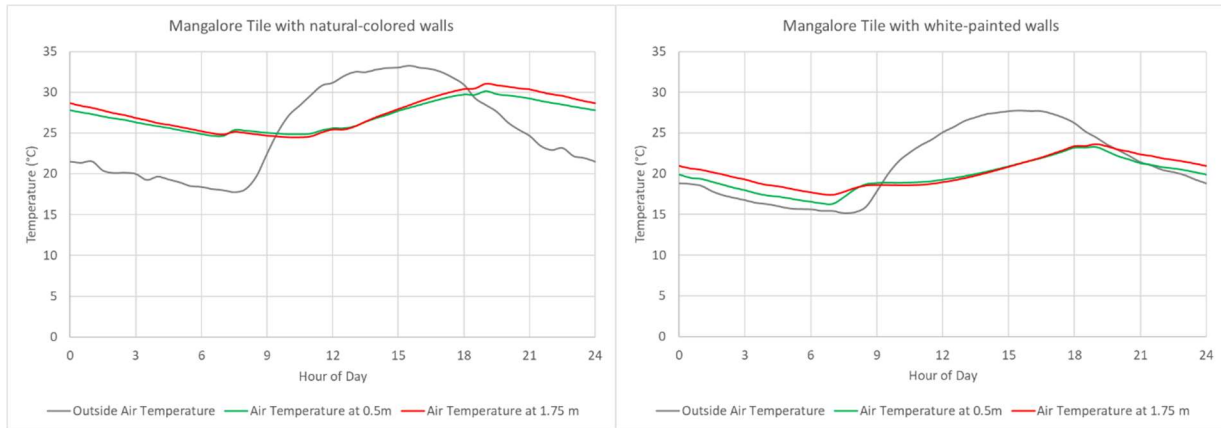
Figure 51: Chamber 2 without (left) and with (right) white-painted walls, with Night Ventilation

To better assess and retest the impacts of night ventilation on the chambers with Mangalore Tile above-sheathing ventilated roofing, the chamber was left closed for two non-consecutive weeks between the night ventilation tests. This approach helped to reduce the fluctuation in the outdoor air temperature, and the resulting data is displayed graphically in Figure 52.
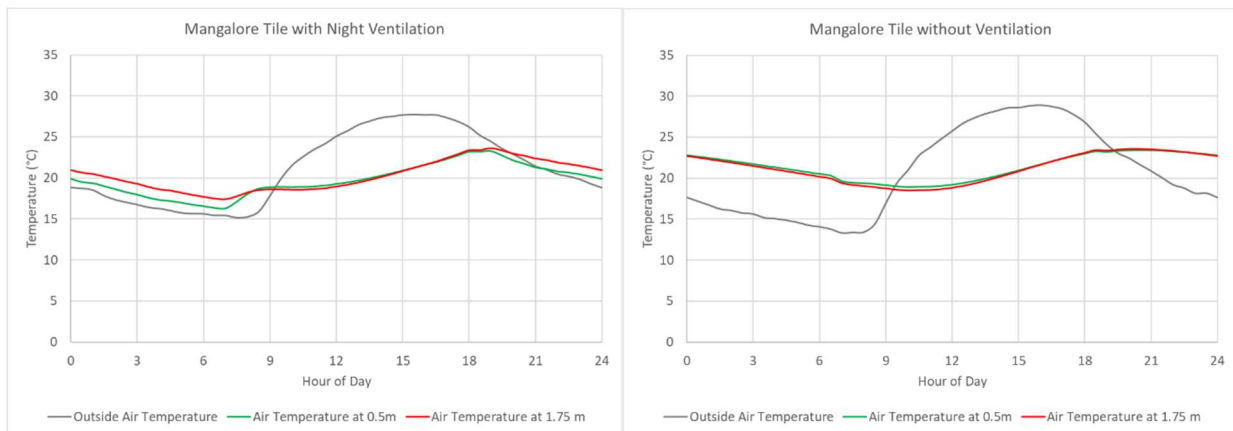
Figure 52: Chamber 2 with (left) and without (right) Night ventilation, walls painted white

Where the numerical results in Table 21 suggest that keeping the windows closed at night will keep the temperature cooler during the day, Figure 52 suggests that such a conclusion does not look at the broader thermal performance. The two periods are not identical and the weather experienced without ventilation had a higher diurnal temperature difference than the period with Night Ventilation. The period without ventilation performs as more of an average of the daily sinusoid, whereas the night ventilation thermal performance stay cooler on the whole; thus reinforcing the advised and practiced trends of night ventilation.

In both chambers, there was no internal heat generated. If internal heat was generated, that would change the suggested window operation schedule. This would be especially true if heat was generated throughout the day where the heat may push the inside air temperature above the outside air temperature.

Through the work of Nelson and Gradillas, Chambers 3 and 4 were constructed with the same floorplan as the other chambers. In lieu of the tin sheet or Mangalore tile roofing, a reinforced concrete slab was poured in place and painted white on top. An image of the original configuration is shown on the left of Figure 41.

In October 2017, the chambers were modified to better simulate the ground level housing in Bhuj, where the houses are built as row houses, also referred to as terraced homes or townhouses. These homes share common side walls and are nearly identical in their layout, but with modifications made in the ornamentation and finishing with the input of the home owners. Some of these homes are shown in Figure 53 below. These homes can be thermally approximated as individual units by assuming that the north and south shared walls are half the thickness as installed and adiabatic on the exterior. To accomplish this approximation using the chambers, the Bhuj-based team installed straw insulation to the north and south sides of the chamber, and covered the straw with white-painted coarse fabric to prevent cows from eating the straw as Gradillas discovered. The conductivity of straw configured in a board application was reported by Neuberger and Kic to be in the range of 0.066-0.089, depending on stalk orientation (Neuberger & Kic, 2017). These values straddle the ASHRAE recommended value of for straw thatch of 0.07 W/m·K (The American Society of Heating, Refrigerating and Air-Conditioning Engineers, 2018). Using the ASHRAE value with the 5 cm thickness, the R-value of 0.714 K·m²/W is akin to 2 cm thick extruded polystyrene, which is available and used commercially as an insulation product in the same thickness. This reinforces the validity of straw as an insulation for short-term testing.

Figure 53: Row homes in Ramdev Nagar, Bhuj, India (January 2018)

Figure 54: Straw Insulation on Chambers 3 and 4 (January 2018)

Test 1: Interior Mud Plaster with Night Ventilation

The first test on the chambers was designed to test the influence of applying a mud-based plaster to the interior of the uncovered east and west walls. Matching the homes in the Ramdev Nagar community, the uncovered east and west walls were painted white, as shown on the right of Figure 54. The mud-based plaster is a technique that is shared with Nepal and is used primarily for aesthetics, although also to reduce air infiltration and longevity in some applications. It can be applied to either an interior or exterior surface and generally requires light maintenance from external weathering. The Bhuj-based artisans were asked to apply the plaster in the same manner that they typically apply it in practice. Figure 55 shows the completed product, which is about 2-3 cm thick overall. The ceiling was painted black in both chambers to cover a radiant barrier installed as part of the Nelson thesis.
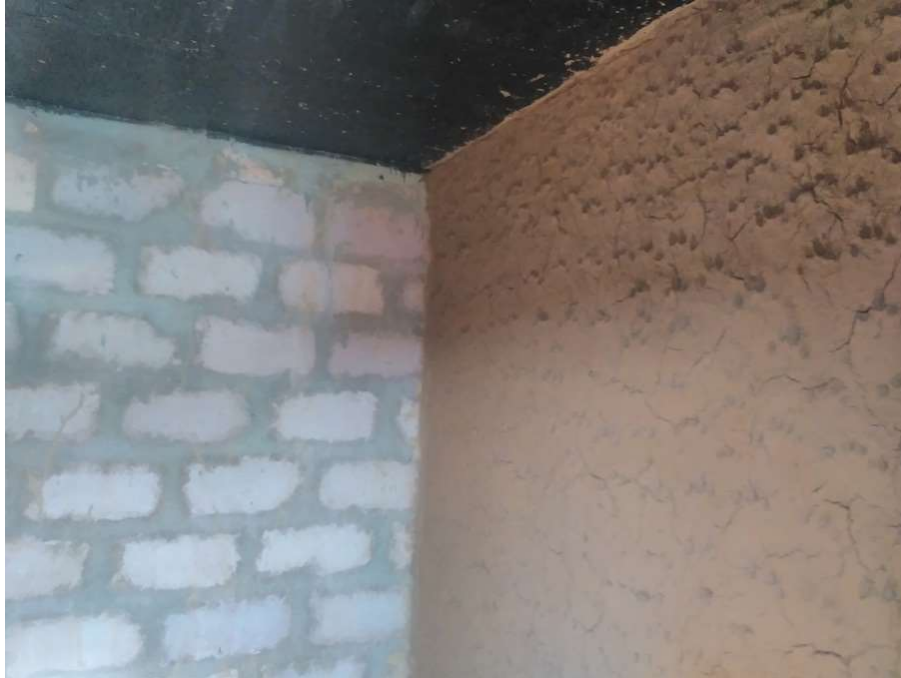
Figure 55: Interior mud plaster on Chamber 4 (photo credit Pradip Rangani)

After the mud plaster was in place in chamber 4, the team installed temperature loggers to track the temperature over 15 minute, synchronized intervals. For each chamber, the team used Onset temperature loggers to track the temperature as a function of time. The team used:

- Two Onset UX120-003M air temperature loggers placed in the center point of the plan and at elevations of 0.5m and 1.75m;
- One Onset U23-003 external temperature logger placed in the center point of the plan to measure ceiling temperature and radiant temperature at 1.2 m height; and
- One UX120-006M four channel temperature sensor to measure the interior wall temperatures at 1.2 m height.

Unfortunately, the U23-003 logger placed in Chamber 3 failed to produce usable data, leaving the comparison points between the interior air temperature, the wall temperatures, and the outside air temperature installed on the site. Table 22 shows the resulting values when the test was run using night ventilation, from November 13 to November 21, 2017.

[°C]	Outside Air Temperature	Chamber 3: North and South exterior insulation, white exterior, black ceiling					
		0.5 m	1.75 m	North Wall	South Wall	West Wall	East Wall
Max	28.79	23.23	23.93	22.81	21.97	23.18	23.06
Min	15.45	16.40	17.72	19.05	19.86	17.97	18.06
Peak Hour	15	18.5	18.25	19.25	19.5	19	19

[°C]	Outside Air Temperature	Chamber 4: North and South exterior insulation, white exterior, black ceiling, mud plaster interior on east and west walls					
		0.5 m	1.75 m	North Wall	South Wall	West Wall	East Wall
Max	28.79	22.90	23.68	22.28	21.97	22.88	22.17
Min	15.45	16.44	17.57	18.80	19.40	18.04	17.89
Peak Hour	15	18.5	18.25	19.25	19.25	19.25	19.25

Table 22: Chamber 3 and 4 Test 1: Setup and results using Night Ventilation (13-Nov-2017 to 21-Nov-2017)

As Table 22 shows, the addition of the mud plaster interior on the east and west walls helped to reduce the peak indoor air temperature by around 0.3°C, with the primary benefits being a reduction in the peak temperatures of the east and west walls by 0.3 and 0.8°C, respectively. It does not go without notice that the north wall also decreases temperature by 0.5 °C, but this is unlikely to be driven by the mud plaster, as the difference is evident across all tests. An initial comparison between the two chambers would have been helpful to rectify this early in the testing stages.

The minimum air temperatures within the chamber remain largely unaffected in the presence of the night ventilation, as the air temperature reflects the open environment outside and less about the chamber itself. No significant impacts are seen in the temperature distribution as a function of time, as the peak temperature times do not substantially change.

Using the Energy Plus simulations described earlier, the team constrained the date range of the simulation to November 20 through November 30th. Doing so allowed the Outside Air temperature to match closer to that which was experienced during the November 2017 test. To incorporate different types of wall types into the Archsim interface, the team altered the floorplan by adding additional zones to the existing model and defining the new zones with the new wall type. To do this, these zones were defined as 1 cm deep and the partition walls were specified to be 1 cm thickness, with zero heat capacity and 1000 W/m·K. The radiative properties set absorptance and emittance of unity, and the inter-zone air movement rate set to 1 m³/sec. Inherently, theses settings seek to reduce the influence of the unphysical partition wall, but in doing so require the assumption that the entire chamber was well mixed. In making this assumption, the variance in air temperature will be reduced, something that the data (Table 22) does not support, as the height-based temperatures vary by 0.75 to 1.5 °C.

For Chamber 4: Test 1, the team modeled the interior east and west mud plaster as an ASHRAE cement plaster/sand aggregate mix of 2.5 cm thickness, with a conductivity value of 0.72 W/m·K (The American Society of Heating, Refrigerating and Air-Conditioning Engineers, 2018) and with values for thermal emittance of 0.9 and solar/visible absorptance of 0.7.

[°C]	Chamber 3: North and South exterior insulation, white exterior, black ceiling				
	As-tested			Simulation	
	Outside Air Temperature	0.5 m	1.75 m	Outside Air Temperature	Inside Mean Air Temperature
Max	28.79	23.23	23.93	30.35	24.35
Min	15.45	16.4	17.72	15.05	17.91
Peak Hour	15	18.5	18.25	15	19

[°C]	Chamber 4: North and South exterior insulation, white exterior, black ceiling, mud plaster interior on east and west walls				
	As-tested			Simulation	
	Outside Air Temperature	0.5 m	1.75 m	Outside Air Temperature	Mean Air Temperature
Max	28.79	22.90	23.68	30.35	24.19
Min	15.45	16.44	17.57	15.05	17.94
Peak Hour	15	18.5	18.25	15	19

Table 23: Chamber 3 and 4: Test 1 As-Tested vs. Simulation

Comparing the as-tested values to the simulation values, the outside air temperatures have a larger amplitude in the simulation, which helps to produce a slightly higher inside mean air temperature than the chamber experienced. However, the minimum temperatures remained higher than the as-tested values, despite the outdoor air temperatures being cooler than the tested version. Similar to the chambers, the simulation was configured without heat gain from the occupants.

The simulation results confirm the results of the test comparison in that the addition of the mud plaster to the interior of the east and west walls are able to reduce the amplitude of the temperature variations, and that there is more decrease in the maximum temperatures than increase in the minimum temperatures. However, while the physical tests showed a decrease in the maximum temperatures of between 0.25 and 0.33°C, the simulations predicted a decrease of 0.16°C. This may be due to the assumption of the conductivity of the mud plaster, which is likely to vary from the ASHRAE value for a concrete/sand plaster mix. Additionally, the two tests use different weather data for the same rough period. In both cases, the result on maximum air temperatures during November weather are clear, but modest.

The team then used the simulation model for the entire year to compare against the ANSI/ASHRAE Standard 55-2017 definition of thermal comfort. This standard takes into account the influence of operative temperature and humidity to determine when occupants would be comfortable "with metabolic rates between 1.0 and 1.3 met and clothing insulation between 0.5 and 1.0 clo who are not exposed to direct solar radiation." (ANSI/ASHRAE, 2017) These bounds correspond to 80% of people satisfied with the thermal comfort conditions.

For the geometry and settings of Chamber 3: Test 1, there are 1,386 hours (15.8%) in the year where occupants are comfortable, and 7,374 hours (84.2%) of the year where occupants would be uncomfortable. For the hottest day of the year, where ambient conditions are 41.9°C using the simulation data, the chamber is expected to experience of maximum air temperature of 34.71°C. For Chamber 4, with the interior mud plaster on the east and west walls, comfort conditions decrease to 1,373 hours (15.7%) of comfort, and 7,387 hours (84.3%) of discomfort within the year. Using the simulation for the hottest day of the year, the maximum air temperature inside the chamber is 33.83°C. The yearly maximum air temperature values show how important the simulation data is in the comparison. The results of the simulation suggest that the addition of the interior plaster will decrease the temperature on the hottest day by 0.9°C, a nontrivial amount.

Similar to other numbers presented, the comfort/discomfort numbers are to be taken with caution if being used directly since the numbers do not suggest if most of the uncomfortable hours are when the temperature is too cold, too warm, or when it is too humid. However, the general trends and quantifications of absolute temperatures can be used as-is.

Test 2: Interior Mud Plaster without Ventilation

Using the existing test setup, the team then left the chambers alone for the period between November 21 and November 28 to look at the influence of Night Ventilation when coupled with the mud plaster. The setup and results of the test are shown below, in Table 24.

[°C]	Outside Air Temperature	Chamber 3: North and South exterior insulation, white exterior, black ceiling					
		0.5 m	1.75 m	North Wall	South Wall	West Wall	East Wall
Max	30.09	21.60	22.16	21.56	20.81	22.01	21.87
Min	12.99	17.52	17.25	17.97	18.61	16.56	16.69
Peak Hour	15.50	20.25	18.50	20.50	22.25	19.75	19.75

[°C]	Outside Air Temperature	Chamber 4: North and South exterior insulation, white exterior, black ceiling, mud plaster interior on east and west walls					
		0.5 m	1.75 m	North Wall	South Wall	West Wall	East Wall
Max	30.09	21.45	21.90	21.18	20.87	22.18	21.15
Min	12.99	17.56	17.27	17.91	18.12	16.80	16.58
Peak Hour	15.50	20.50	19.50	21.00	21.50	20.25	20.50

Table 24: Chamber 3 and 4 Test 2: Setup and results without ventilation (21-Nov-2017 to 28-Nov-2017)

As Table 24 shows, the addition of the mud plaster interior on the east and west walls helped to reduce the peak indoor air temperature by between 0.15 and 0.25°C, with the primary benefits being a reduction in the peak temperatures of the east and west walls by an average of 0.3°C. The north wall decrease of 0.4 °C may be driven by a variation in the straw covering, as supported by the results of the entire range of tests between the two chambers.

The minimum temperatures within the chamber remain largely unaffected. In the absence of night ventilation, the peak temperature times are delayed by an average of about half an hour.

Similar to Test 1, Test 2 was simulated using EnergyPlus. To compare the measured values from November 21 to November 28, 2017, the team used the ISHRAE dates of November 20 to December 30 to best match the Outside Air Temperature values. For the duration of the test, the ventilation windows remained closed and thus, the infiltration rate is assumed to be constant. The resultant values are shown graphically below in Figure 56. Within the figure, solid lines are measured values, and dashed lines are simulated values. All values are indicative of an average day for the duration of the two representative periods.
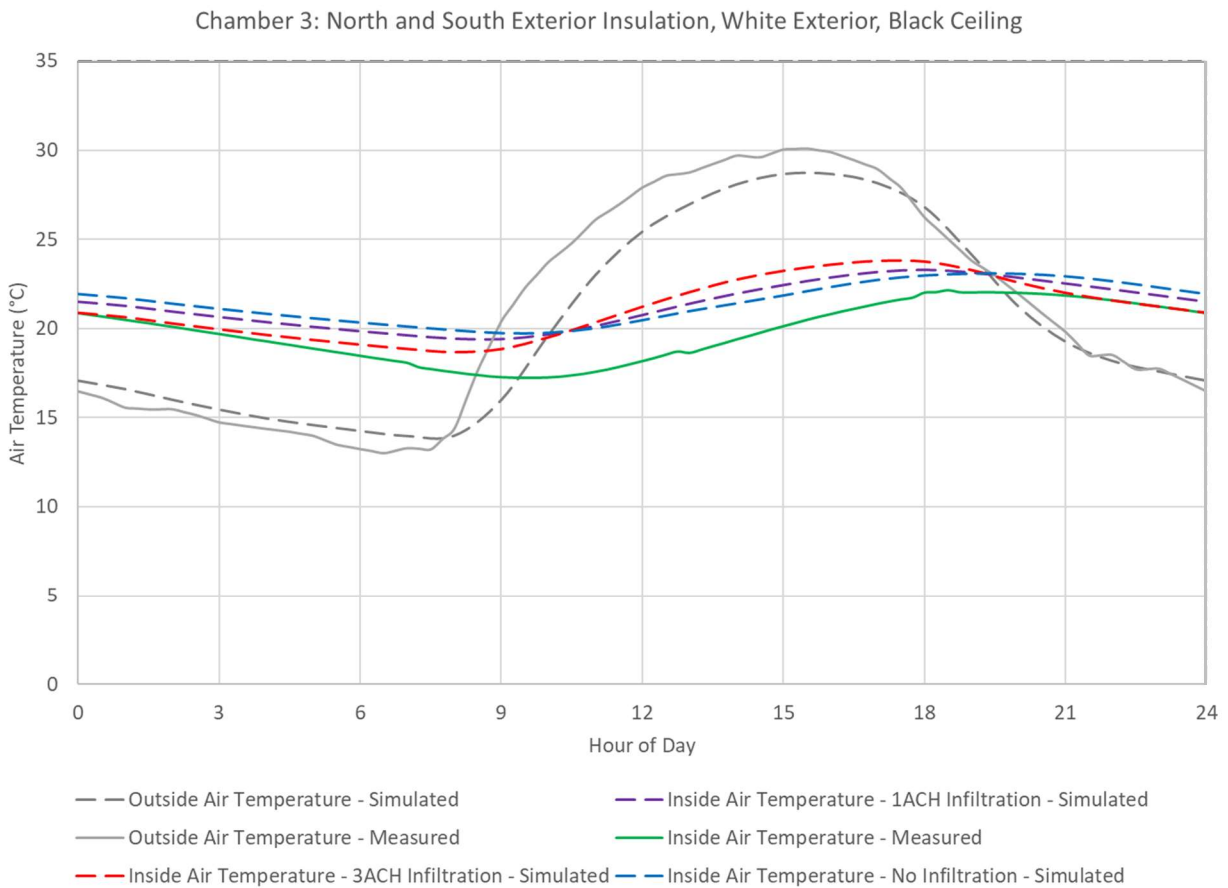
Figure 56: Chamber 3 Test 2, measured vs simulated values

Within the figure, the Outside Air Temperature profiles has reasonable agreement with the measured value. However, while the outside air temperature values are generally lower in the simulated case than the measured case, the resultant inside air temperature simulated values are higher than the measured values. In an attempt to explain this difference, the team questioned the zero infiltration assumed and modeled the cases using increasing infiltration air change rates. Air change rates, defined as air changes per hour (ACH), are a way to define how quickly the air within the chamber is being circulated through the space. For a reference, 6 ACH is the value used by Nelson to evaluate a condition where windows are left ajar, and 1 ACH is the value used by Nelson to evaluate when the windows

remain closed. While the windows remained closed in the setup of this experiment, the infiltration rates are assumed to be constant, unchanging with time.

With the inclusion of the infiltration rates, the simulated values migrate towards the measured values during the non-sunlight hours, but deviate during the day. Matching the profiles of the air change rates with the measured values may suggest that there is some modest infiltration, but the zero infiltration approximation holds as reasonable. These conclusions are the same for Chamber 4, as represented in Figure 57.
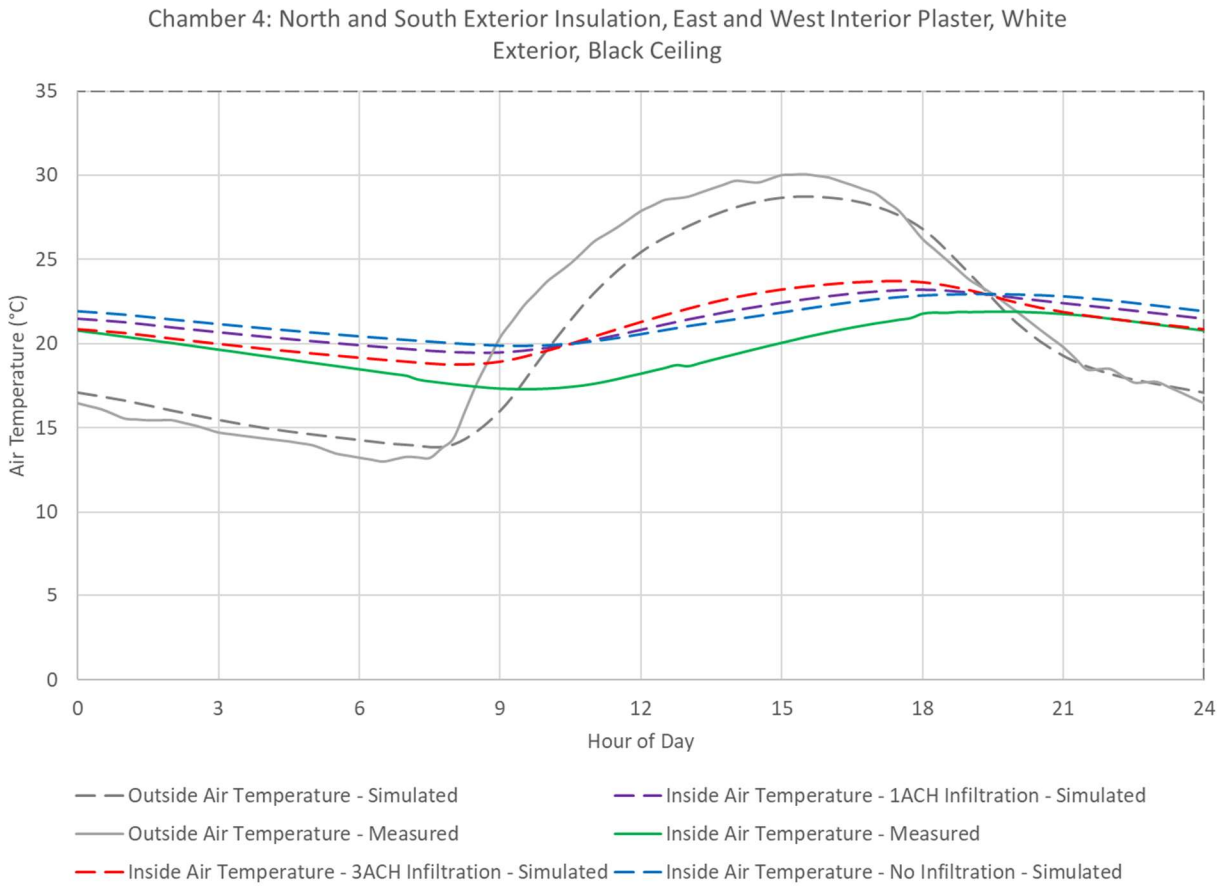
Figure 57: Chamber 4 Test 2, measured vs simulated values

The performance of the interior plaster on the east and west walls did little to drastically change the overall profile. However, the simulation and experimental results agree that a modest (~0.15°C) decrease in peak temperatures can be achieved by adding internal plaster to the east and west walls. The experimental results suggest no impact at night, while the simulation results predict a similar magnitude modest increase in minimum air temperatures at night. Overall, the differences are too small to show graphically on the same scale as Figure 57, and instead are shown numerically in Table 25, below.

94

[°C]	Chamber 3: North and South exterior insulation, white exterior, black ceiling				
	As-tested			Simulation	
	Outside Air Temperature	0.5 m	1.75 m	Outside Air Temperature	Inside Mean Air Temperature
Max	30.09	21.6	22.16	31.34	25.11
Min	12.99	17.52	17.25	10.2	17.23
Peak Hour	15.50	20.25	18.5	16.00	19.00

[°C]	Chamber 4: North and South exterior insulation, white exterior, black ceiling, mud plaster interior on east and west walls				
	As-tested			Simulation	
	Outside Air Temperature	0.5 m	1.75 m	Outside Air Temperature	Mean Air Temperature
Max	30.09	21.45	21.9	31.34	25.02
Min	12.99	17.56	17.27	10.2	17.36
Peak Hour	15.50	20.50	19.50	16.00	18.00

Table 25: Test 2 Setup and Numerical Results

Test 3: Influence of radiant barrier in chamber with night ventilation

Similar to the testing within Chamber 1, Test 3 on Chambers 3 and 4 reconfiguring the tests to test the impact of a constant radiant barrier. To do this, the mud plaster was removed and aluminum foil was applied to the ceiling of Chamber 4. Using night ventilation, the test ran from November 29 to December 8, 2017.

[°C]	Outside Air Temperature	Chamber 3: North and South exterior insulation, white exterior, black ceiling					
		0.5 m	1.75 m	North Wall	South Wall	West Wall	East Wall
Max	27.45	21.81	22.81	21.49	20.77	21.87	21.76
Min	14.77	15.95	16.90	18.01	18.82	17.17	17.26
Peak Hour	14.50	18.25	17.75	19.25	19.75	19.00	19.00

[°C]	Outside Air Temperature	Chamber 4: North and South exterior insulation, white exterior, aluminized ceiling					
		0.5 m	1.75 m	North Wall	South Wall	West Wall	East Wall
Max	27.45	21.78	22.65	21.05	20.74	22.04	21.23
Min	14.77	16.02	16.92	17.90	18.52	17.02	16.95
Peak Hour	14.50	18.25	18.25	19.50	19.00	19.00	19.00

Table 26: Chamber 3 and 4 Test 3: Setup and results with night ventilation (29-Nov-2017 to 8-Dec-2017)

Table 26 shows that the addition of the aluminum radiant barrier applied directly to the ceiling made no significant changes to the maximum or minimum temperatures of the chambers. The peak temperature times also show no influence from the radiant barrier presence. However, when represented graphically (Figure 58), the aluminized ceiling coating has an impact outside of these two data points.

In Figure 58, Chamber 3 is represented in red and orange, and Chamber 4 is represented in green and light green. The darker colors represent the 1.75m measurements, and the lighter colors the 0.5m measurements.
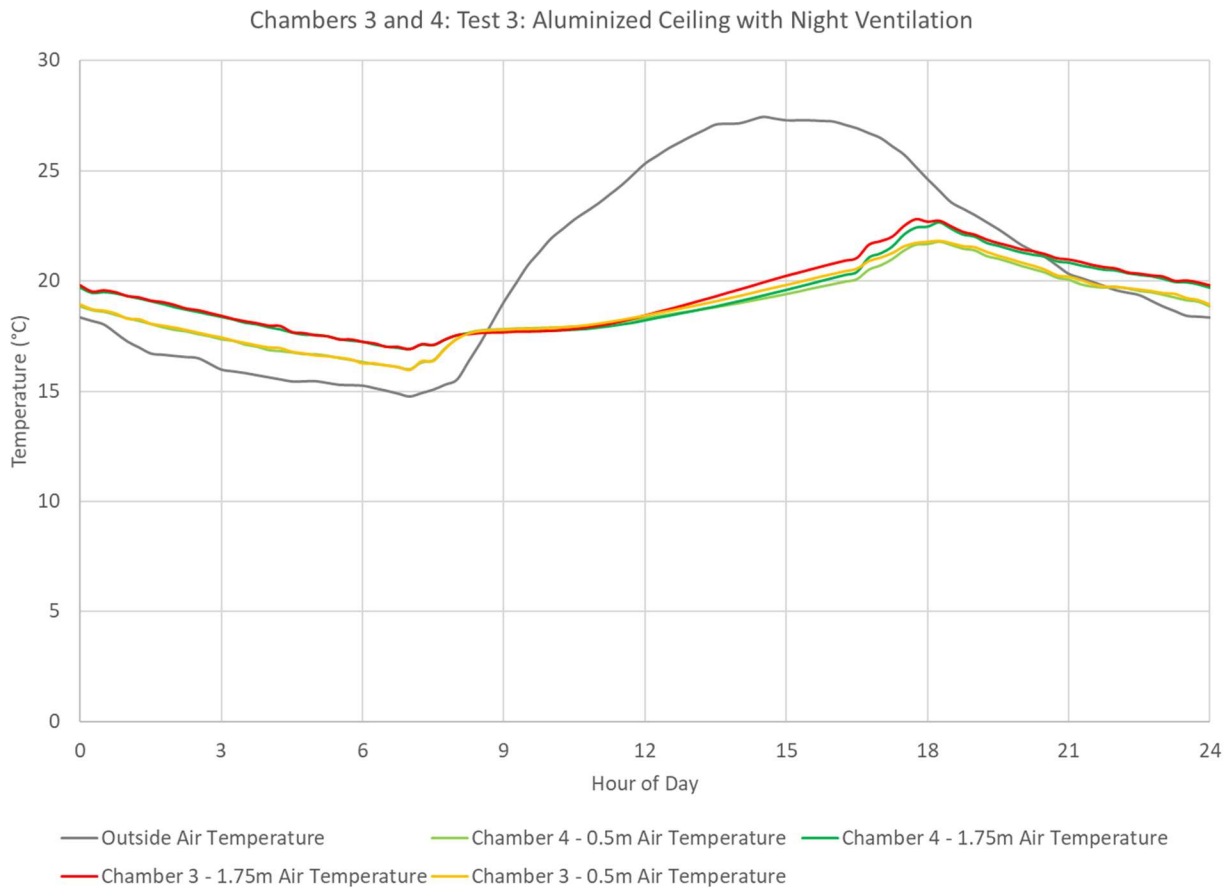
Figure 58: Chambers 3 (black ceiling) and 4 (aluminized ceiling), Test 3, Radiant Barrier Ceiling with Night Ventilation

Figure 58 shows that the aluminized ceiling coating allows the interior air temperature to remain cooler during the day without a substantial detriment to the nighttime temperatures when ventilation is in effect. The aluminized ceiling was able to reduce the inside air temperature by 1°C for a two hour period. While this two-hour period does not coincide with the hottest times of the day, it does produce a cooler indoor air temperature beginning at high noon and ending at 6 pm. The team feels reasonably confident that the results from the chambers are not biased due to discrepancies in construction.

96

To further validate this, the team used EnergyPlus to compare against the measured values. For these simulations, the chamber was assumed to have 6 ACH after nightfall, and to be sealed during the day. The roof layers were modified such that the roof geometry were two mated planes with the lower layer having a 1mm thickness and the surface properties of the variable interior. The outer layer remained the same, as a white painted concrete slab. Whereas the experiment ran from November 29 to December 8, 2017, the simulation used the ISHRAE values for December 12 to December 20 to match the outside weather conditions. The results are displayed below, in Figure 59, where the coloring is the same as Figure 58, but the simulation results have been added as dashed lines.
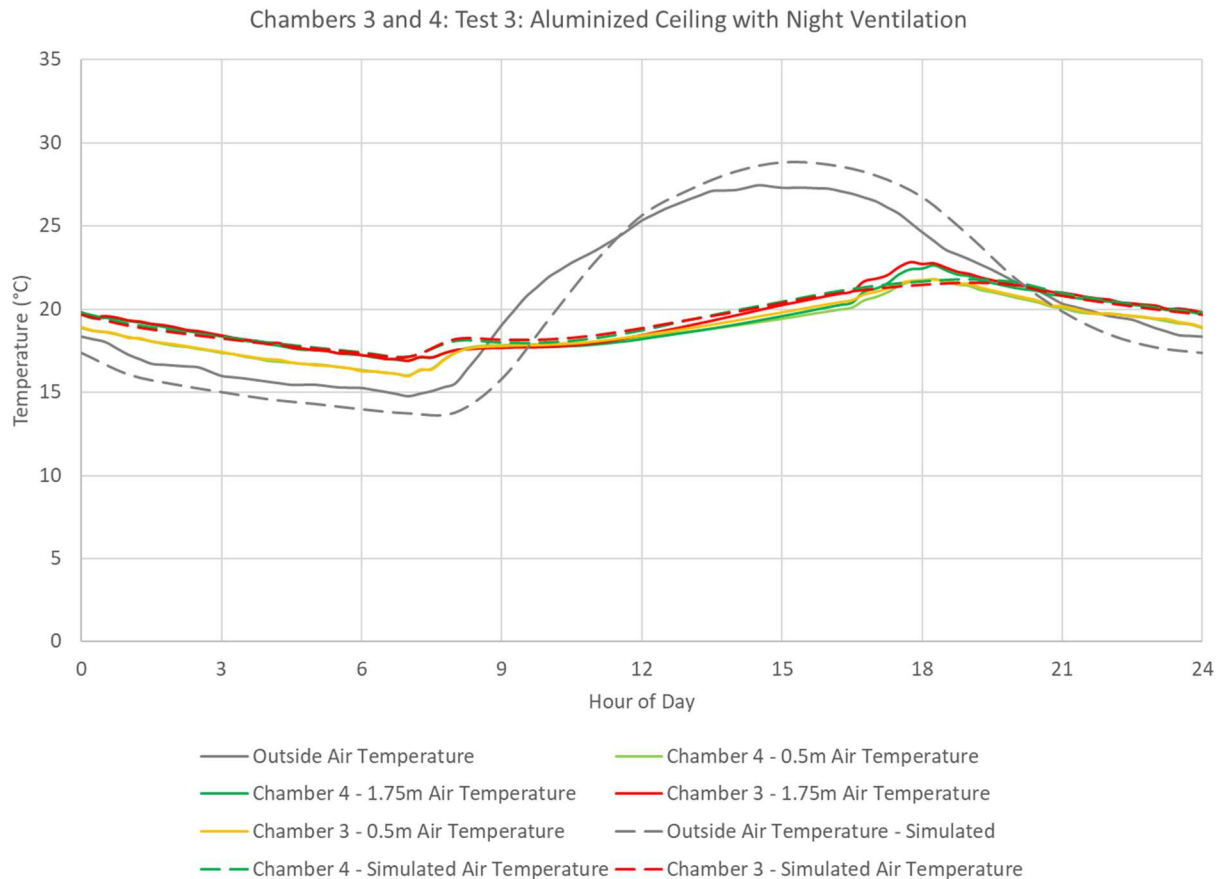
Figure 59: Chamber 3 (black ceiling) and 4 (aluminized ceiling): Test 3, measured vs simulation results

Even outside of the slightly different weather patterns, the simulation predicts no substantial change in the mean inside air temperature with or without the aluminized ceiling. While the conclusion from the simulations align with the conclusion presented in Test 3 of Chamber 1, it deviates from the experimental results. Test 3 of Chamber 1 concluded that no major influence was to be found by adding the aluminized ceiling coating, but was different from Test 3 of Chambers 3 and 4 in that Chambers 3 and 4 already had other heat reduction strategies employed. Chamber 3 and 4 had exterior insulation on the north and south facades, and a white-painted RCC roof slab, where Chamber 1 had a galvanized corrugated sheet roof.

Driving further to determine the root cause of why the aluminized inner layer has varying impacts on the internal temperature, this could be due to both changes in thermal absorptivity and the impact of the thermal mass, which may store more heat as opposed to releasing it to the chamber, which may prolong the heat flux. Starting at the top surface of the roof, the solar absorptivity of the corrugated sheet was determined experimentally to be 0.28, where the paint was assumed to be 0.22. On the scale from zero to unity, this subtle uniform change is unlikely to create the resultant temperature difference. However, the aluminized ceiling in Chamber 1 was applied directly to a fresh piece of galvanized corrugated sheet (Room temperature absorptivity of 0.142), whereas the aluminized ceiling that was applied to the roof of the RCC chamber was referenced against a case where the ceiling was painted black (expected Room temperature absorptivity of 0.90). This difference is critical in the RCC case as addition of the aluminum to the ceiling changes the ceiling from being near a black body to being near a perfect reflector. The aluminum foil was tested to have an absorptivity of 0.071 at room temperature.

While the simulation results suggested marginal air temperature changes with the addition of the aluminum ceiling covering, the use of the EnergyPlus simulation allowed the team to test the impact of the switch from a black body (Thermal Absorptivity = 1) to a perfect reflector (Thermal Absorptivity = 0). Additionally, the simulation aimed to look at performance in the heat of the dry summer season (April and May), when the solar contribution and heat flux through the roof would be the highest.
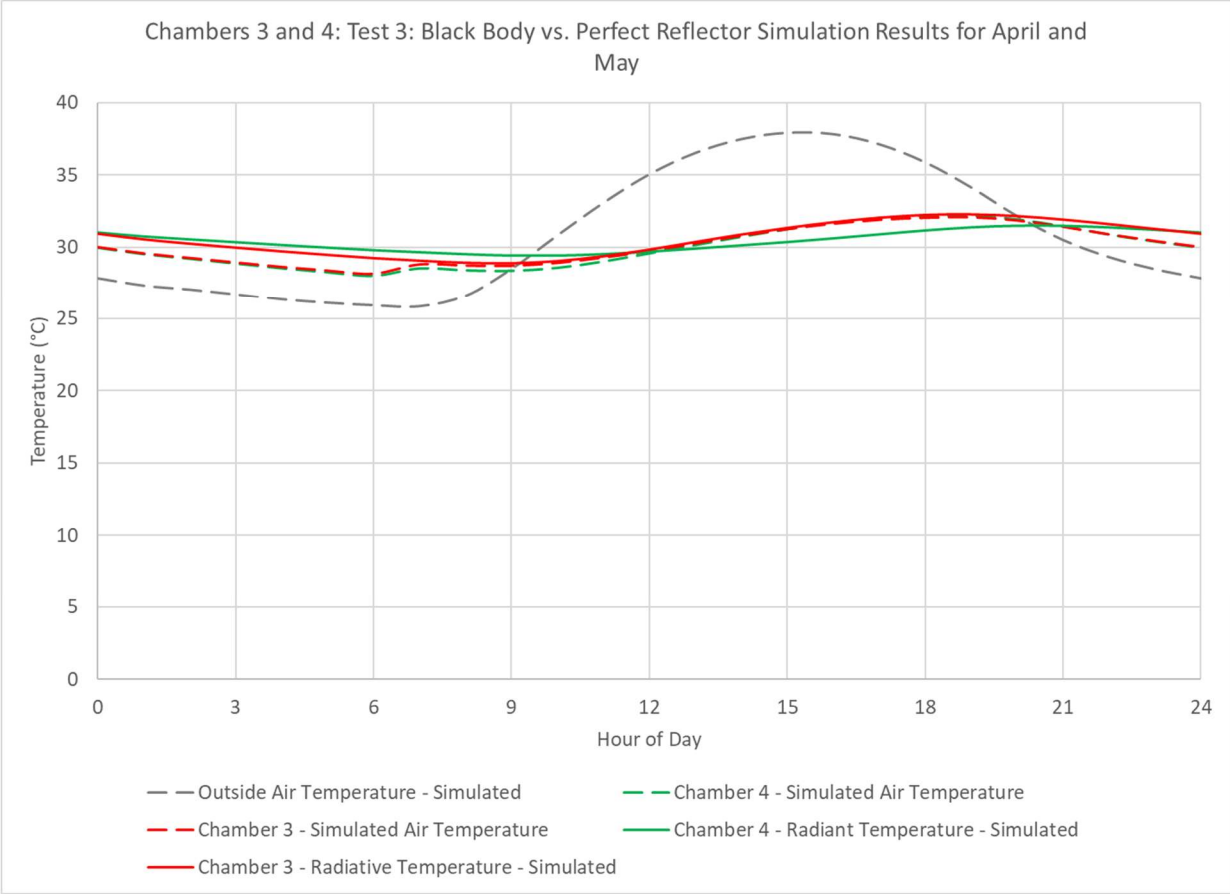
Figure 60: Simulated Results for Blackbody (Chamber 3) and Perfect Reflector (Chamber 4) Ceilings

Figure 60 shows the results of the modeling efforts, displayed for the months of March and April, where the mean air temperature again shows marginal impacts from the addition of the aluminized ceiling coating. However, Figure 60 also includes the 'average day' values for the mean radiative temperature, which is more sensitive to surface property changes and reflects both the surface properties and temperatures of the surrounding surfaces. The simulated mean radiative temperatures vary by 1.2°C at the peak difference and are more in line with the variation seen in the RCC test chambers. These results suggest that the Energy Plus approximations for air movement within the chamber may be more stagnant than what is actually present. This hypothesis is partially reinforced within the simulation outputs by the uniform temperature difference that is present between the inside face and immediately adjacent air temperatures which, when plotted against each other, the inside face adjacent air temperature averages between 0.75 and 1.85°C cooler than the face itself.

In the absence of ventilation, data was collected from the chambers from December 8 to December 15, 2017.

[°C]	Outside Air Temperature	Chamber 3: North and South exterior insulation, white exterior, black ceiling					
		0.5 m	1.75 m	North Wall	South Wall	West Wall	East Wall
Max	26.89	21.49	21.83	21.18	20.93	21.70	21.50
Min	13.51	18.13	17.85	18.42	19.29	17.32	17.41
Peak Hour	15.50	18.75	18.75	20.50	18.75	18.75	18.75

[°C]	Outside Air Temperature	Chamber 4: North and South exterior insulation, white exterior, aluminized ceiling					
		0.5 m	1.75 m	North Wall	South Wall	West Wall	East Wall
Max	26.89	21.18	21.54	20.81	20.89	22.07	21.00
Min	13.51	18.19	17.96	18.62	18.98	17.30	17.21
Peak Hour	15.50	18.75	18.75	21.25	18.75	18.75	18.75

Table 27: Chamber 3 and 4 Test 4: Setup and results without ventilation (8-Dec-2017 to 15-Dec-2017)

As Table 27 shows, the addition of the radiant barrier applied directly to the ceiling reduced the average of all data streams maximums by 0.2 °C, with peak air temperatures decreasing by 0.3 °C. Numerically, this variation exists from the maximum and minimum temperature values since the impacts are on a longer timescale, as seen in Figure 61.

Chambers 3 and 4: Test 4: Aluminized Ceiling without Ventilation
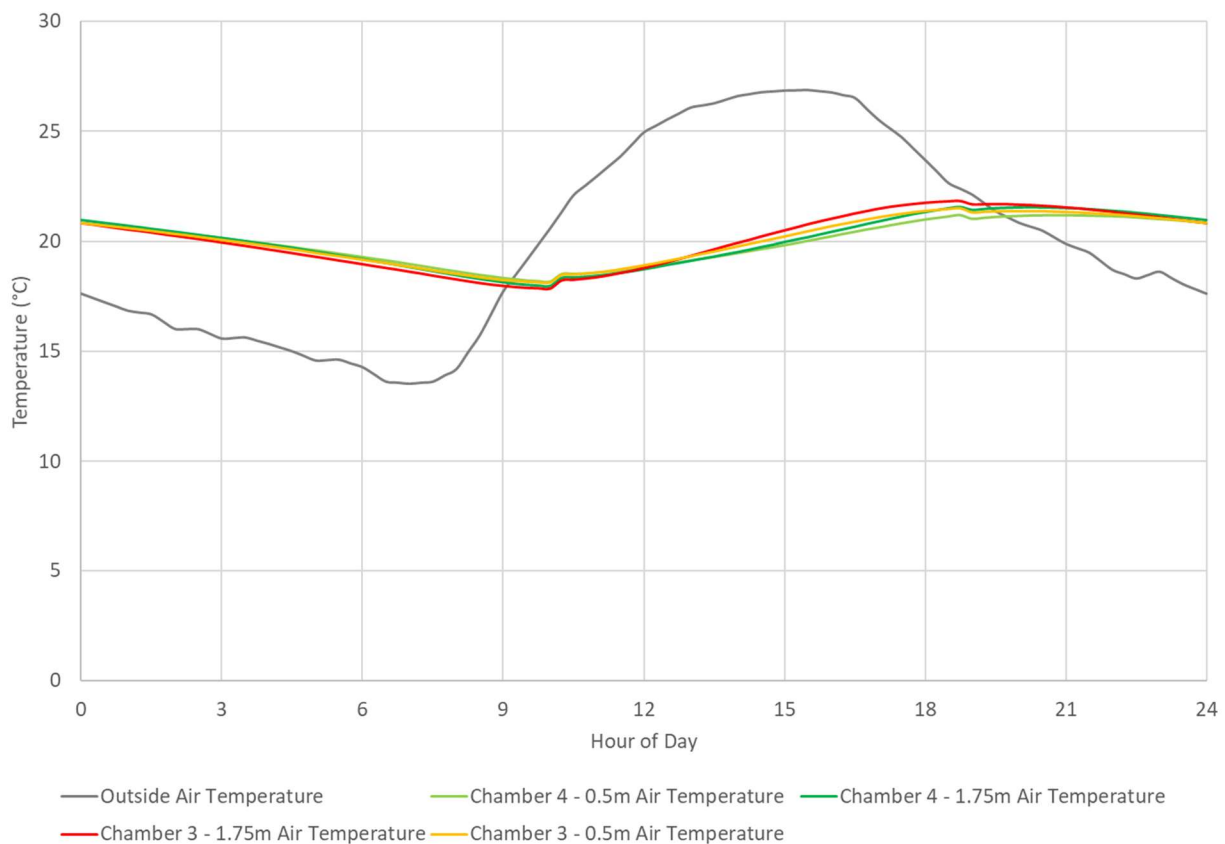
Figure 61: Chambers 3 (black ceiling) and 4 (aluminized ceiling), Test 4, Radiant Barrier Ceiling without Ventilation

Similar to test 3, the application of the aluminum ceiling coating reduces the mean ambient temperature in the test chamber by up to 1°C during the middle of the day. However, in the absence of the night ventilation, a marginal deviation continues through the nighttime hours. These tests confirm the applicability of a highly reflective ceiling coating on structures that current have black body-like ceiling coatings.

Although not a perfect comparison, the results from the above tests allow for elementary generalizations on how the roof typologies perform thermally with respect to each other. It is not a perfect comparison since the chambers are being compared across different time intervals and slightly different weather patterns. However, providing this comparison can provide insight on the relative ability for certain roof typologies to shield occupants from extreme heat events. The subsequent chapter on *in situ* housing in Ramdev Nagar, Bhuj, India provides full scale, long term, and parallel comparison of four iterations of double layer (above-sheathing ventilation) roofing styles, along with commentary on social acceptance of the different roofing styles.

Beginning with Chamber 1, the application of the white paint to the exterior walls of the chambers allowed the structure to remain 1.5 to 2.5°C cooler during the heat of the day, while also keeping the night 1 °C cooler. As Figure 53 shows, this practice is already being widely utilized in the Ramdev Nagar community for both aesthetic and thermal reasons.

Comparing the tin sheet roof with the Mangalore tile above-sheathing ventilated roofing, the comparison allows both chambers to have the same wall treatments, but the wide variation in outside air temperature hinders the ability to make a conclusion based on the data available. For a better comparison, the *in situ* housing provides a better value, but is limited to double layer/above sheathing ventilated roofing. Nelson's thesis provides simulation results to answer that question, and concludes that the RCC slabs remained more than 6 °C cooler than the galvanized sheets. Reductions in maximum air temperature are likely to be less than that amount.

Comparing the Mangalore tile above-sheathing ventilated roofing with the RCC roofing with North and South exterior insulation, the RCC slab roofing permitted the peak internal air temperature to remain up to 1°C cooler, but with maximum temperature half an hour earlier than in the Mangalore tile roof. The minimum temperatures were about equal between the two chambers with night ventilation.

Adding in the comparison to the mud plaster, the RCC roof with north and south exterior insulation and interior mud plaster on the east and west walls remained cooler than chamber without mud plaster, by about 0.4 °c at the peak temperature, with no impacts to the minimum temperature when night ventilation was present. This implies that the RCC roof with north and south exterior insulation (mimicking the row housing) and interior mud plaster on the east and west walls remained up to 1.4°C cooler at the peak temperature than the Mangalore Tile above-sheathing ventilated roof.

The radiant barrier efforts did not have a significant impact. Further implementation of the radiant barrier borrows from Nelson's thesis in applying the alternating radiant barrier with air gap, which was simulated to reduce the peak air temperature by 4 °C compared to a tin sheet roof. Further discussion of this concept, including thermal conductivity testing of small-scale prototypes, are included in 'Local Experiments'.

Across all chambers, the minimum values for inside air temperatures were greater than the outside minimum temperature by 1 to 5 °C, meaning that night ventilation can be further implemented to help reduce next-day peak air temperatures.

Bhuj Housing

Purpose and Construction

In addition to the scale chambers at MIT and in Bhuj. The research team, constructed four second story homes to look at the impacts of material choices within the above-sheathing ventilation. These chambers were constructed by Hunnarshala in Bhuj based on the results of the field experiments within the prototype test chambers and are in the Ramdev Nagar neighborhood. Using homeowner input, the Hunnarshala team developed a housing design that would substantially fit within the budget outlined by incentives from the national government's Housing for All program, subsidies from the state government, and land grants from the local government. These homes were built in the summer of 2016 and fit for occupancy that fall. Illustrations provided by The Hunnarshala Foundation provide dimensions of the structures, and are shown in Figure 62.

As the sketches help show, the homes are two-story row housing designs that encompass two sleeping rooms, a kitchen, wash room, bath room and courtyard on the ground level. The second level can be left open for families relying on government assistance alone, or another two rooms and terrace can be added with family financing. The structure rest on concrete footers and is supported through a reinforced concrete (RCC) frame with 23 cm thick sandstone walls. The roof of the ground floor is a poured RCC slab, and a parapet wall is constructed of similar sandstone blocks to provide the base for further home additions. For the homes constructed with a second story, this space adds two more sleeping areas, as well as a terrace for social gatherings. After physical construction has been completed, the walls are then covered with plaster and typically painted with light colors or whitewashed with hydrated (slacked) lime.

Ridge vent

Tin sheet

Cross Section of Housing for All Home with
Double Layer Tin Roof and Ridge Vent

N

2.10

0.90

ROOM 3   ROOM 4   TERRACE

0.70

2.90

2.10

ROOM 2   ROOM 1   VERANDA   COURTYARD

Ridge tile

Cross Section of Housing for All Home with
Double Layer Clay Tile Roof

Wooden beam

N

2.10

0.90

ROOM 3   ROOM 4   TERRACE

0.70

2.90

2.10

ROOM 2   ROOM 1   VERANDA   COURTYARD

GL ± 0.00

4.72

COURTYARD
BELOW

N
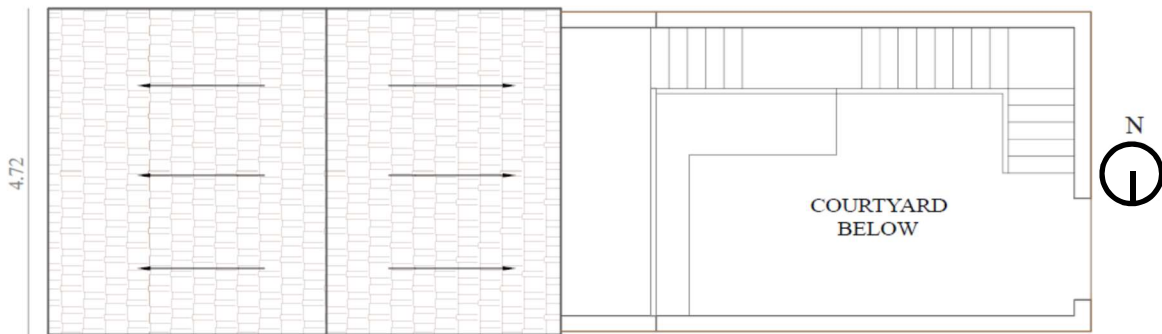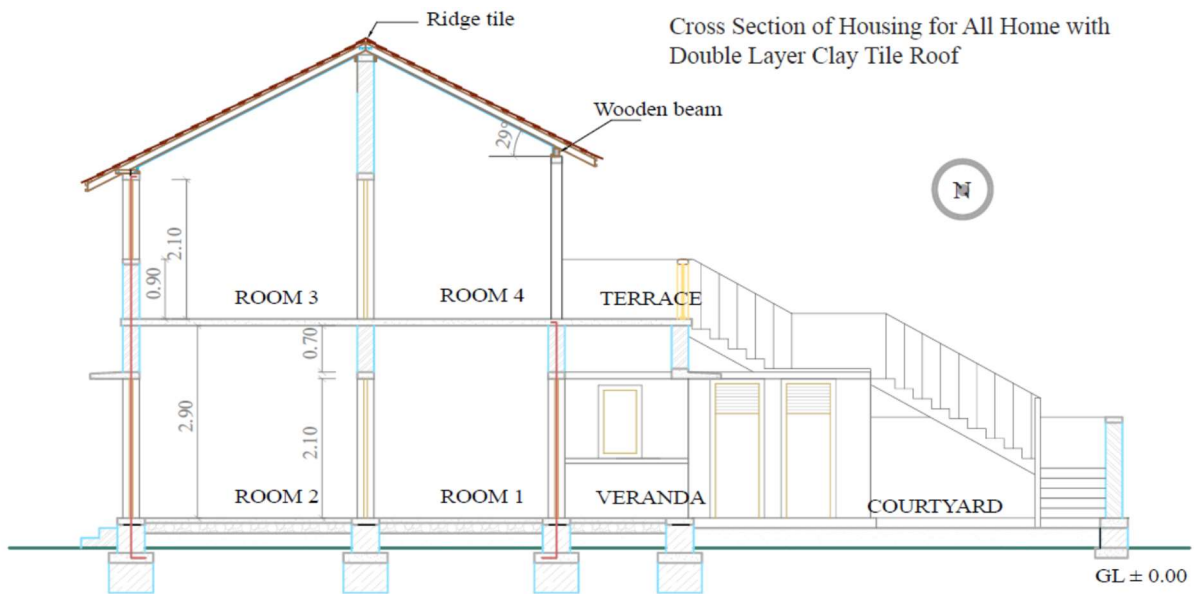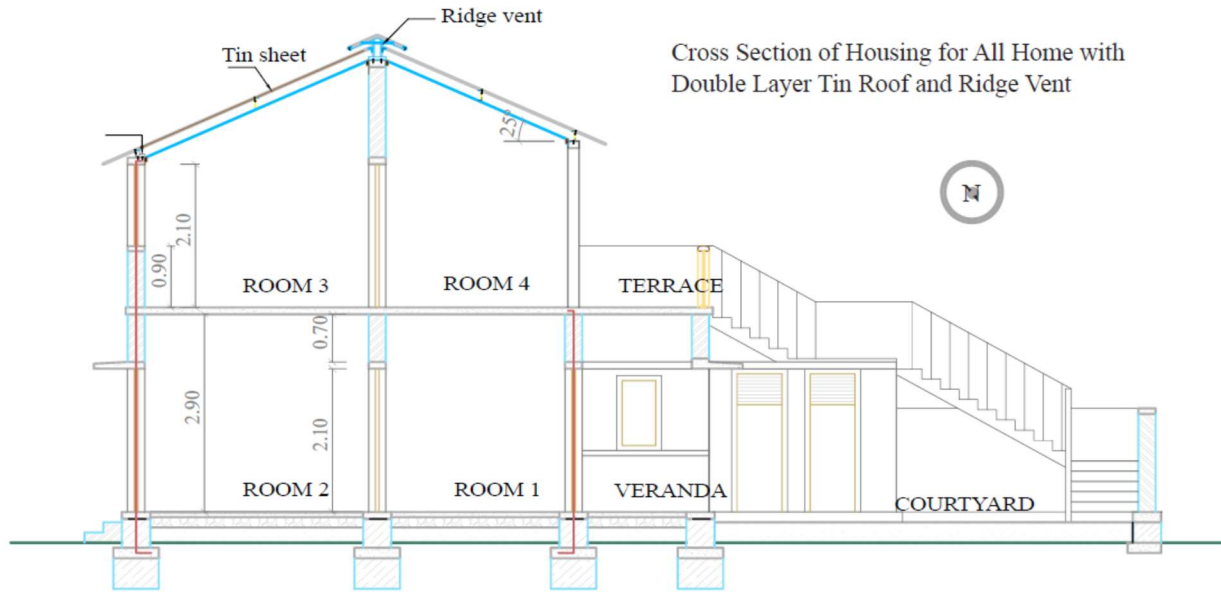
Units in Meters (m)

Figure 62: Housing for All section views and plan view (Hunnarshala, Nelson)

105

Figure 63: Ramdev Nagar homes under construction, Summer 2016 (Photo Credit Tejas Kotak)

Three of the four homes are shown during construction in Figure 63. All four homes all had a peaked roof, and the ridgeline was shared a North-South direction. The roof types were:

- A two-layer roof composed of local, traditional Mangalore tiles as the upper layer, with a layer of aluminum foil-faced cardboard facing an air cavity. Below the 15 cm air cavity, mud rolls create an air-impermeable layer between the interior of the home and the air cavity.
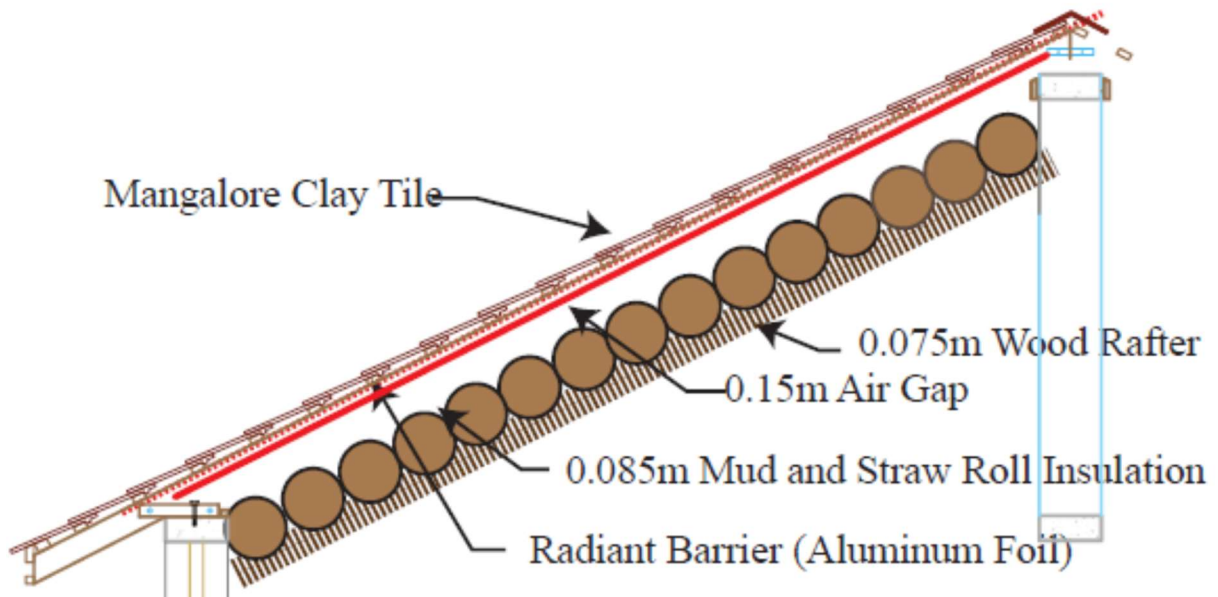
Figure 64: Mangalore Tile with Mudroll Ceiling roof section (Nelson, 2017) and as-built

An important distinction of this home is that the homeowners have allowed the Hunnarshala Foundation to use their second story as a field office, and only inhabit the home during the evenings, when it is used for sleeping. This leads to a different occupancy schedule that a typical bedroom. The home is painted white on all four walls, and each window has a wooden shutter.

- A two-layer roof composed of local, traditional Mangalore tiles as the upper layer, with a layer of aluminum foil-faced cardboard facing an air cavity. Below the 15 cm air cavity, a wooden ceiling creates an air-impermeable layer between the interior of the home and the air cavity.
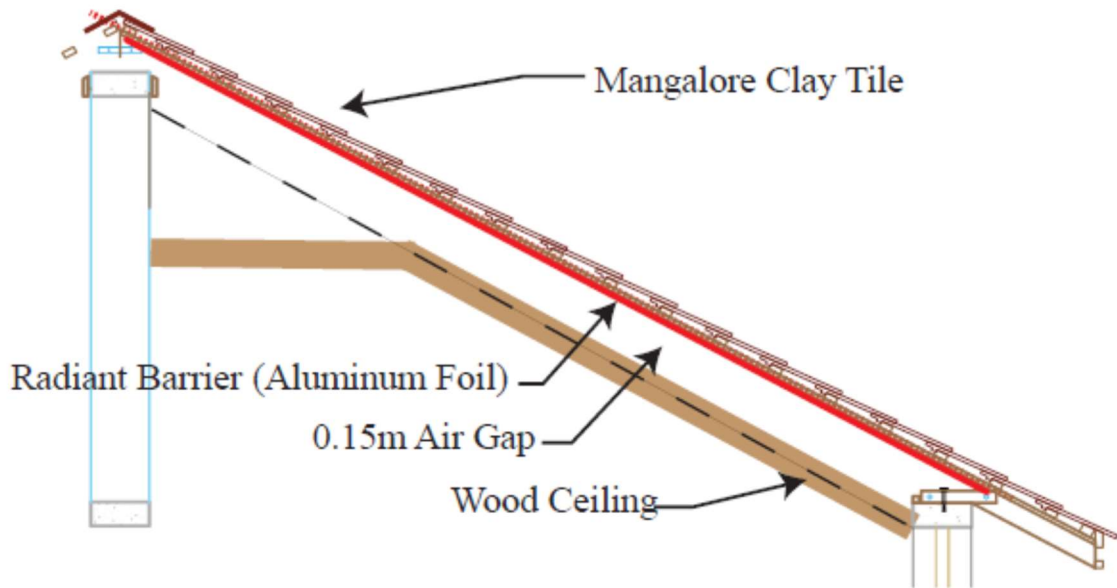
Figure 65: Mangalore Tile with Wood Ceiling roof section (Nelson, 2017) and as-built

This home was painted white on the east, south, and west faces, and was largely used as a storehouse for quilt-work and bedding that the family produced as a cottage industry. As such, the homeowners reported that the windows and doors tended to remain closed throughout much of the day and night. This would remove the night ventilation component that Nelson advocated for, and cause the air temperatures to be greater for the duration of a 24-hour day.

- A two-layer roof composed of white-painted exterior, aluminum foil-faced interior corrugated galvanized iron (CGI) sheet. Below the 15 cm air cavity, a wooden ceiling creates an air-impermeable layer between the interior of the home and the air cavity.
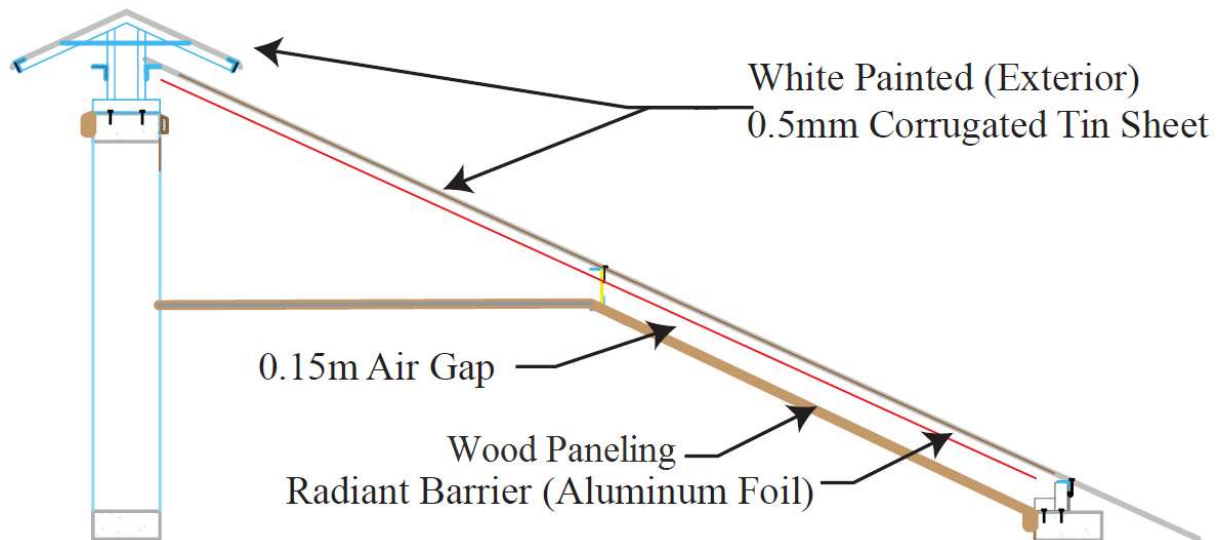
Figure 66: Corrugated Metal Sheet with Wood Ceiling roof section (Nelson, 2017) and as-built

An important distinction of this home is that the south-facing window has security bars but no shutters, meaning that airflow through both this South-facing window, and a similar window on the east face would remain unobstructed. However, in fall of 2017, the team observed that the homeowners had placed a quilt over the window to block the sunlight reaching into the space during the day. This quilt would also help impeded airflow. The outside walls of this home were painted white on all four sides with the exception of a 10" brown stripe highlighting the RCC frame running to the peak of the roof. Additionally, in this home, the central wall ran between the floor and ceiling to provide privacy between the two upper rooms.

- A two-layer roof composed of white-painted exterior, aluminum foil-faced interior corrugated galvanized iron (CGI) sheet. Below the 15 cm air cavity, a layer of 4mm foil-faced bubble wrap faces the air cavity while a tin sheet supports the bubble wrap and helps to ease fire safety concerns.
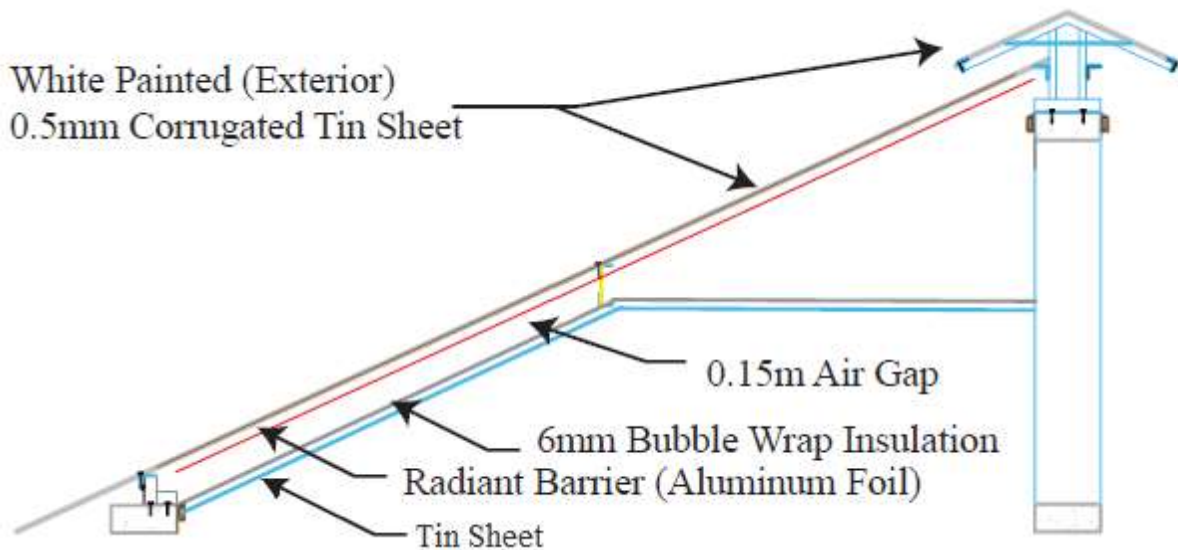
Figure 67: Corrugated Metal Sheet roof with Bubble Wrap and Metal Sheet roof section (Nelson, 2017) and as-built

This home was the last to be painted (March 2017), and was whitewashed on the east, south, and west faces. A water storage tank was also installed in the home summer of 2017 to help provide pressurized water to the courtyard, kitchen, and wash areas below.

Within each home, the team used Onset HOBO® UX120-006M four-Channel Analog Data Loggers with four steel temperature probes placed within each home to measure the south wall, ceiling, air, and radiant temperatures on 30-minute synchronized intervals. The rough placement of these meters are shown in Figure 68 and vary slightly from each other due to concerns about homeowner interference and ease of installation.

110

CROSS SECTION

1.5m
52°
2.1m
2.1m
1.75m
2.4m

PLAN VIEW

1.5m
1.5m
4.72m
1.5m
0.8m
1.5m

⊕ Air Temperature ◉ Inside South Wall Temperature ● Mean Radiant Temperature ○ Inside Ceiling Temperature

Units in Meters (m)
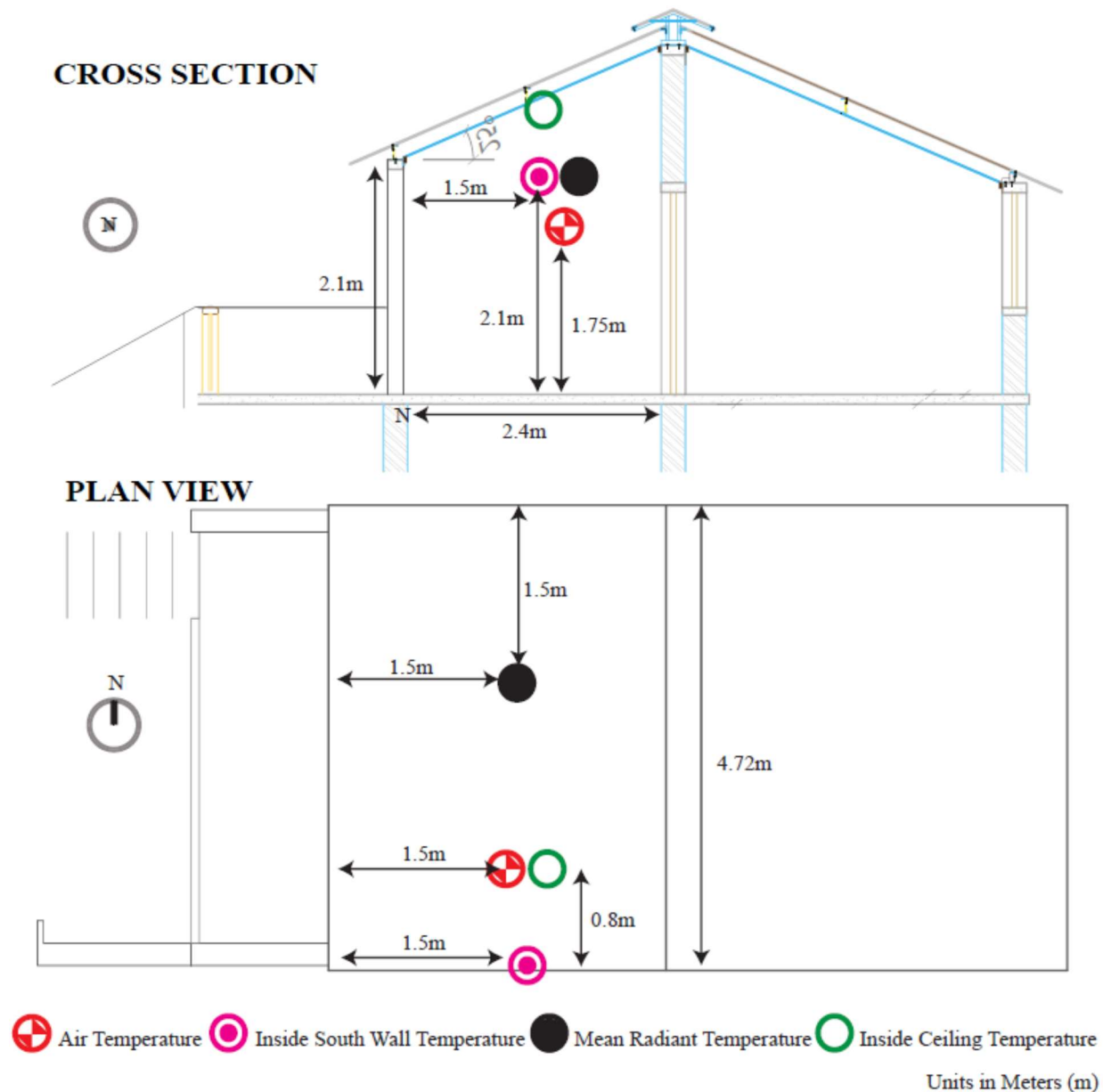
Figure 68: Sensor Placements within the double layer roof typologies (Nelson, 2017)

These data points were collected at the same synchronized intervals as an Onset HOBO® Micro Station (H21-USB) recorded data from wind speed (S-WSB-M003), wind direction (S-WDA-M003), solar radiation (S-LIB-M003), and temperature/relative humidity (S-THB-M002) sensors. The team installed all of these sensors in January of 2017, and the sensors were launched on January 21, 2017. The team then recovered data monthly and continued collecting data through May of 2018. This allowed the team to monitor the performance of the homes remotely and to assess and correct any metering issues that may have presented. Additionally, the team monitored an informal home from January of 2016 through May of 2017, allowing the team to compare the thermal performance of the test chambers with the informal home.

Figure 69: Informal Home exterior (Gradillas, 2015) and interior (Nelson, 2017)

Measurement Results and Discussion

Similar to the test chamber data, the data recovered from each of the homes was averaged hour-for-hour over a duration of interest and compiled into an 'average day', which allows the team to eliminate noise and look at the overall thermal performance. Looking at the air temperatures, a typical day for an entire year (January 2017 to January 2018) is shown in Figure 70.
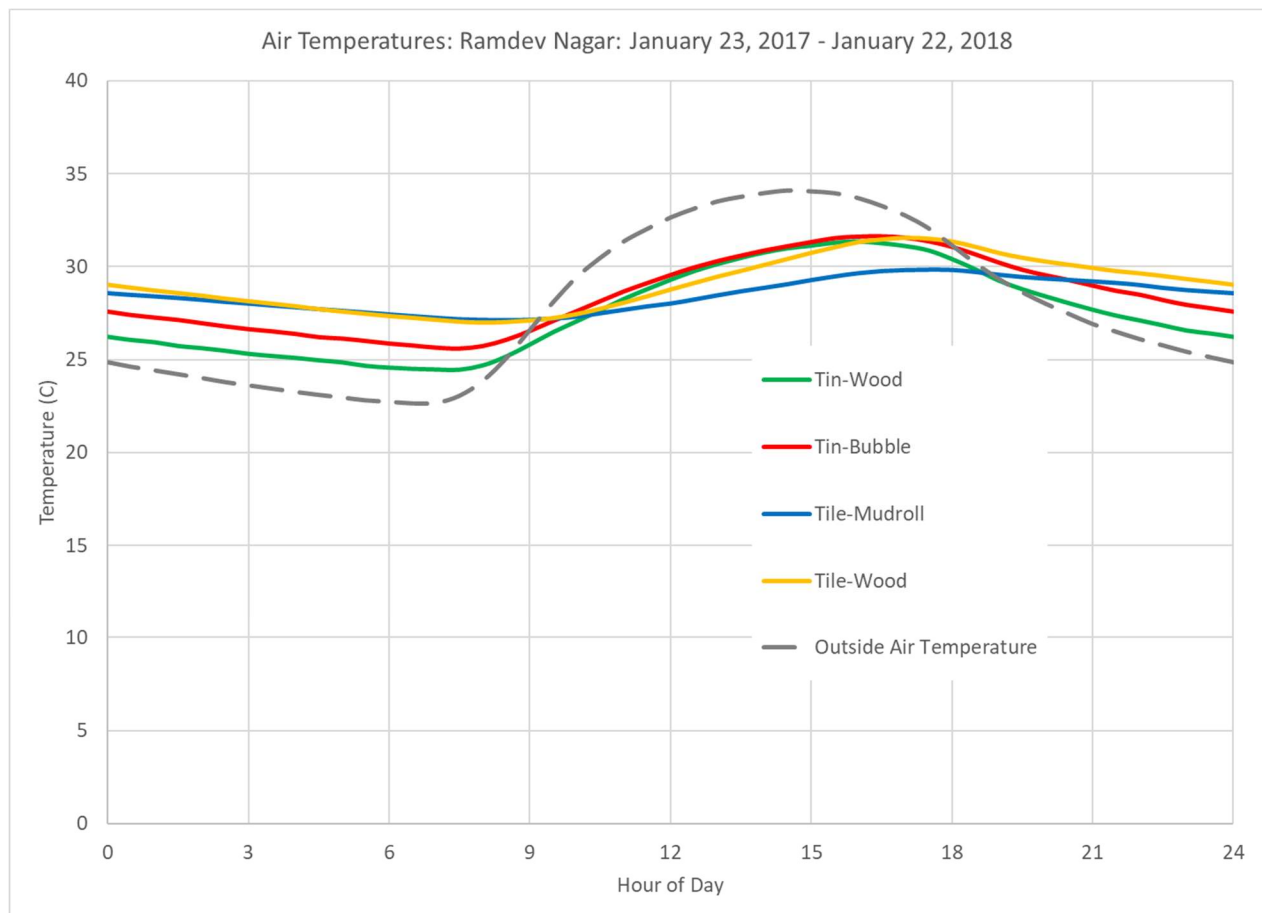
Figure 70: Air Temperatures in Ramdev Nagar homes, January 2017 to January 2018

Figure 70 shows that in comparison to the outside air temperature, all of the homes with the above sheathing ventilation are cooler than ambient temperatures throughout the heat of the day. Between those homes, the white-painted corrugated metal sheet roofing homes are the warmest during the day and the coldest during the night. In comparison to the outside air temperature, the roofs with the tin upper layer reach a maximum temperature 2.6°C less than the peak outdoor temperature, albeit roughly one and a half hours later. At the peak heat of the day (14:30), the air temperature within the homes with the metal roofs is slightly over 3°C cooler. These homes are also the coolest at night in comparison to Mangalore Tile exterior roofing, on average being 2-3°C warmer than the outdoor air temperature. Between the two metal exterior roofing assemblies, the wood ceiling remained an average of 1.35 °C cooler than the bubble wrap and metal ceiling during the night, and 0.3°C cooler during the day.

The Mangalore tile with mudroll interior remained coolest throughout the day, but performed similarly to the Mangalore tile with wood interior during the night. Similar trends held for the radiative temperature and the ceiling temperatures, although the ceiling temperatures showed a different influence throughout the evening.
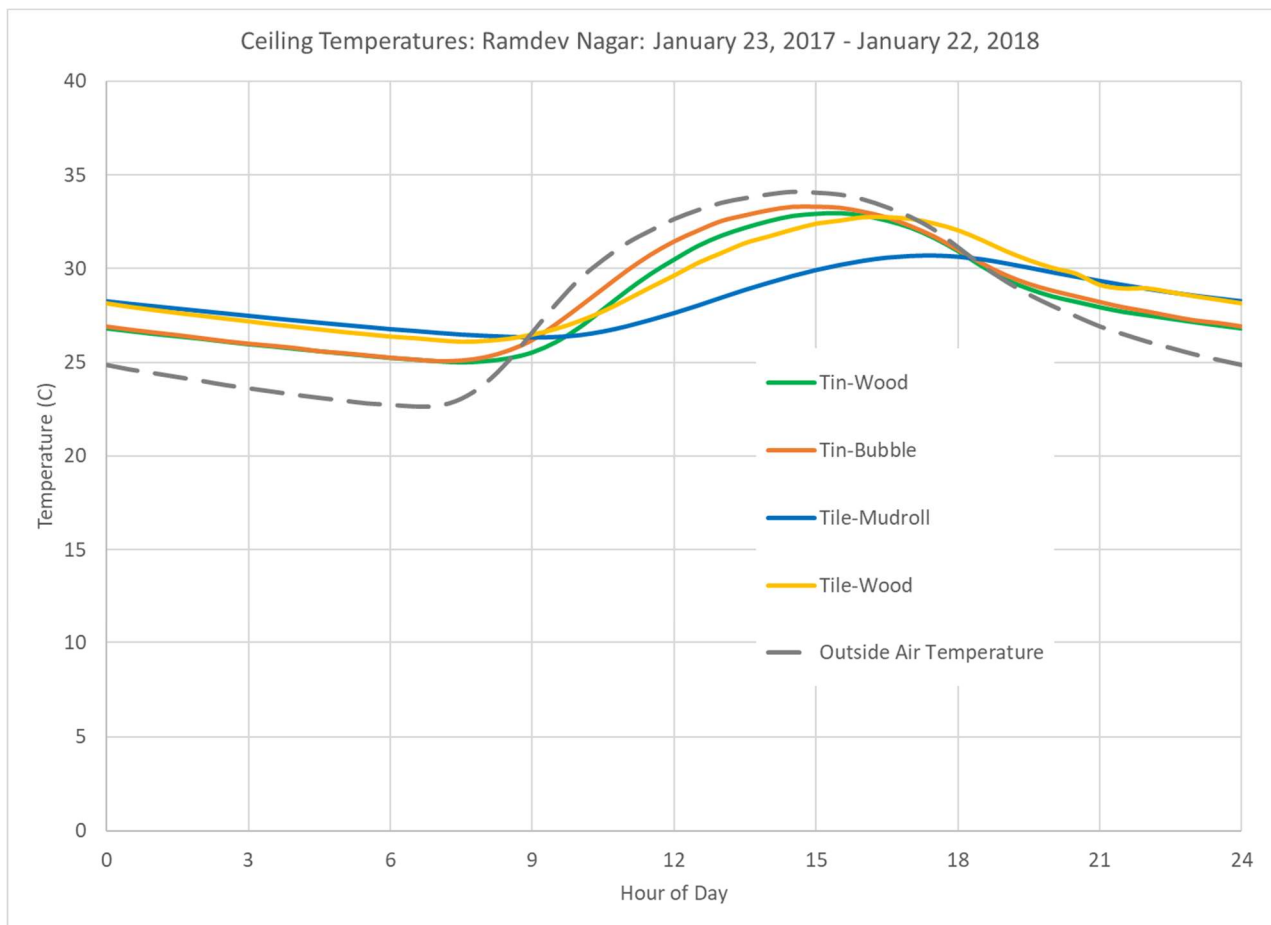
Figure 71: Ceiling Temperatures in Ramdev Nagar homes, January 2017 to January 2018

While the ceiling temperatures are closer to the outside air temperature throughout the day than the inside air temperature, the ceiling temperature shows a clear distinction in the inside face of the ceiling during the night. The low mass metal roofing systems perform similarly to each other, as the temperature profiles are match each other near perfectly. This is without regard to the inner layer. The higher mass Mangalore tile systems on the other hand, stay a consistent 1°C warmer than low mass metal sheeting systems.

Based on these profiles, the exterior layer drives the performance of the roofing system, especially during the night. At night, the addition of mass to the outer layer of the system is detrimental to the interior ceiling temperature in the hot climate of Bhuj. The reverse is true during the day, where the additional of thermal mass to the exterior layer of the system is beneficial. This added mass helps to keep the chambers cooler throughout the year. Moving even farther to a high mass system, the Tile-Mudroll combination remains the coolest throughout the day, keeping the inside of the chamber 5°C cooler than the outside air temperature during the hottest point of the day.

Pursuing this logic further may push the argument for an RCC inner layer in place of the mudroll. The research team would like to heavily discourage this as adding large amounts of mass to the ceiling will increase the chances of failure during an earthquake, leading to structural failures and unsafe conditions.

Where the yearly data is helpful for academic audiences, the homeowners in Bhuj were most concerned with the performance during the hottest period of the year, April and May. The air temperatures for these months are shown below in Figure 72.
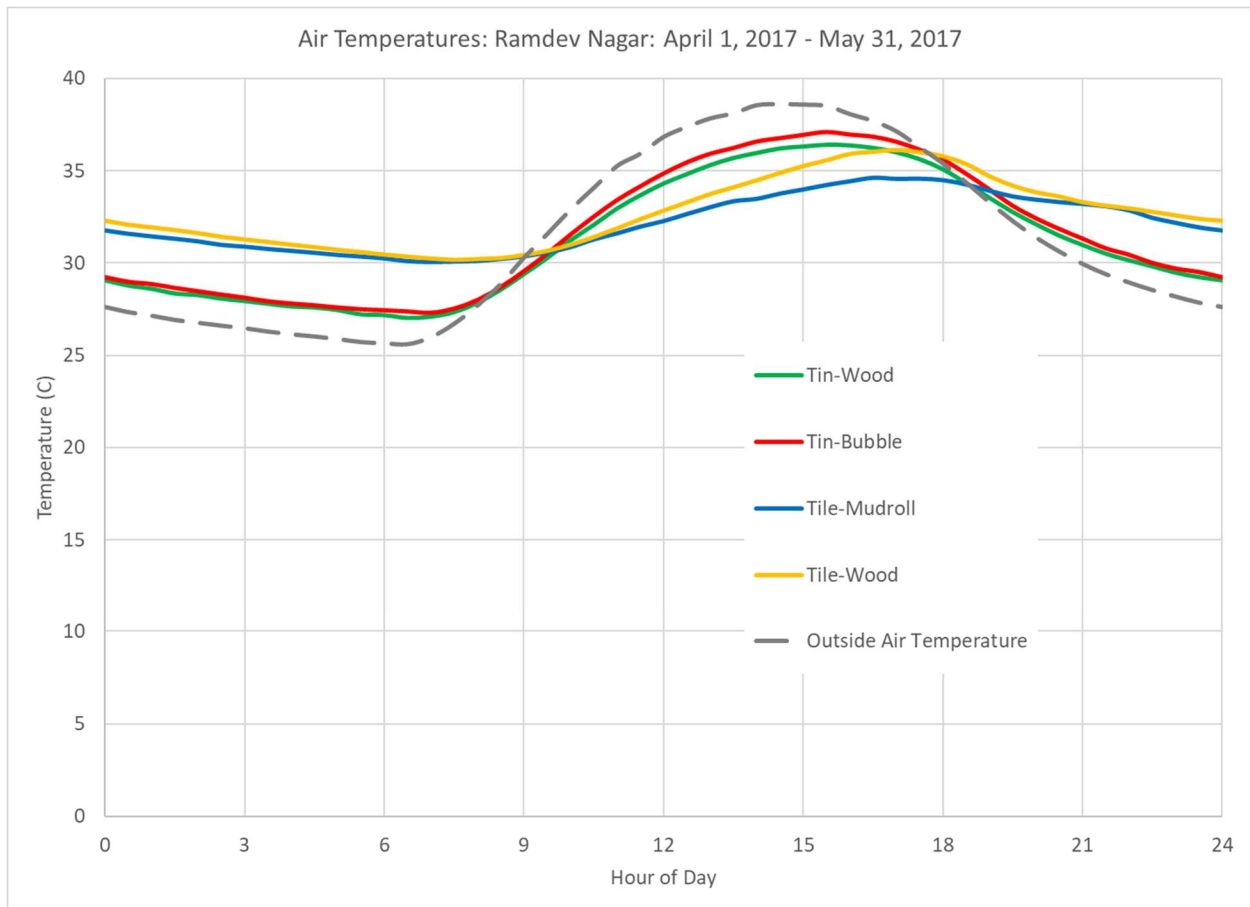
Figure 72: Air Temperatures in Ramdev Nagar homes, April 2017 and May 2017

As the summer months show, the Mangalore tile roof systems remain coolest throughout the day, and warmest throughout the night. In fact, the pairing of the outer surface profiles are consistent up until monsoon season in June of 2017, when the separation begins to become apparent and remains apparent until the end of the monitoring period. Where the homes were largely unoccupied during the January 2017 visit, the tile and wood roof home had been occupied by August of 2017, and this change can be due to the fact that the home's doors and windows went from being largely open to remaining closed for security regions.

In the hottest months of the year (April and May), the Mangalore tile systems allow the air temperature to remain roughly 5°C warmer than the outside air temperature during the night, and 4-5°C cooler during the day. The Mangalore tile with mudroll roof system remains 5°C cooler while the Mangalore tile with wood ceiling system remains 4°C cooler than the outside air temperature at the peak point in the day. The air temperatures in the homes with metal sheeting roof systems only provide a 2-2.5°C cooler air temperature than the outside air temperature during the heat of the day. During the night, these systems are similarly 2°C warmer than the outside air temperature.
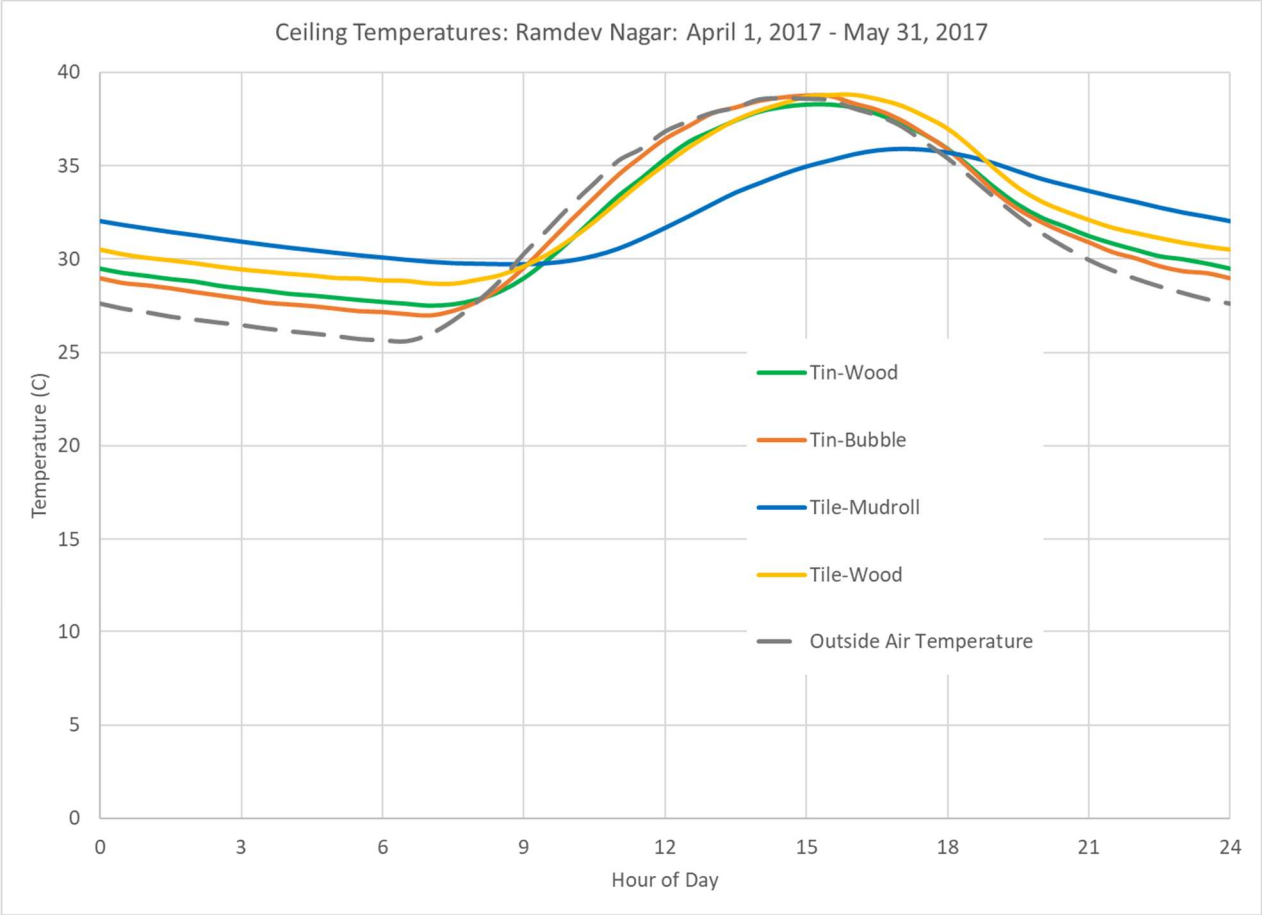
Figure 73: Ceiling Temperatures in Ramdev Nagar homes, April and May 2017

During the summer months, the ceiling temperatures have a different role than throughout the year. The Tile-Mudroll combination continues to remain coolest throughout the day, owing in part to the thermal mass. The other three systems slightly lag the outside air temperature, exceeding it as the temperature decreases in the early evening. The table below lists the values of each system at the time of the warmest and coolest outside air temperature, for April and May 2017. The values are color coded within each column for easier identification.

Air Temperatures [°C]	Warmest Outside (14:30)	Coolest Outside (6:30)
Outside	38.62	25.61
Tin-Wood	36.22	27.03
Tin-Bubble	36.78	27.38
Tile-Mudroll	33.77	30.11
Tile-Wood	34.9	30.35

Table 28: Air Temperatures Corresponding to the Warmest and Coolest Outside Air Temperature for an average day (April and May 2017)

Lastly, these above thermal performance numbers have little meaning to the homeowners who currently live in informal or improvised housing. As mentioned above, an informal home was also instrumented with a steel-encased thermocouple attached to an Onset HOBO® UX120-006M four-channel analog data logger from January 20th, 2016 to May 21st, 2017. The data collected by this UX120-

006M was every five minutes and aligned with the top of the hour, similar to the others. The team used this dataset and selected the half-hour increments that correlated with the four second level homes, as well as curtailed the comparison period to a time period when all of the loggers were recording air temperature. In this case, that was between January 20th, 2017 and May 21st, 2017. The results of this comparison are shown below, in Figure 74. The informal home was also located nearby to the Ramdev Nagar community, so outside air temperature changes between the two locations due to the Urban Heat Island effect can be ignored.
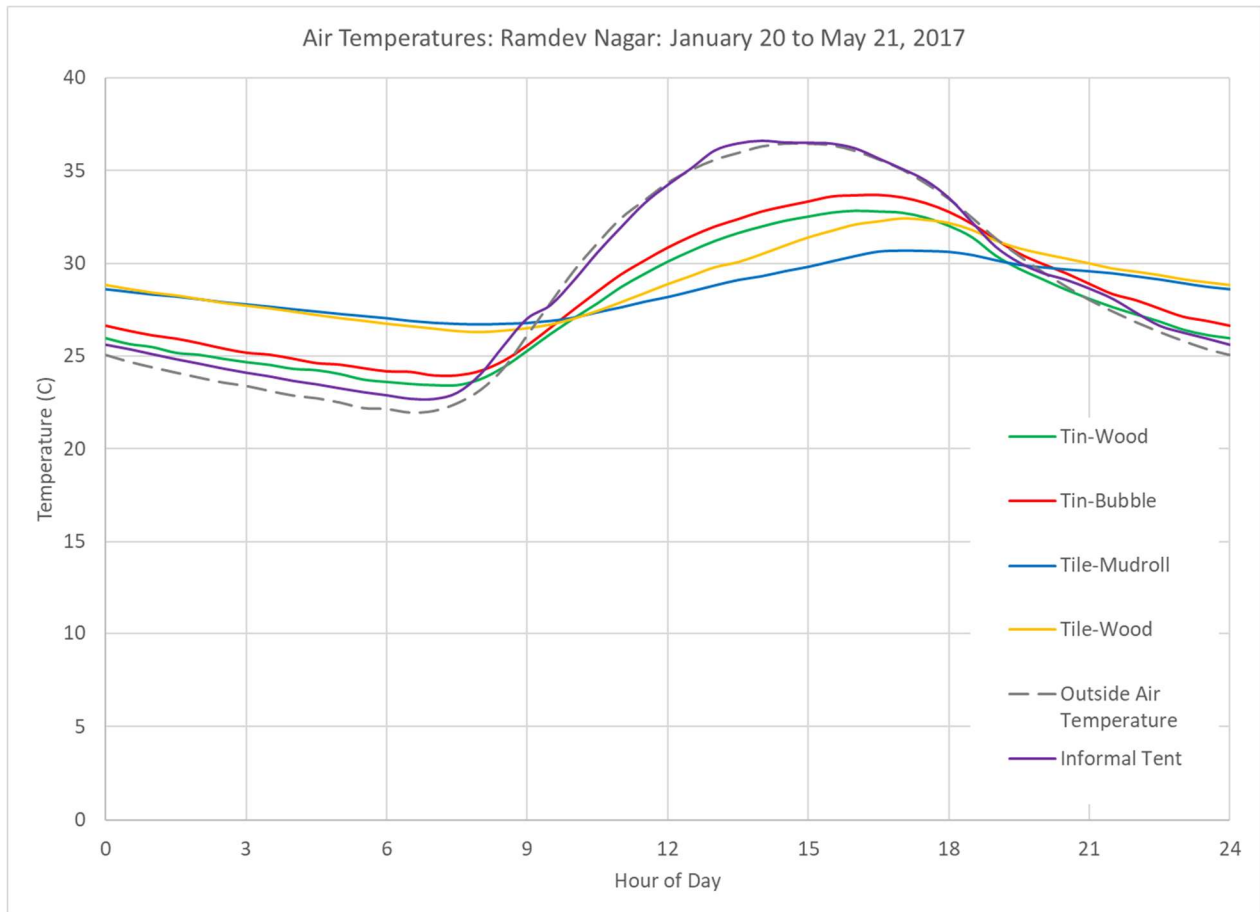
Figure 74: Air Temperatures in Ramdev Nagar homes, January 20 to May 21, 2017

As Figure 74 helps show, the air temperature within the informal tent housing are largely indicative of the outside air temperature for the Spring and Summer months. This is not surprising, as the informal tent is air permeable, and the elevated temperatures at night may be due to occupants sleeping in the space or residual heat in the ground below the home.
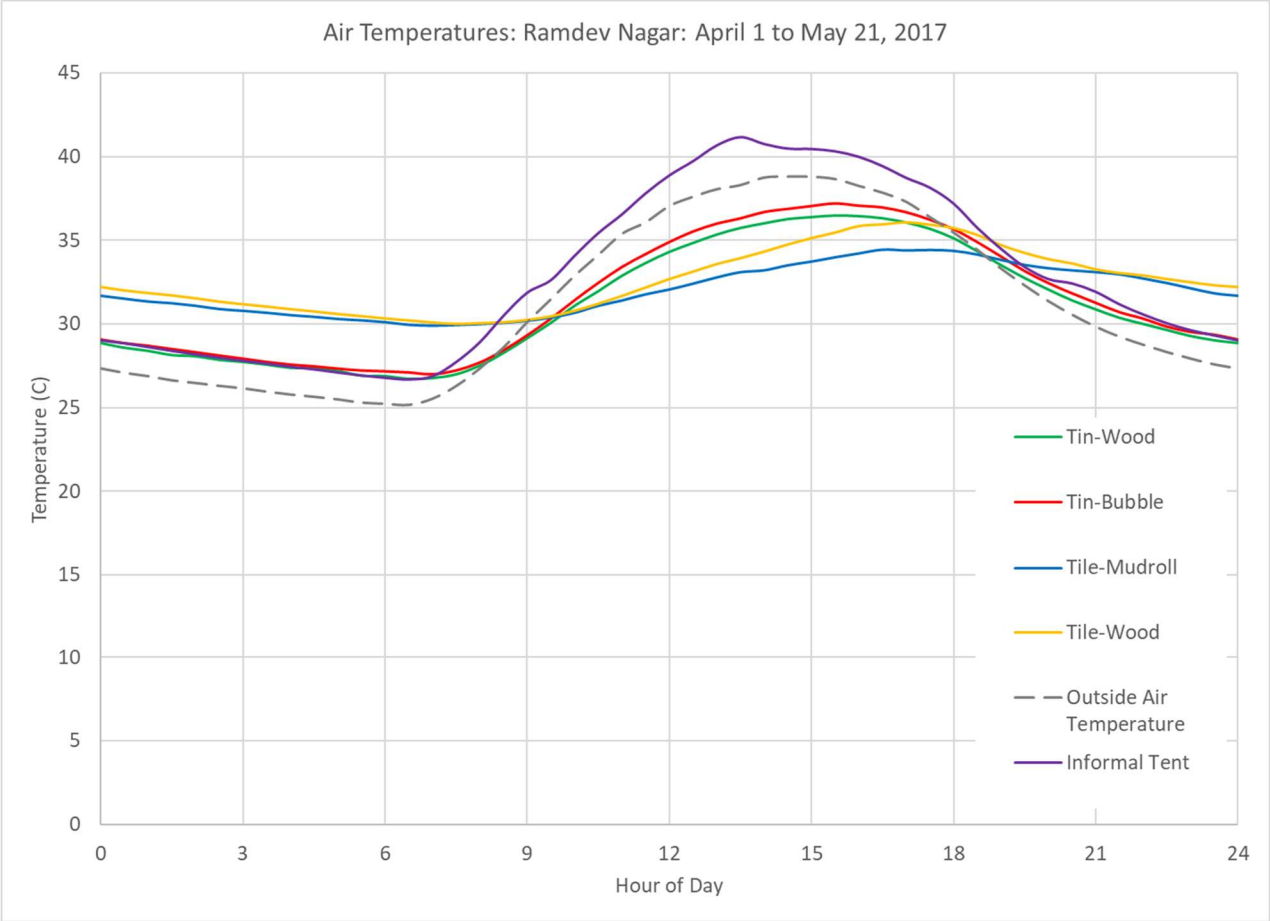
Figure 75: Air Temperatures in Ramdev Nagar homes, April 1 to May 21, 2017

Looking closer at the summer months in Figure 75, it becomes apparent that the informal tent housing can become up to 3°C warmer than the outside air temperature during the day, and remains around the same temperature as the metal sheeting roof systems during the night. This changes the narrative slightly, where the previous comparisons were to the outside air temperature, as the informal tent housing produces much warmer air temperatures during the day, the double layer roofing system coupled with a more substantial structure helps to provide a significant step toward thermal comfort.

Air Temperatures [°C]	Warmest Outside (14:30)	Coolest Outside (6:30)
Outside	38.81	25.16
Tin-Wood	36.48	26.72
Tin-Bubble	37.20	26.99
Tile-Mudroll	34.44	29.90
Tile-Wood	36.07	30.00
Informal Tent	41.17	26.68

Table 29: Air Temperatures Corresponding to the Warmest and Coolest Outside Air Temperature for an average day (April 1 to May 21, 2017)

As the passive features of these homes are primarily designed for increased thermal comfort and decrease mortality during heat waves, it may be of more importance to look at the performance of the home during these extreme weather events. To compare the test houses against the informal tent

home, the team confined the data to the day with the hottest outside air temperature of the duration of the mutual measurement periods. This day, 13 April 2017, reached a maximum outside air temperature of 45.5°C. Similar to the previous data, the informal tent climbed to 3°C warmer than the outside air temperature. The test homes remained between 5 and 9.5°C cooler at this point in the day.

Air Temperatures [°C]	Warmest Outside (14:00)	Coolest Outside (7:00)
Outside	45.53	27.11
Tin-Wood	39.19	29.85
Tin-Bubble	40.22	30.90
Tile-Mudroll	37.45	32.30
Tile-Wood	35.98	32.81
Informal Tent	48.61	26.87

Table 30: Air Temperatures Corresponding to the Warmest and Coolest Outside Air Temperature for the hottest day in the measurement period (April 13, 2017)

With this data, the tile roof systems remain cooler than the metal roof systems, and both remain substantially cooler than the informal tent. The research team is unsure why the wood system performance was cooler during this day, but implementation of nighttime ventilation could be attributed to a 1.5°C change in temperature several hours later.

Based on data of district-level mortality rates in India from 1956-2000, the team applied the data points listed in Table 30 to a log-linear extrapolation of Burgess' projected total death rate in rural India as a function of temperature (Burgess, Deschenes, Donaldson, & Greenstone, 2017). The three temperatures of 48.5°C (Informal Tent), 45.5°C (Outside), and 36°C (Tile-Wood) would produce mortality rate elevations of 11.0%, 8.4%, and 3.5%, respectively. These values are all given to a baseline normalized value between the 22-24°C temperature range. As such, the passive thermal housing helps to reduce the mortality rate within the structure by 7.5 percentage points, a non-trivial number. Assuming that the occupants of the home are a representative sample of the population, this would be a conservative estimate if occupants remained proactive about remaining hydrated and staying out of the direct sunlight.

Outside of mortality rates, these conclusions have significant implications for comfort as well. Figure 76, adapted from Nelson, shows the implications of the shift of temperature from the peak outside air temperature to the temperature of the Tin-Wood home at the same time. Within this figure, the horizontal axis is the average temperature over the previous 30 days, which is 30.2°C in this case. As the figure shows, the outside air temperature is significantly outside the range of the 80% acceptability comfort standards for the three listed comfort standards. On this plot, the informal tent home would be off the top of the chart, and so the chart shows a conservative case.

While the test homes greatly reduce the temperature, the values are still 2-5°C out of the specified comfort ranges. Of course, there is more to the comfort standards than temperature alone, and so ceiling fans or standing fans would likely be utilized if possible. It should be noted that in the case of the informal home, or a single-layer metal roof, utilization of a ceiling fan may not be an optimal choice, as it may increase the heat transfer from the hot ceiling into the space. Nelson elaborates

further on this decision. For the two-layer roofing design testing in the homes, there is less consideration required, and a ceiling fan should be appropriate.
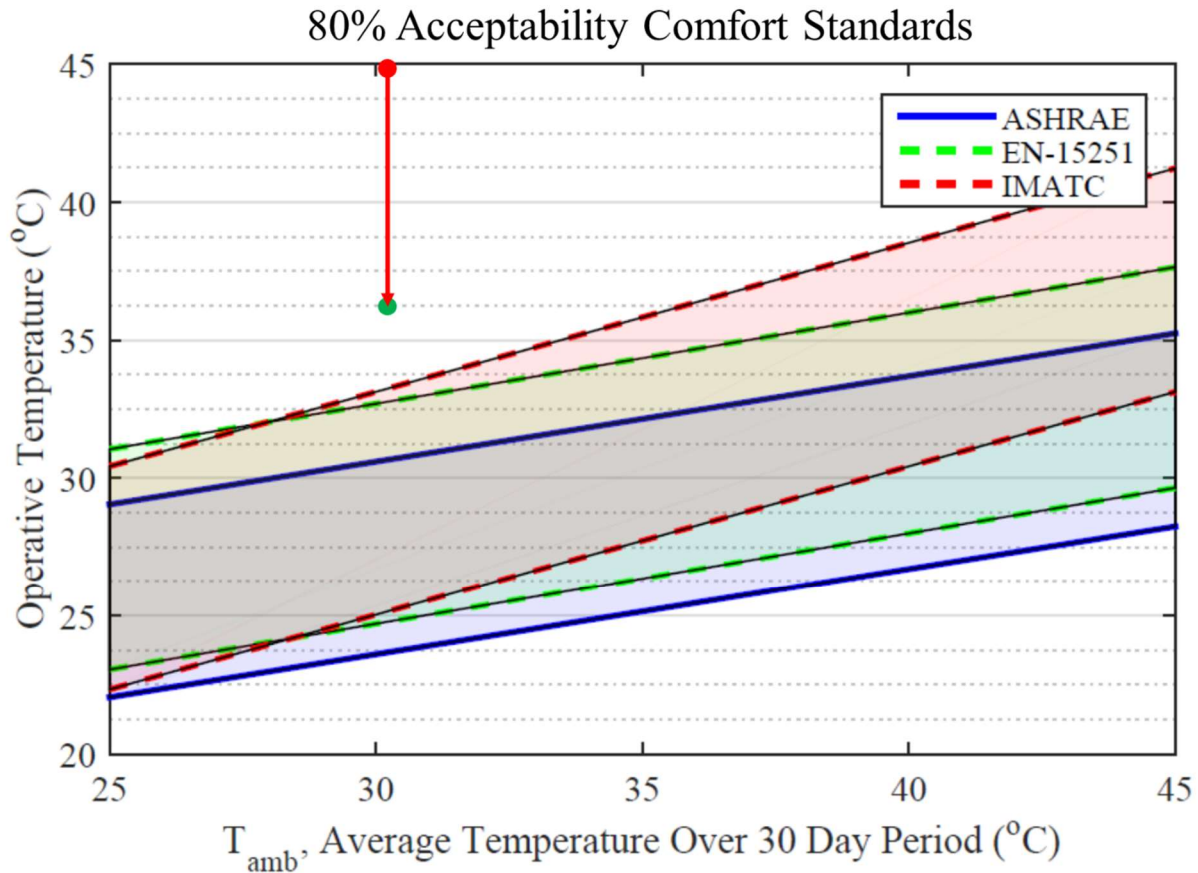
Figure 76: Acceptability of Various Thermal Comfort Models, adapted from Nelson

Conclusions

This information helps to validate the influence of modifications to the double layer roofing system (above-sheathing ventilation). Where the mass of the outside layer helps to maintain a cooler indoor air temperature throughout the day, it also remains warmer throughout the night. Adding in the thermal mass and insulative properties of the mudroll allows the home to remain coolest throughout the heat of the day, based on the homes tested. Especially in comparison to the informal tent baseline, the Mangalore tile and mudroll combination helps keep the home nearly 7°C cooler at peak daily temperatures.

Further, the in-depth look at the extreme weather events (~45°C) is of extreme importance for the associated reduction in increased mortality rates, where utilization of Burgess allows the team to claim a reduction in the mortality rate of 7.5 percentage points over the outside air temperature condition and on a normalized mortality rate near 22°C. When applied to comfort standards, the as-built homes are unlikely to fully meet the comfort conditions with stagnant air conditions. Coupled with increased air movement or evaporative (swamp) cooling systems, the as-built test homes can help meet the upper limits of the comfort standards.

Nepal Housing

While not a core component of this thesis, this chapter has been added to help communicate and apply observations drawn from the January 2017 and January 2018 trips to new and existing construction in Nepal. This chapter presents observations on building construction quality, data and results from one year of temperature monitoring, and suggestions for under-utilized applications of locally-sourced materials within the building.

Introduction and Background

Building on the lessons learned from thermal avoidance strategies in Bhuj, the research team sought to apply elements of the design to another Hunnarshala project in Nepal. Although climatically different, Nepal experienced a 7.8 magnitude earthquake in April and of 2015, directly causing nearly 9,000 deaths, 23,000 injuries, 594,000 homes destroyed, and 280,000 homes damaged (Barry, 2016; Government of Nepal: National Planning Commission, 2015). Consequently, over 8 million people have been affected by the earthquakes, in addition to the repairs necessary for infrastructure and services (Simkhada, van Teijlingen, Rant, Sathian, & Tuladhar, 2015).

With Hunnarshala's existing experience in building earthquake-resilient homes, a Hunnarshala Foundation and Lumanti Support Group for Shelter ("Lumanti") collaboration has provided engineering support for residential building activities in Nepal. Contributing to this collaboration, the research team offered to provide recommendations for the thermal aspects of building construction in and around the Kathmandu Valley within Nepal.

The research team traveled to the region in January of 2017 to assess the existing building typologies, social perspectives, building construction, and thermal performance. During this initial visit, the team focused their efforts on villages in the Chitlang region (27°38'18.30"N, 85° 9'57.98"E), as well as a remote religious community in the Chagam region (27°55'27.30"N, 85°51'53.34"E). As part of the initial assessment, the team installed data loggers to measure point temperatures and weather conditions in the Chitlang village and performed an initial assessment of the building typologies and construction methodologies.

From the field visits outside of the urban environment, the team learned about reconstruction efforts using both the indigenous housing methods and newer reinforced concrete (RCC) methods. Funding for this new construction is assisted by a grant from the government of Nepal to families impacted by the earthquake (The World Bank, 2017), and supplemented with savings or loans from banks and financial cooperatives.

The first indigenous housing typology, seen in the valleys and mid-level regions around Kathmandu, stems from the Newari tradition and are historically constructed from stone and mud mortar, with a bitumen-coating corrugated metal sheet roof and mud plaster wall coatings. In practice, the ground level is typically used as a dry storage area for farm products or as shelter for animals, leaving the second floor for living and sleeping areas, and the third floor for a kitchen and eating area.

Figure 77 shows a typical house constructed in the Newari style. It is not atypical to build houses into slight hills, and this house exhibits many of the characteristics common to the regionally indigenous housing style. The walls are made of a stone and mud mortar, with larger squared-off rock as the corner stones of the building. This particular house has been reinforced with timber within the wall construction to help reinforce the wall. However, due to the limits and expense of acquiring long timbers for construction, this practice is not universal. An existing technique of using flattened oil barrels as the roofing layer was common practice up until recently, and the bitumen remaining on the steel sheeting also helps to protect the metal from oxidizing. The bitumen remains fluid though, and several homeowners mentioned that condensation would form on the roof at night, causing a black line to appear on the ground where the bitumen-carrying condensate runs off the end of the roof. In lieu of recycling oil containers, galvanized corrugated metal sheeting is commonly used to repair the roofing of these homes.

Figure 77: Newari Architecture, Chitlang, Nepal

Figure 78: Timber-reinforced Stone and Mud construction, Chitlang, Nepal
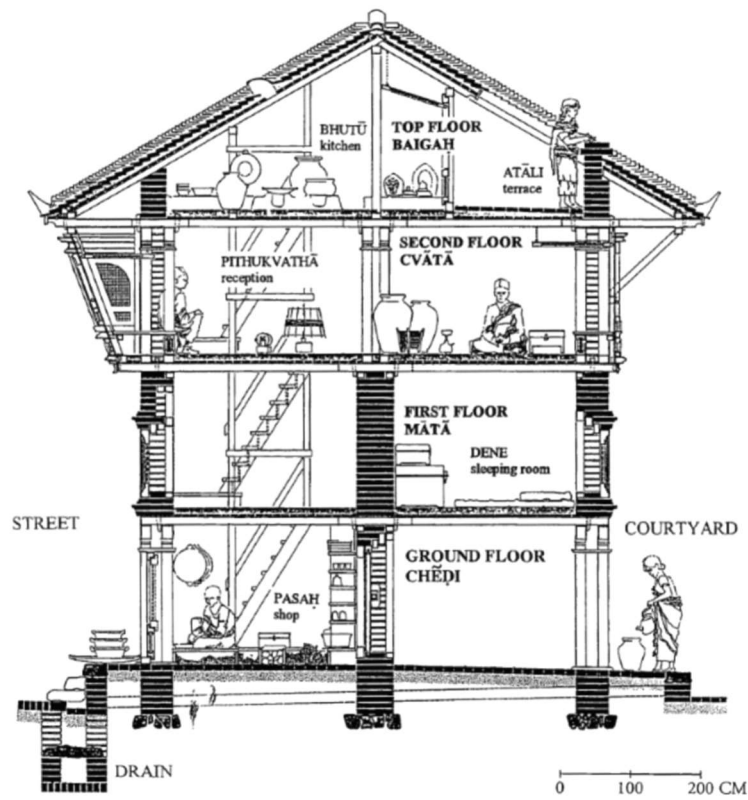
Figure 79: Cross Section of a typical four-story Newari structure (Gutschow, 2011)

For more affluent families, the public-facing outside façade of the home may have additional plaster coats and paint. While primarily aimed at aesthetics, this practice is also helpful in extending the longevity of the mud mortar, which helps to bind and secure the stones within the wall. During the 2015 earthquake, weak mud mortar frequently played a role in delamination of wall cross-sections and building collapse (Dizhur, Dhakal, Bothara, & Ingham, 2016). Restoration efforts have been slow going and hampered by social and economic influences.

Figure 80: Newari architecture surface coatings, Chitlang, Nepal

Based on discussions with the community and the project managers, the population of Nepal is emigrating from the rural villages to the Kathmandu valley for education and jobs, returning only to their ancestral villages for holiday and familial events. Despite this trend, reconstruction in the rural villages continues as the urbanites seek to rebuild their family homes for older family members. This pursuit is complicated by the lack of building expertise outside of the older generations. In interviews with the project managers, the project managers stated that the skills learned in the Nepali building trades would command higher incomes outside of Nepal, and so the Nepali building industry was lacking an appropriately-skilled labor force. The implications of some of the lost institutional knowledge is observable in the recent building construction, and mentioned later in this chapter.

The team also traveled to the Chagam religious community in January of 2017 to understand building trends in an extreme resource-constrained environment. This particular community is a group of 200 Tibetan nuns whose homes were substantially destroyed by the 2015 earthquake and were left homeless until Hunnarshala helped reconstruct their homes with support of the American Jewish World Services (Dolma, 2016). The nuns live in an area that is located high on a mountain, a day's walk to the nearest road and a day's walk from the border between Nepal and Tibet. The remoteness of such a location represents an extreme design constraint for Nepal, but the housing style is typical of this region, and a related building style was observed nearer to Kathmandu in Chitlang.

These rural homes share many similar characteristics and building methods to the traditional multi-story Newari architecture, but overall construction is limited to a single story. The roofing is typically metal sheeting, where the attic space is either a nonfunctional space separated from the main living area by a lightweight cement board ceiling, or is a cooking and storage space supported by wooden joists with perpendicular lath strips holding a mud floor layer.

The Chagam community utilized the former approach, opting for a cementitious board separating the living space from the attic space, and helping interior aesthetics, acoustics, and thermal performance over the bare metal roofing. Structurally, this housing style (Figure 81 and Figure 82) incorporates a modified ring beam into the construction through a reinforced concrete band at the height of the ceiling or a steel frame tied back to the foundation for earthquake protection. Further, where plastering the walls is commonplace for aesthetic reasons, it improves the thermal performance as well through a reduction in the infiltration rate. Older work from Houghten and Ingels (1927) showed a decrease of the air infiltration rate through a plain 8 ½" thick brick wall of 99% with the addition of two coats of prepared plaster, at a 5 mph wind velocity (Houghten & Ingels, 1927). Lecompte (1987) later confirmed that a 90% - 99% decrease in air infiltration rates can be attained by pointing joints and plastering brick walls (Lecompte, 1987). To put this in perspective to a Nepali homeowner, assuming a 2.5 m high, 4 m wide wall at an 18°F (10°C) air temperature difference across the wall and a 5 mph wind velocity, this would correlate to an energy savings of 25.0 kg of wood over a 12 hour period due to the infiltration through the one wall alone. The plastered wall values determined by Houghten and Ingles suggests burning 0.24 kg of wood over that same 12 hour period. Granted, such a difference relies on the definition of what 'bad workmanship' is, and this may be an incorrect baseline for applications in Nepal, as industry-accepted publications only predict an 80% reduction in infiltration due to overall building construction (Rutkowski, 1986).

For a sense of scale, Nepali homes typically burn on the order of 6-10 kg of wood per day in the colder months to heat existing homes (Antony, 2018). Using the above assumptions, this would be on the order of an average air temperature increase of 7-8°F (~4°C). To reduce the fuel required for heating or increase the temperature with the same amount of fuel, infiltration through the walls and around doors and windows would need to be reduced, as well as heat loss through solid surfaces such as the walls, roof, floor, doors, and windows.

Figure 81: Chagam nunnery reconstruction project (construction in progress, January 2017)

Figure 82: Chitlang rural reconstruction (Completed project), Right photo courtesy of Vadim Kuklov

Structurally, the homes been built in collaboration with the Lumanti-Hunnarshala team have been built with the help and involvement of architects and engineers, which show in the continuity of ring beams and load distribution throughout the wall. Outside of this sample, there were many instances where the reconstruction effort did not make use of these building trades, and compounded with the flight of skilled laborers, some of the most profound examples were apparent in homes that were built using Reinforced Concrete (RCC).

126

In the Nepali context, much of what the research team observed within new construction was masonry-infill reinforced concrete construction. RCC is not new to Nepal, but according to the representatives of Lumanti and Hunnarshala in Nepal, it is socially perceived as being stronger and as a symbol of progress and achievement, as opposed to the subsistence farming stone and mud construction.

The flight of skilled laborers is also apparent in several homes visited by the research team in January 2018. On the material side, the team observed that the process for firing bricks lacked temperature-based controls and the powdered lignite fuel was hand fed based on instinct, leaving the final products to be of varying quality. The final bricks used in construction often had signs of deep cracking and void defects by the time they arrived on the job site. When placed in a structure, these inconsistencies will allow the bricks to spall from frost/thaw cycles and compromise the integrity of the brick wall. Where much of the masonry will remain exposed to the climatic elements during the lifetime of the building, the crumbling failure of the masonry walls poses an immediate danger to occupants during an earthquake when the wall may fall or cascade inwards, or when the wall is unable to help buffer the loads placed on the overhead concrete slab.

In Lumanti's role as a social mobilizer and coordinator, the representatives have had little success in convincing homeowners to reconstruct using the a more conventional stone and mud approach as opposed to the more expensive RCC. On the structural side, the conventional stone and mud approach has been strengthened by adding ring beams and by reinforcing the corners of the homes with reinforced concrete, where the stones act as the formwork. Traditionally, some of the ring beams and column support has been accomplished through large timber, which are cost-prohibitive to acquire in the building market. Lumanti's method helps promise a lighter ceiling structure, lower emissions, and more traditional home at lower cost than a comparable RCC structure. However, part of the complication is that much of the financing for new construction outside of the Kathmandu valley comes from relatives in the Kathmandu valley itself, who see RCC being used for new construction.

From the trips to the field and outside of the Kathmandu valley, the research team was able to characterize the typical reinforced concrete home as a two-level dwelling with a central staircase and plaster-covered masonry infill (Figure 83). In these homes, vertical RCC columns are formed and poured on site on top of a previously-prepared concrete footing. These RCC columns are left with exposed rebar to tie into the floor slabs after the walls have been infilled with brickwork. Typically, halfway to three-quarters up the wall, a ring-beam is placed to add rigidity and lateral support to the wall. Ideally, the rebar inside of the ring beam would be tie into the columns. The team was unable to observe these tie-ins in the non-Hunnarshala/Lumanti buildings. Each floor slab is also constructed of RCC and integrated into the columns. According to the design, the weight should then be supported by the RCC columns, so that there is marginal weight on the brickwork.

Within these structures, there was no dedicated central heating, cooling, or insulation. However, more affluent buildings had a liquid propane non-vented space heater that could be turned on

to provide some relief. While having a heater does suggest that the occupants are uncomfortable enough to seek one out, the occupants claimed that they rarely used the heater. Whether by cost or choice, the lack of a dedicated vent on the heater negatively impacts the indoor air quality when the heater is in operation and carbon monoxide and carbon dioxide are allowed to build up (Greiner, 1997).

Figure 83: Active RCC Construction projects (Chitlang, Nepal). Left: Builder constructed, Right: Owner constructed

Within the building construction, the research team was alarmed to find many structural concerns in such new construction. The ring beam, a layer of wood or concrete that horizontally supports a masonry wall, were not integrated into the building columns or integrated between other elements of the ring beam. Without this connection, the masonry walls are at risk of falling in an earthquake. As Figure 83 shows, there were also several cases where wooden window frames structurally support the masonry above, where a window header should be in place. Structural issues are also present in builder-constructed housing and raw materials.

Figure 84: Left: RCC column, Right: Brick delivery (Chitlang, Nepal)

As Figure 84 shows, the current method of pouring RCC columns leaves large voids between the aggregate within the column. While small voids are normal, and even preferable, in RCC mixes, the voids that the team observed in some buildings was excessive. Elements of the steel rebar could be seen

through the external voids, presenting significant risks of water contacting the uncoated steel rebar, causing rusting, promoting oxide jacking (rust jacking), spalling of the concrete, and an overall degradation of the system's structural performance. Further, the voids themselves represent a loss of strength and possible structural failure (Son, Pilakoutas, & Neocleous, 2006). While post construction surveys and inspections from authorized inspectors may help improve build quality, the surface can be covered by a skim coat of plaster or cement, and the voids may go unnoticed.

Figure 84 also shows construction bricks used for masonry infill in the Chitlang area. While it is not uncommon for bricks to be damaged or chipped during packing and shipping (The Brick Industry Association, 2007), the bricks seen around the job sites frequently had cleaves, deep cracks, or non-trivial chips that would increase the chance of masonry degrading at an accelerated rate. Strength-wise, the research team was unable to do any testing to determine the strength or load carrying capacity of the brick.

Of these criticism, many of this issues are not new to the building industry (Jigyasu, 2002). Lewcock proposed a number of criticisms of North Yemenese constructing in 1983 following the 1982 Dhamar earthquake, attributing the destruction of typical Yemeni housing to the following:

" …The builders have become skimpy and careless; building materials and mortars are often poor, foundations weak, wooden ring beams are inadequate and often are not properly joined, and roof beams are of poor quality and too short, with bearing over only a short distance into the walls." (Lewcock, 1983)

In a vacuum, these criticisms are valid, but Barahkat proposed that these failures were all part of the economic pressures that have led homeowners and builders to cut costs by excluding traditional reinforcements (Barakat, 1993). A loss of a skilled workforce can also produce the same effects.

Thermal Considerations

Prior to the field visit to Nepal, the main focus of the research team was on the thermal performance of the housing in Nepal. However, experiences on the ground necessitate a coupling of efforts to improve earthquake resilience, reduce maintenance requirements from unskilled laborers, and improve thermal comfort. Based on the team's interactions with homeowners during both trips, homeowners actively stated that they were predominantly concerned with earthquake safety, economics, and maintenance. However, when asked about their thermal comfort, they quickly said that they were frequently thermally uncomfortable in their home. The social and cultural climate allow the team to have a magnified impact on introducing the concepts of air infiltration and building insulation to the building context.

In Nepal, especially in rural areas, the lack of thermal comfort can be deadly. Recently, these issues were highlighted as a young woman died from lighting a fire indoors to stay warm and the subsequent lack of oxygen (Bowman, 2018). Unfortunately, this is not an isolated incident. Since 2007, at least eight other deaths have been reported from carbon monoxide poisoning, smoke inhalation, or lack of oxygen, all from indoor heating fires (Preiss, 2016). The issues of thermal comfort are even more

prevalent for newborns, where 99% of the 4 million annual worldwide neonatal deaths arise in low-income and middle-income countries (Ahman & Zupan, 2007), and of those, the majority die of complications associated with colder weather, such as hypothermia and pneumonia (Lunze & Hamer, 2012; Lawn, 2005).

To assess the need for improving thermal control in the home, the research team installed an Onset Computer Corporation HOBO Micro Station Data Logger (H21-USB) with a basic weather station setup at the Chitlang office of Hunnarshala in January of 2017 (27°38'18.30"N, 85° 9'57.98"E). Using the Temperature/RH sensor (S-THB-M002) protected by a Solar Radiation Shield (RS3-B), the setup was attached to exposed rebar on the RCC structure (Figure 85) and set to log the outdoor conditions every half hour.

Figure 85: Onset Computer Corp. HOBO H21-002 weather station installed in Chitlang, Nepal

Data from the weather station was recovered in January of 2018 and the daily maxima, averages, and minima are shown in Figure 86 as a function of the year.
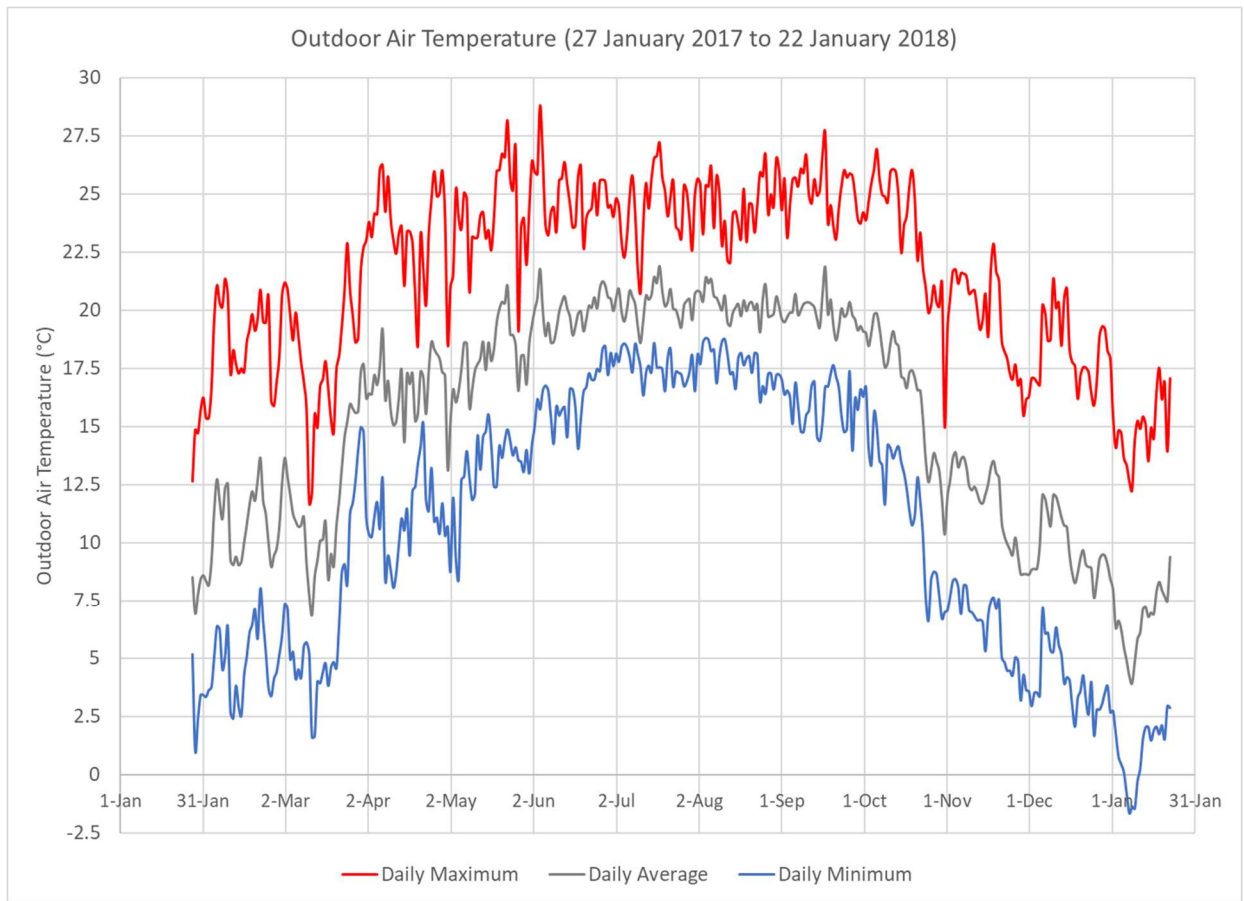
Figure 86: Outdoor Air Temperature in Chitlang Nepal: 27 January 2017 to 22 January 2018

From December to February, the minimum temperatures are typically 2.5 °C, much warmer than we had anticipated, with daily maxima reaching 15-20 °C. With such large diurnal shifts, a dedicated heating system is not explicitly required if the more comfortable temperatures (the daily highs) can be retained through the uncomfortable temperatures (nighttime, daily low). To do so perfectly, a theoretical home would require a large amount of thermal mass, an effective insulation system, and an appropriately sized means to ventilate the home during the comfortable periods. In the summertime, the system would be flipped such that the daily low temperatures would be held through the hottest part of the day, much as the research team has been striving for in Bhuj.
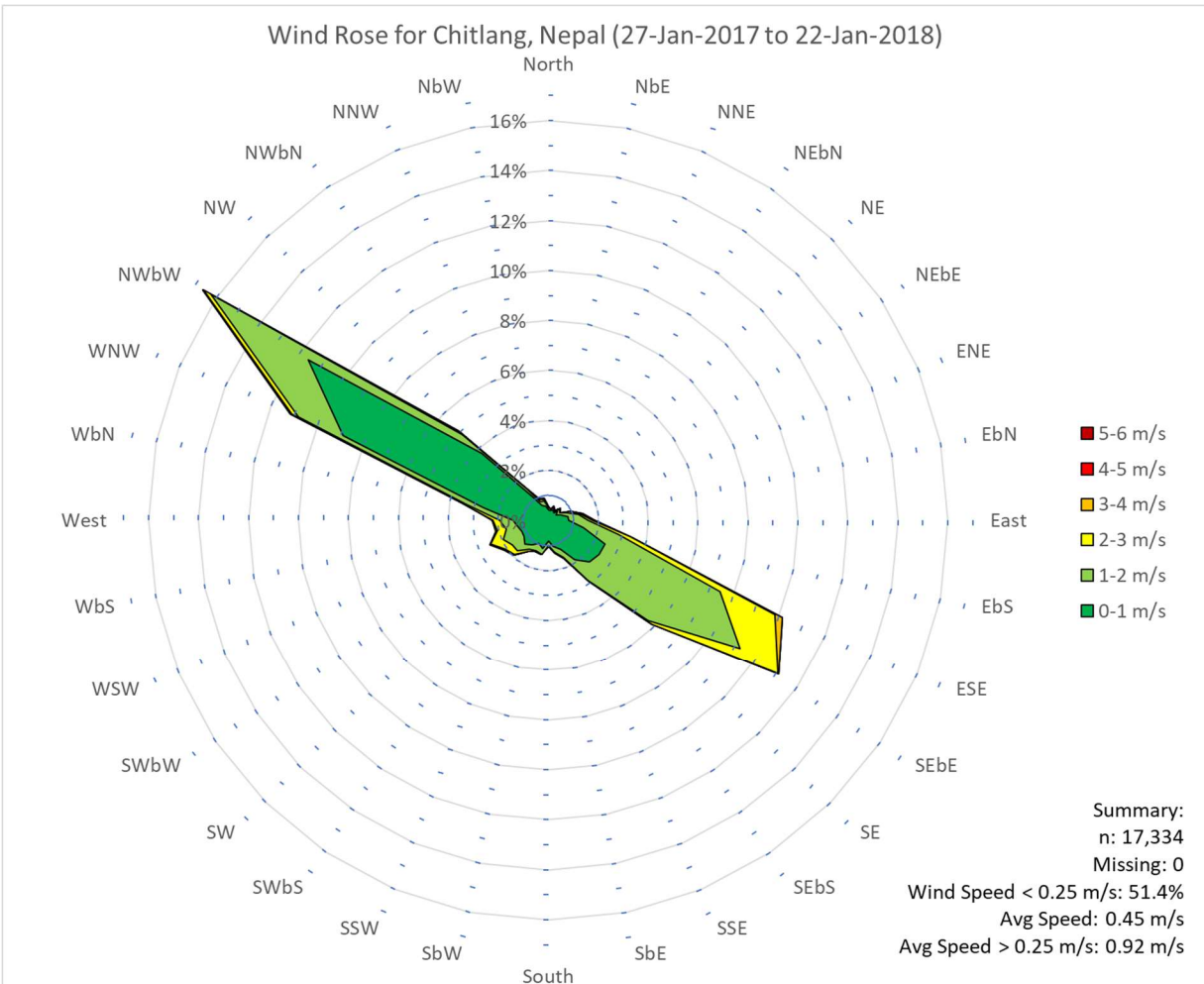
Figure 87: Wind Rose for Chitlang, Nepal (27-Jan-2017 to 22-Jan-2018)

The weather station at Chitlang also gathers information on the wind direction, speed, and gust speed. The data of which can then be post-processed and displayed as above. Figure 87 is a Wind Rose for Chitlang, Nepal based on the collected data. To read a Wind Rose diagram, the outside of the radial chart is the direction from which the wind is coming, and the magnitude is the percentage of time the wind is coming from that direction with a magnitude illustrated by the color matched to the legend. The Rose helps designers to understand the implications of building orientation and openings throughout the building. On the thermal side, the prevailing wind direction is helpful as it helps to define the greatest risk of infiltration within the building. Given a limited budget, the Chitlang Wind Rose illustrates that homeowners should work to prevent air infiltration from the WNW and ESE directions, or the façade most similar to those faces. This information is also helpful since the any wind-driven rain would hit those two facades, but lacks specificity per season to help understand the implications for indoor comfort.

132
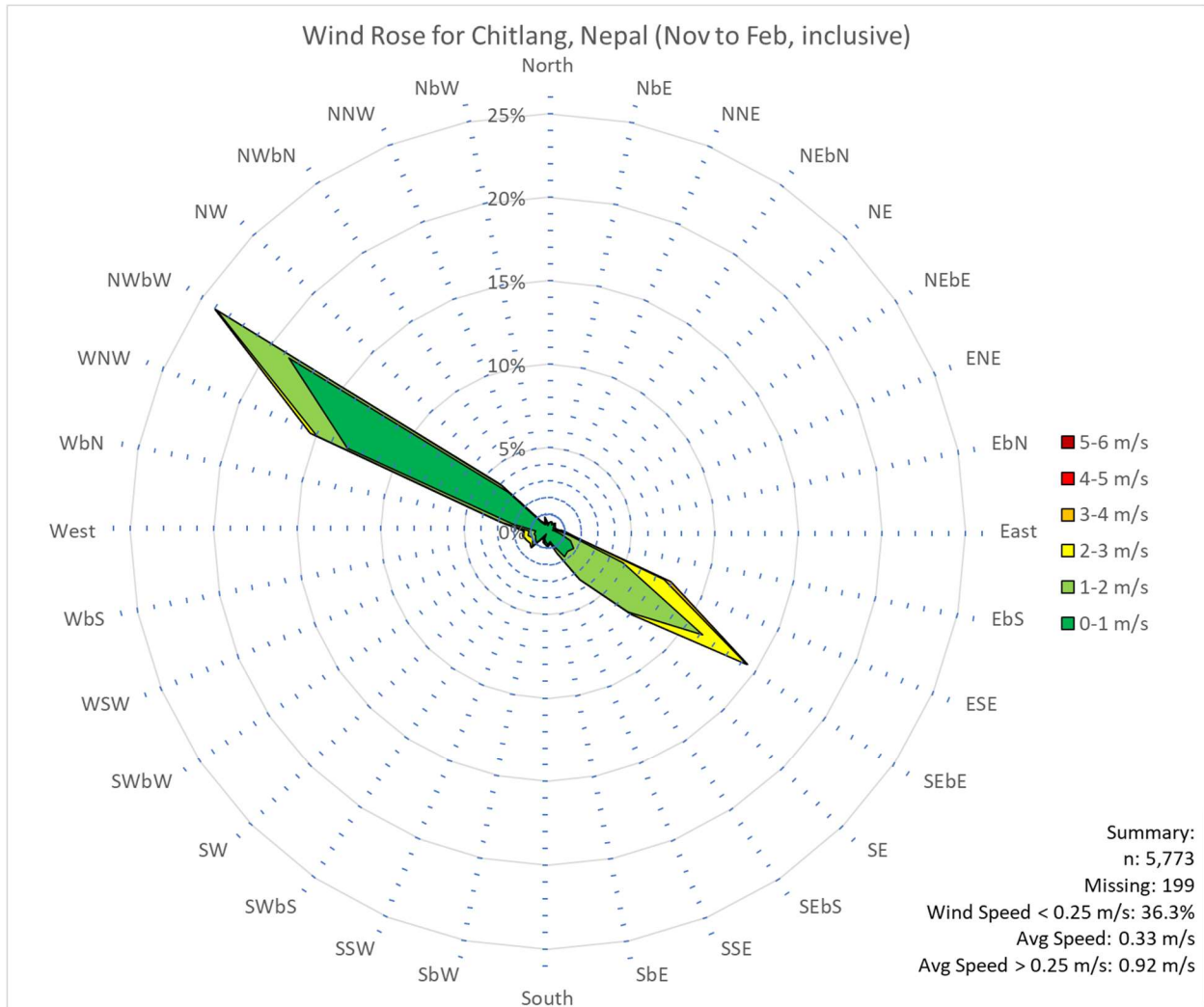
Figure 88: Wind Rose for Chitlang, Nepal (November to February, inclusive)

Figure 88 refines the data from Figure 87, and only displays the wind data for the colder months (1-November to 28-Feb). Figure 88 shows that, during the colder months, the predominant wind direction is from the NWbW magnetic (303.75°). While it may be premature to claim this wind as the dominant source of heat loss, landscape elements may help to reduce the wind hitting a building while windows facing NWbW would greatly aide in ventilation through the space. For Nepal, given that the highest wind face is NWbW and that little sun hits that face, it makes more sense to protect that wall from the wind-associated heat transfer than to encourage ventilation openings in that direction.

The house in Figure 77 and Figure 78 served as the lodgings of the Hunnarshala field staff working in the Chitlang region and, in January 2017, the research team installed one Onset Computer Corporation HOBO UX120-006M four-channel analog temperature logger to measure temperature at the same time stamps as the outdoor logger using steel temperature sensors (TMC20-HD). With the Hunnarshala staff occupying the residence, it made it possible to ensure data continuity for the duration of one year until the MIT-based team members returned in January of 2018. One sensor was offline for

a period of eleven days during early May 2017 due to rodents eating the sensor cables, but the cable was replaced by the Hunnarshala staff with a spare left behind for this reason.

The team installed four sensor points in both the traditional home (Figure 77 and Figure 78) and the RCC building that served as the Hunnarshala field office (Figure 89 Left).

The four sensor points were all installed in the main occupied room and were:

- Ceiling temperature,
- South wall temperature (embedded in the south wall 2 cm. from the inner surface),
- Air temperature (centered in the room, roughly 25 cm from the ceiling), and
- Radiant temperature (an air temperature sensor placed inside a black-painted 4" metal sphere, centered in the room and roughly 25 cm from the ceiling).

Figure 89: Left: RCC Home serving as the Hunnarshala field office, Right: Radiant Ball installed in the Traditional home
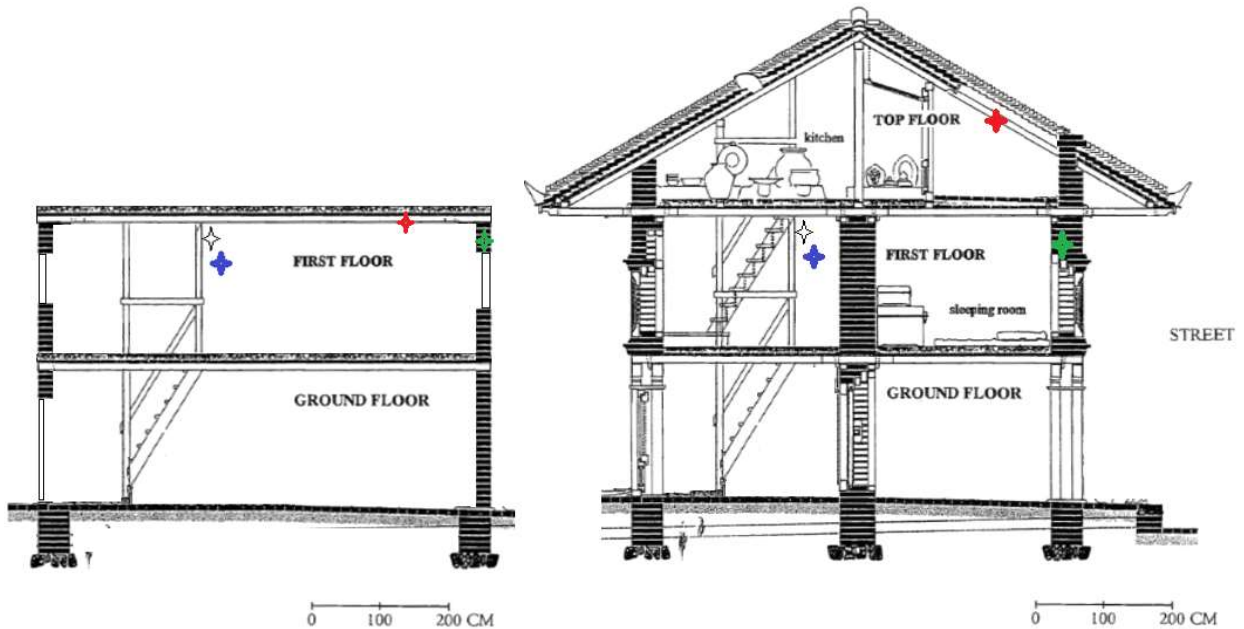
Figure 90: Left: RCC Home data points, Right: Traditional Home data points (Red: Ceiling, Green: South Wall, Blue: Air, Yellow with black border: Radiant), Image adapted from Gutschow

134

Between the two homes, it should be noted that the two metering positions for the roof and ceiling temperatures are different placements. In the traditional home, the sensor is placed between two sheets of the roof when they overlap. This point is reached from the attic space, which is separated from the main living space, and the other metering points, by a mud floor. In the RCC structure, the ceiling of the living space is the roof of the structure, whereby it is directly exposed to the exterior on the upper surface. While these values are similar in that they measure the interior temperature of the roof/ceiling layer, they vary in their influence on the air temperature inside the living area.

After collection of the data, each month was aggregated into a 'typical' 24-hour day during the month. The results make it possible to compare different temperatures during the month with minimal noise and look at the performance throughout the day. Figure 91 shows the results for February 2017.
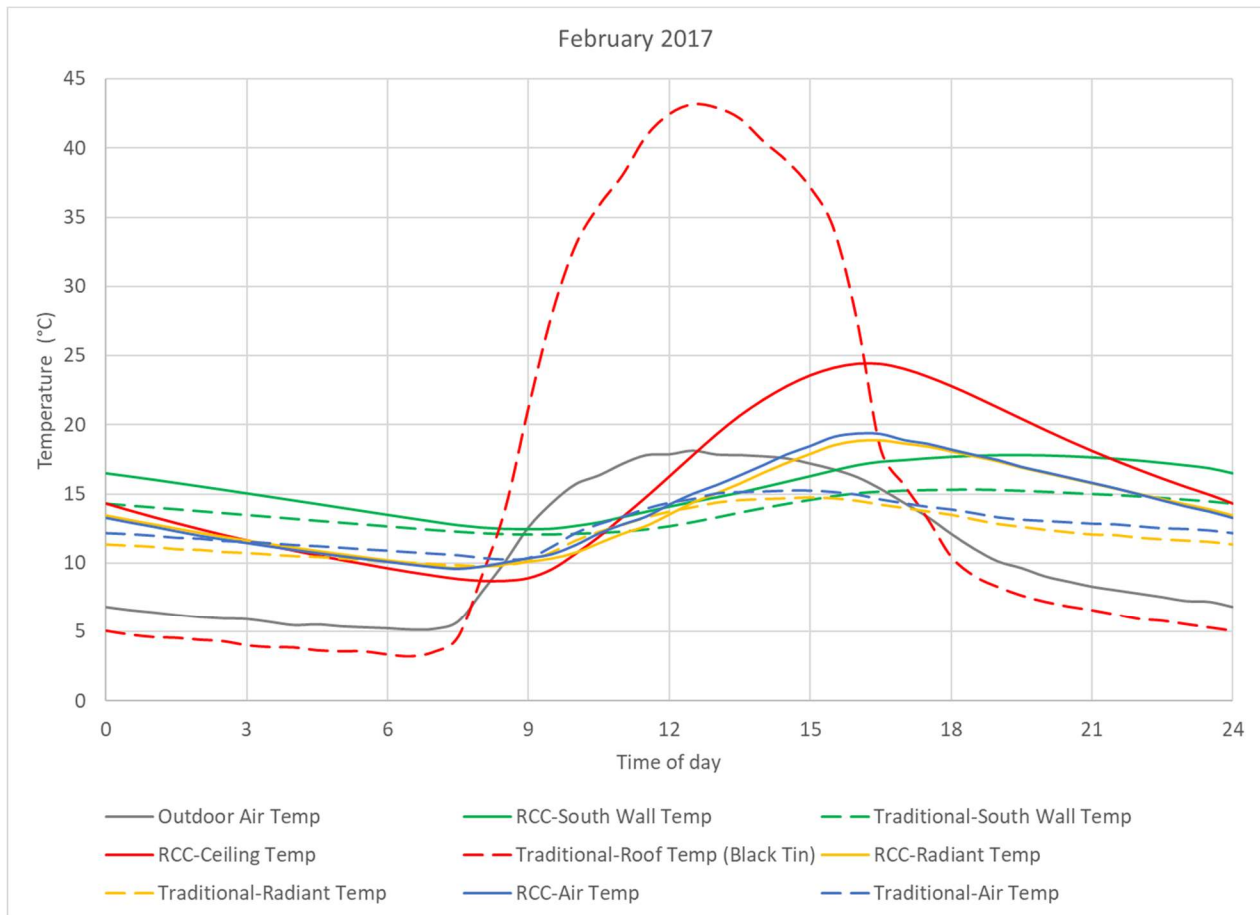
Figure 91: Average day for Chitlang in February 2017

In Figure 91, the Outdoor Air Temperature reaches a minimum of 5 °C shortly after 6 AM, and reaches a maximum of 18 °C shortly after noon. However, both the RCC and the traditional home are warmer than the outdoor conditions during the night. In the absence of dedicated heating systems, this residual warmth is a function of the thermal mass of the structure, or the ability for the structure to retain heat within the core of the building, away from the lightweight roof. The high thermal mass of the 45-60 cm thick stone and mud walls, and the mud floors and ceilings on the traditional home are excellent examples of the thermal mass in a structure. Within the data, the importance of thermal mass is shown as the air, radiant, and south wall temperatures remain within a narrower band throughout the

day than the RCC. Another way of stating this is that the temperature profile of the traditional home is closer to being uniform throughout the day, where the RCC building, with less thermal mass, more readily moves towards the outdoor temperature.

The delay in the RCC temperature profiles can best be attributed to delays in the midday elevated temperatures propagating through the roof slab. An alternative hypothesis would suggest that a space heater could be used to heat the space and contribute heat during the tail end of the workday, but the timeline of data does not support the radical temperature swings that accompany a heater starting or cycling throughout its operation.

For the homeowners, the interior condensation issues that they were noting on the traditional homes is due to radiative heat loss from the roof to the night sky. This heat loss results in a surface that is cooler than the air itself, and is lower than the dew point required for moisture in the air to condense. Using the data, the team compared the outside air conditions to the temperatures of the interior of the roof for both homes. Specifically, the team was looking for conditions where the interior of the roof temperature was lower than the dew point temperature of the outside air conditions. Using this condition implicitly assumes that the vapor pressure remains constant, and that there are no sources of humidity inside the home, an assumption that falls apart when the building is occupied or used for cooking.

For a significant majority of the year (March to December), there were no points at which the outside dew point was below the ceiling temperature. However, during the months of January and February, both the traditional and RCC homes experience periods where condensation can occur. For the traditional home, there is a 54% daily likeliness of condensation on the interior of the roof during January, and an 81% daily likeliness of condensation occurring during February. In a traditional home, the condensation is most likely to form during the early morning hours, between 3 AM and 7 AM. For the RCC home, there is a 16% daily likeliness of condensation during January and a 37% daily likeliness of condensation during February. In an RCC home, the condensation is most likely to form between 8 AM and 11 AM.

Reconciling the social responses collected by the research team with the data collected by the temperature monitoring equipment is tricky at best. Whereas condensation on an inclined metal sheet is likely to bead and roll down to the eave, RCC has a lower probability of generating condensation and may also absorb modest amounts of moisture, giving the appearance that it does not condense. Nonetheless, the collected data suggests that innovation in the roofing can increase nighttime temperatures in the living space, thereby increasing thermal comfort.

Many of these comparisons assume that the ventilation schedules and ventilation rates are on the same order of magnitude as each other. However, it is unknown if the building is well ventilated throughout the day, and at what times. Changes in the ventilation patterns could account for some of the variation, and be employed with beneficial results. Especially within the winter months, it would be beneficial to open the windows and doors during the day, when the outdoor air temperature is warmer, and close the windows and doors during the night, to help limit the heat loss to the outside.
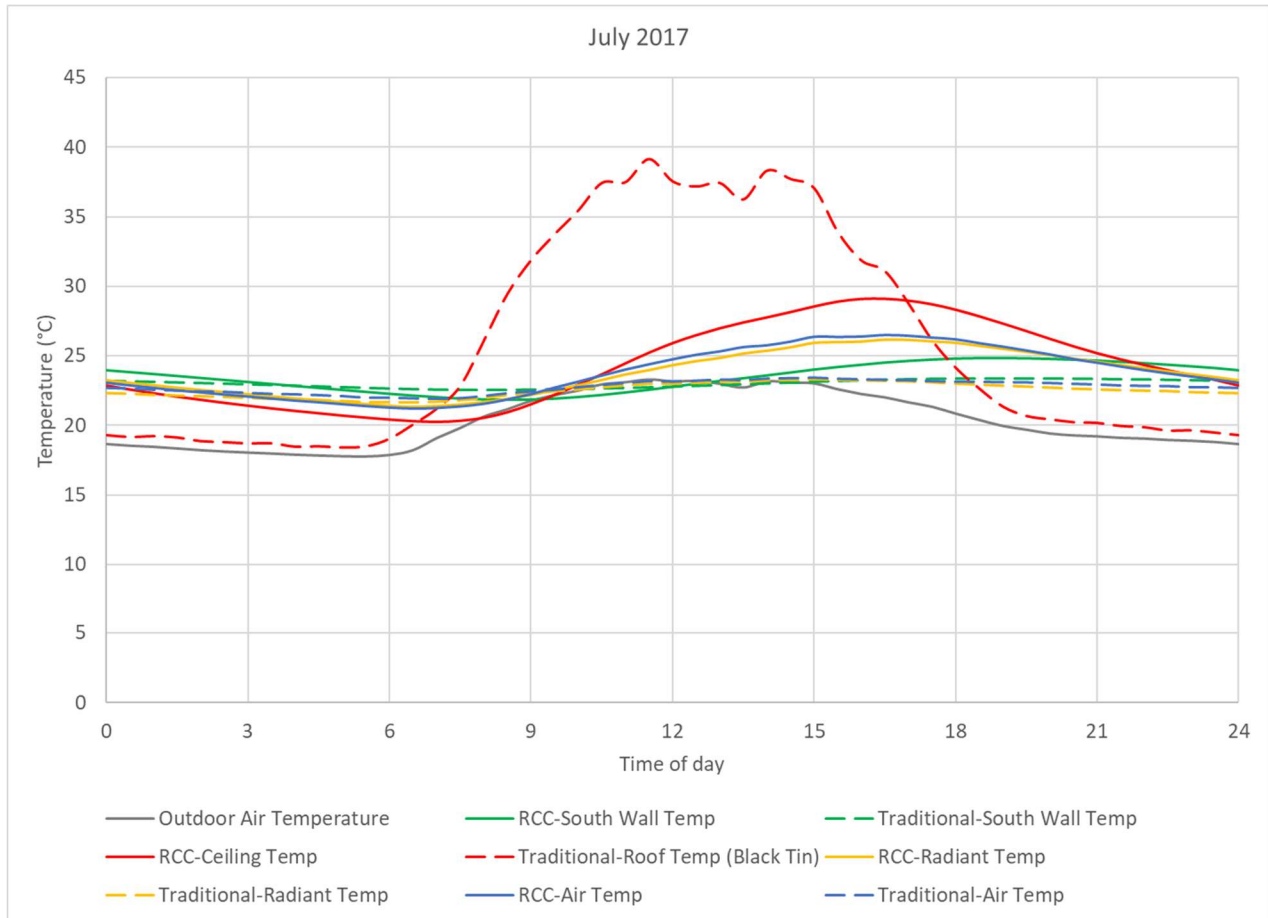
Figure 92: Average day for Chitlang in July 2017

Similar to Bhuj, Figure 92 shows a potential for nighttime cooling to reduce the temperature during the peak of the day. The 4 °C gap between indoor and outdoor air temperature is sufficiently large that using the existing thermal mass can yield a benefit. For the RCC structure, the addition of wall insulation may also yield a benefit as it will decouple the influence of the walls with the air temperature. In this structure in particular, the 10 cm thick masonry has relatively little insulating value (R-value = 0.16 m²*K/W), and does not play a large role in maintaining thermal comfort with the exception of reducing infiltration through the living space. In comparison, the insulating value of an equally thick layer of fiberglass or polystyrene is fifteen times as insulating as concrete.

Where the Traditional Black Tin Roof temperature rises substantially during the day, the radiant temperature and other values inside the space do not reflect this substantial rise due to the intermediate mud floor that is present in the traditional home. This intermediate mud floor can be seen in Figure 90 on the right. This implies that the cooking space on the top floor may be uncomfortable on an air temperature basis, which can be reduced by opening operable windows to ventilate the space at all times given that the outside air temperature is lower than the roof temperature for the entire 24-hour day.

As presented earlier in the chapter, there are several structural elements that should be remedied prior to addressing thermal considerations. While typical methodologies would separate those considerations, there are mutual benefits between some of the structural and thermal remedies.

While looking at some of the homes constructed with architectural and engineering support, several of the wall stones were loose and cavities in the wall construction present concerns of out of plane failures and air infiltration. As Figure 93 shows, the resulting cavities are much larger than a weep hole or designed void would require. Increasing the consistent use of mortar throughout the wall section would help to alleviate these potential issues and inhibit inter-stone movement during an earthquake.

Figure 93: Loose and missing stones in a typical home construction, showing baseball sized cavities. (Chitlang, Nepal)

Out of plane failures are of significant concern because while the building itself may not collapse, the wall may crumble and the constituent stones crumble inward upon a sleeping occupant. Figure 94 shows an image of an out of plane failure that was seen in a building near the Chitlang region, still standing nearly three years later. These types of failures and wall collapses were the most commonly observed failure mode (Dizhur, Dhakal, Bothara, & Ingham, 2016). Fortunately for the occupant, this wall failed on the exterior side, but could easily have also failed on the interior side.

Figure 94: Out of plane failure of mud and stone wall (Chitlang, Nepal)

The use of plaster on these walls would also help in reducing infiltration of air through the wall itself. As the American Society of Heating and Ventilating Engineers showed in 1927, adding a plaster coating to a masonry wall can reduce the heat loss by infiltration through the wall by 99.55% (Houghten & Ingels, 1927). Granted, eliminating infiltration is not a silver bullet to achieving thermal comfort, but it is a significant first step towards that goal. The same plasterwork that reduces infiltration heat losses is also helpful in ensuring the structural longevity of the mortar mentioned in the paragraph above, helping reduce intensive maintenance in the process. Long term, adding insulative components (such as straw, pumice, timber or aerogel) to the plaster can allow the plaster to serve as an exterior insulation, reducing heat flows and providing a tighter thermal coupling of the building interior to the wall mass temperature. Adding plaster to the interior will also help to reduce the air infiltration and heat loss, although it will reduce the influence of the wall's thermal mass in moderating the interior air temperature.

During interviews with homeowners, the research team heard several complaints of the condensation on the interior of their metal sheet roofs and the data in Figure 91 supports the potential for condensation to occur. The potential for condensation can be reduced with the addition of roof insulation. One homeowner, on the advice of a relative in Kathmandu, decided to add straw to the exterior of his roof to reduce the condensation. He stated that the condensation has not returned since doing this, and he will continue doing this in the future. However, he was uncertain of why more people did not do this, and the homeowner was asked in the middle of January, before most of the conditions are ripe for condensation formation. The straw used by this homeowner (Figure 95) is waste material from the field, and can be easily replaced with fresh straw when the existing straw begins to degrade. An advantage of this approach is that it helps avoid concealed condensation which can form within the insulation (Al-Homoud, 2005).

Figure 95: Metal sheet roof with straw covering (Chitlang, Nepal)

In a similar fashion, Nepali women typically weave straw mats that will become sitting mats, mattresses, rugs, and runners. While currently only used in small amounts, the same concepts and weaving method can be used as a wall or roof insulation material in the homes. As mentioned in the Local Experiments chapter, the woven mat has a thermal conductivity of 0.0556 W/(m·K), much the same as an equivalent thickness of tiled and lay-in panels. However, applying the 1.87 cm thick mat to a 25.4 cm block masonry wall would double the thermal resistivity of the wall, thereby reducing the heat transfer through the wall by half (Rutkowski, 1986). This has significant impacts for the heating requirement, which is predominantly wood scavenged by female members of the family in the rural areas of Nepal (St. Clair, 2016). Further, this has larger implications in that poorer households are highly dependent on the forests to sustain their day-to-day livelihood (Sapkota & Oden, 2008).

Applying a layer of the straw mat to the wall, ceiling, and floor of a 4m x 6m x 2m home in Nepal would decrease the peak heating requirement by 51.3%, to 0.6 kg of wood per hour from 1.2 kg of wood per hour. Another way of looking at this is that the heating load with the straw mat insulation would turn the interior conditions for a -6°C outdoor air temperature day into what would typically be a 3.7°C outdoor air temperature day, 9.7°C warmer. A second layer of straw mat would then reduce those numbers to 37% of the original value, 0.44 kg of wood per hour, or a typical 6.5°C outdoor air temperature day. Reducing the infiltration would then take these values a step further to 35% of the original value, 0.42 kg of wood per hour, or a typical 6.9°C outdoor air temperature day.[12]

---

[12] Computed using the Air Conditioning Contractors of America (ACCA) Speed-Sheet for Manual J: Residential Load Calculation (Rutkowski, 1986) to do a sizing estimate for a basic structure. The structure was defined as a 4m deep by 6m wide by 2m high structure made of 12" unfinished block walls, a solid core wooden door, no subfloor insulation, and a ventilated attic space. Single glazed windows and wooden framed windows were assumed to occupy one square meter per face, with a 'semi-loose' envelope leakage rate. Input values were based on table lookups from ACCA's Manual J version 7. Memphis, Tennessee was used as an example city to define a 99% Outdoor Winter design condition at 21°F at a heating design condition of 57°F, achieving a 20°C delta.

Conclusions and Recommendations

The conclusions and recommendations in this chapter are based off of the analysis of scale, field, and full size test homes, observations and point measurements in the field, as well as laboratory-based testing of thermal conductivity and surface reflectivity of selected materials found in and around the Bhuj area. This chapter serves to summarize the results that directly influence design decisions, as well as provide a concise description of the intellectual contributions from this work. Finally, based on the results of experimental data, community input, and simulations, a series of hypotheses are offered for preparation of future work in the field.

Conclusions from Previous Work

Based on measurement results from higher performing buildings, Gradillas concluded that buildings that stayed cooler throughout the day tend to have high thermal mass exterior surfaces that are protected from direct solar radiation and tend to utilize nighttime ventilation with low daytime ventilation. Critically, Gradillas noted that any building characteristics that help contribute to thermal autonomy hinge on a combined and unified approach with other building elements. For example, implementing a nighttime ventilation schedule would have little impact on homes that were unprotected from solar heat gains throughout the day.

Among the tests performed, double-layered, insulated roofs decreased daily high indoor temperatures by an average of 1.5°C compared to single-layer, uninsulated roofs. The performance increased to an average of 2 to 2.5°C less than the single-layer, uninsulated roofs when night flush ventilation and sealed daytime conditions were incorporated into the schedule. Ultimately, the ceiling temperature of a double-layer metal sheet roof with an upper radiant barrier remained anywhere from 9 to 11.5°C cooler than the single-layer non-radiant barrier counterparts. This design maintained daily high surface temperatures within 1°C of indoor air temperatures. With respect to the roof, the metal sheet double-layer insulated roof was able to keep the peak indoor air temperature nearly 8°C cooler than the outdoor air temperature, where the uninsulated clay tile roof only kept the indoor air temperature 3.8°C cooler than the outdoor air temperature, a 4.2°C difference. (Gradillas, 2015)

Nelson built off of the pre-existing work to provide recommendations for housing based on three major roofing themes: low heat capacitance if using single layer roofing, adding insulation to a traditional thermally massive slab construction, and lowering the emissivity of the ceiling surface. Nelson recommended the use of a double layer corrugated metal roof with a ventilated air gap and mud roll insulation.

For the walls, via field work, Nelson confirmed that 15cm thick straw applied to the exterior of the walls led to a 1-5°C decrease in maximum air temperatures. Although not stated, the building modification also includes the change of exterior wall color from natural sandstone to white plaster. Based on simulation results, Nelson concluded that the change in wall absorptivity alone would reduce the peak operative temperature by 2°C.

Using a combination of two-dimensional computational fluid dynamics and field test chamber experiments, Nelson concluded and recommended that ceiling fans should not be used in conjunction with single-layer metal roofing, due to the increased convection from the hot roof into the air below. Standing fans would help to reduce this convection.

Conclusions from This Work

Field and Scale Chamber Testing

Through this work, the team has designed and implemented various thermal avoidance strategies that are electric independent. Beginning with the small-scale test chambers located at MIT, the team worked to develop a relationship between the stand-alone chambers which were the focus of Gradillas and Nelson, and the slab roof row housing, which have been built in Ramdev Nagar, Bhuj, Gujarat, India. Using multiple small scale chambers equipped with night ventilation, the team determined that the row housing will remain cooler than the stand-alone housing due to the absence of solar radiation on the north and south faces (those walls shared with a neighboring home) and the increase in thermal mass dampening due to the tighter thermal coupling of these walls to the indoor environment rather than the outdoor weather conditions. This modification alone lowered the peak indoor air temperature by 1.7°C. Additionally, where Nelson had concluded from simulation that the addition of white wall paint would reduce the peak operative temperature by 2°C, scaled physical chambers in this work found that the addition of white wall paint would reduce the peak air temperature by 0.7°C.

While these are numerically different, the two values are different ways to measure the temperature of a chamber, and will change based on the area of the wall compared to the entire area of the chamber exterior, as well as insolation levels. After the movement of the core structure to a row-housing configuration and the addition of wall paint to establish a new baseline, the team showed that the roof now has even a greater significance on the internal temperatures of the home. Where the core row-housing/white wall structure experienced a 2.4°C cooler peak indoor air temperature than a standalone exposed structure, the addition of white paint to the roof of the chamber had the single greatest reduction in peak indoor air temperature, reducing the peak indoor air temperature 4.0°C further (6.8°C compared to original standalone exposed structure). The team continued to test multiple iterations and, of these, determined that adding exterior insulation to the east and west facades (the front and back of the Ramdev Nagar row housing) will help reduce the peak interior air temperature another 2.0°C. Testing these results in a full scale chamber, the team determined that the daytime maximum temperature would decrease by 1.5-2.0°C, and that the nighttime average temperature would also decrease by 1°C. These numbers are on the conservative side of the scale presented by Nelson, but are within range.

Where both Gradillas and Nelson had discussed the importance of surface coatings through radiant barriers, this research presents laboratory experiments looking at the surface optical properties. The team developed the following chart for the absorptivity and emissivity of selected samples brought back from Bhuj. Please note that while the chart reads absorptivity values, infrared absorptivity may be approximated as being equal to emissivity when the incident radiation is of the same wavelength profiles, or near the same temperature. The values presented in Table 31 may be used for simulation purposes or comparison purposes to additional materials, representing a value to both academics and practitioners alike.

The solar absorptivity to infrared emissivity values are useful for application to solar-exposed surfaces, with the intention that surfaces much less than unity can be used to help reflect solar wavelengths while also emitting infrared wavelengths. For the ceiling applications suggested by Nelson, only the infrared values apply. Low infrared absorptivity surfaces, such as the aluminized surfaces, would be helpful for these applications.

Absorptivity Material	501.5 nm (Solar Range, 5780 K)	9,670 nm (Infrared Range, 300 K)	$\dfrac{Absorptivity_{Solar}}{Emissivity_{Infrared}}$
Aluminum foil, shiny side	0.04 ± 0.02 (n=2)	0.07 ± 0.05 (n=7)	0.57
Aluminized Bubble Wrap 4 mm thick	0.22 ± 0.07 (n=6)	0.08 ± 0.05 (n=11)	2.75
Aluminized Bubble Wrap 6 mm thick	0.21 ± 0.06 (n=6)	0.11 ± 0.03 (n=8)	1.91
Mylar, coated side	0.02 (n=1)	0.07 ± 0.04 (n=5)	0.59
Mylar, substrate	0.11 ± 0.02 (n=2)	0.77 ± 0.01 (n=5)	0.14
Galvanized Iron ("Tin sheet")	0.32 ± 0.02 (n=44)	0.14 ± 0.11 (n=12)	2.29

Table 31: As-tested Absorptivity Values for Selected Materials

In the same vein of research, the team looked at the thermally conductivity of various locally produced fibrous materials to determine potential application as insulation. The team assessed three materials produced for different applications in the home. These materials included a straw mat intended as a mattress or floor runner from Nepal, a Jute basket weave rug from India, and a coconut fiber mattress from India. Tested under steady-state conditions for a variety of thermal setpoints, the results are reproduced below.

Material (Origin)	Thermal Conductivity	Thermal Resistivity
Straw Mat (Nepal)	0.0556 W/(m·K)	0.3364 (m²·K)/W
Coconut Fiber Mattress (India)	0.0472 W/(m·K)	0.4117 (m²·K)/W
Jute Rug (India)	0.0734 W/(m·K)	0.2546 (m²·K)/W

Table 32: Natural Fiber Materials Summary

The results highlight how these materials are suitable for use as a thermal insulating material. However, the team noted that all of these materials were perceived to be more likely to combust than other commercially-available insulation products, such as fiberglass, commercial cellulose insulation, and mineral wool. This is not all-encompassing though, as some commercially available products are easy to ignite and/or produce dangerous fume. For the natural fiber materials, adding a thin layer of gypsum plaster, which is a common interior surface coating, increased the protection from combustion, but also increased the thermal conductivity of the entire assembly. With the addition of the gypsum plaster, the samples have a conductivity on the same order of cement fiber slabs (Coconut Fiber Mattress) and high density hardwood (Straw Mat and Jute Rug).

Material (Origin)	Thermal Conductivity, with plaster	Thermal Resistivity, with plaster
Straw Mat (Nepal)	0.1141 W/(m·K)	0.2113 (m²·K)/W
Coconut Fiber Mattress (India)	0.0616 W/(m·K)	0.3822 (m²·K)/W
Jute Rug (India)	0.1380 W/(m·K)	0.1536 (m²·K)/W

Table 33: Natural Fiber Materials Summary

Bhuj Housing

Applying previous work from Gradillas and Nelson, the team built a second story of four test homes in Bhuj, India in summer of 2016, and instrumented the homes in January of 2017, along with an informal tent home, all of which had pitched roofs. The temperature logging of the second story interior of the test homes and the ground level of the informal tent allowed the team to look for overall temperature profile changes, as well as look at performance during extreme weather.

Figure 96 shows the average daily inside air temperature as a function of the time of day in the metered homes in Ramdev Nagar, Bhuj, Gujarat, India. Across an extended time period, the Tile-Mudroll roofing style implemented by Nelson remains the coolest throughout the day, although it also remains warmer at night. During the heat of the day, near 2 PM, the thermal mass of the Tile-Mudroll roofing helps maintain the air 3.5°C cooler than the tin roofing with an air cavity and 7.5°C cooler than the informal tent home. Further, the tile roof types peak much later in the day, when the heat of the day has passed. For families that only use the second floor living space in the evening, the tin roofing with an air cavity may be a better choice due to the lack of occupancy during the heat of the day.
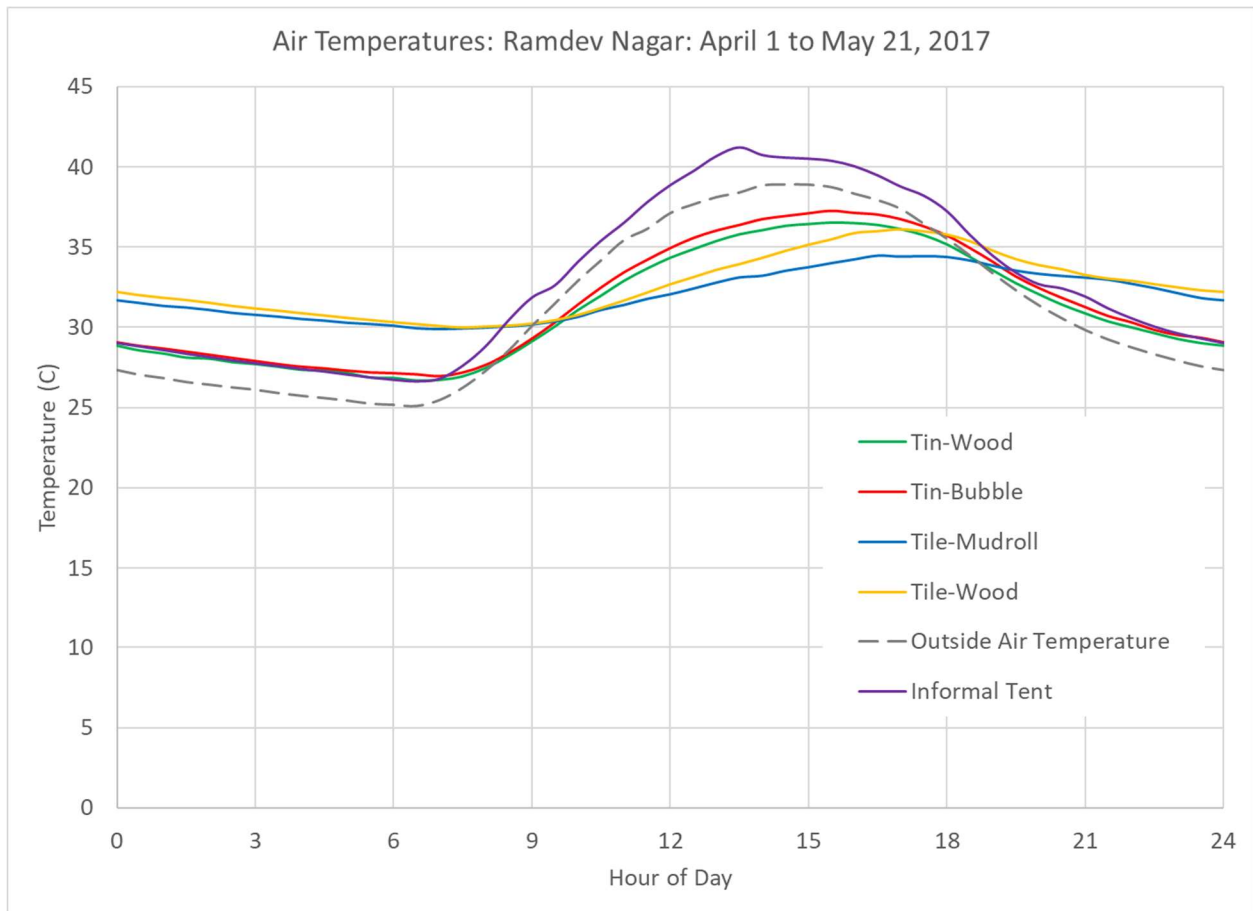
Figure 96: Average Daily Air Temperatures for the five metered homes in Ramdev Nagar (April 1 to May 21, 2017)

For a family that utilizes the second floor living space throughout the day, the ability for the roof to keep the space cool during the heat of the day is more important. The hottest day during the measurement period was April 13, 2017, when the outside air temperature reached 45.53°C (113.95°F) at 2 PM in the evening. Using the data collected by the instrumentation at that same time, the team was able to look at the range of temperatures between the different homes.
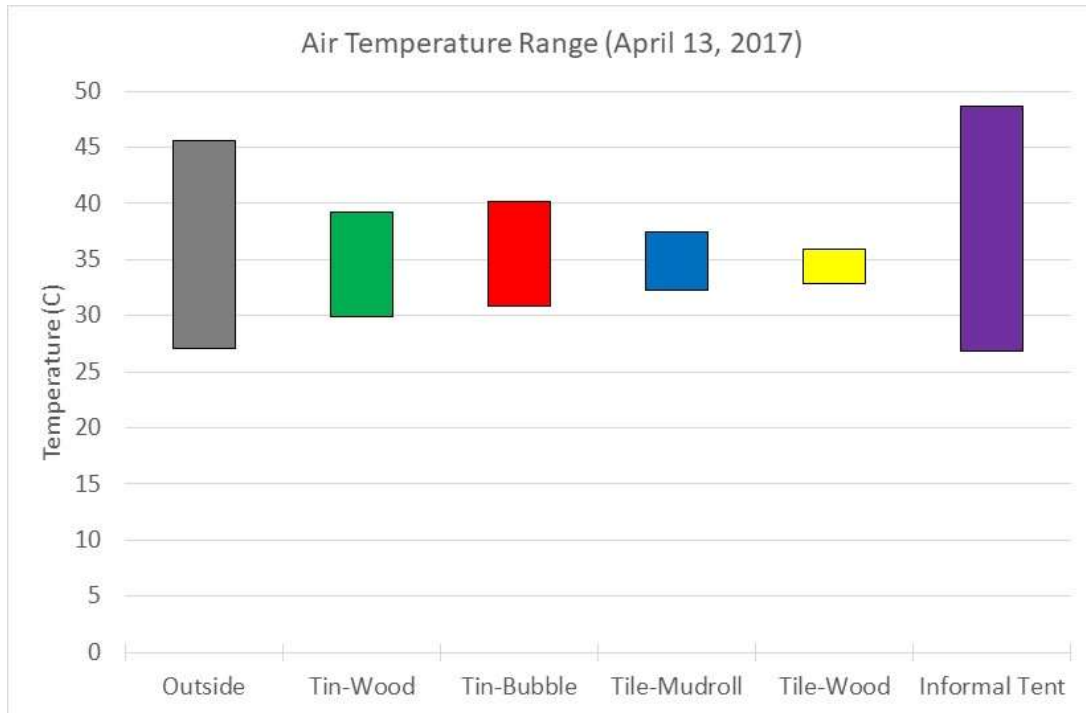
Figure 97: Air Temperature Range at Maximum and Minimum Outside Air Temperature over 24 hours (April 13, 2017)

Using the data, the tile roof structures remain between 7 and 8.5°C cooler than the outside air temperature during the heat of the day, although they stay roughly 5.2-5.7°C warmer during the night. Compared to the informal tent housing though, the Mangalore Tile roof with wood ceiling and above sheathing ventilation remained 12.6°C cooler compared to the peak outdoor air temperature. This is a substantial improvement in performance, and has the capacity to lower the mortality rate by 7.5 percentage points compared to the informal housing. Where the elderly and newborns are most likely to be impacted by extreme heat events, this reduction in the mortality rate directly affects those populations, who are also more likely to be around the home for the duration of the day. On the thermal comfort side, the reduction in internal temperature does not meet the thermal comfort standards as it is currently set. However, these air temperatures are in the absence of personal fans or evaporative coolers, which are additional methods that can help make the home more comfortable.

In both January 2017 and 2018, the team traveled to Nepal to extend some of the lessons learned to a Nepali climate. Prior to travel, the team had intended to look primarily at insulation and other means to retain heat within the structures. However, during the visits, the team became aware that building construction quality was an overarching theme, encompassing seismic, thermal, and air quality concerns.

To address some of these concerns, the team recommends adding and maintaining plaster on the exterior walls to help reduce shifting of blocks during an earthquake, as well as reduce the infiltration through the wall itself. From observations in the field, even newly constructed homes have cavities that are cause for concern. The existing mud-based plaster may be a good starting point, but future work may consider adding fiber or insulating beads to the exterior plaster to help reinforce the structure and decrease thermal conductivity through the wall. Additionally, adding a binder to the plaster mix may help reduce moisture movement through the wall and aid in durability.

On the roof of several homes, the local traditions of using metal sheet roofing are a wise choice for a seismic zone. However, these metal sheets provide little thermal resistance and allow condensation to form in the winter months. Adding insulation to these roofs will help to reduce condensation buildup and retain heat better, allowing for a reduced heating load or increased indoor temperature.

With the baseline work of Gradillas, Nelson, and this thesis, the team has had the opportunity to continue building and improving the overall design of the homes alongside with input from the homeowners and the local partner, Hunnarshala. There are several avenues that the team suggests for further research, including improving the performance of the inclined roof, improving the performance of the flat roof, dissemination of the working knowledge to the region, cross testing the approach in laboratory setups and different geographic environments, and introducing a more active control scheme to airflow within the air cavity. Several of these are discussed below.

Improving performance of the pitched roof with above sheathing ventilation

This roofing style has been enormously beneficial in reducing the peak indoor air temperature within the house. To help improve this approach, the team has looked into the feasibility of shifting the Mangalore tile from a clay color to a lighter white color. To achieve this, the team has done spot testing of the relative absorptivities with a water-based and oil-based white paint. However, the homeowners have stated that they prefer the clay color over the white color. Figure 98 shows an initial effort to test the implication of two types of white paint on the temperature of the tile in the midday sun. Note that the water-based paint has a much lower surface temperature than the oil-based paint, and that the water-based white tile is 10°C lower than the natural Mangalore clay tile.
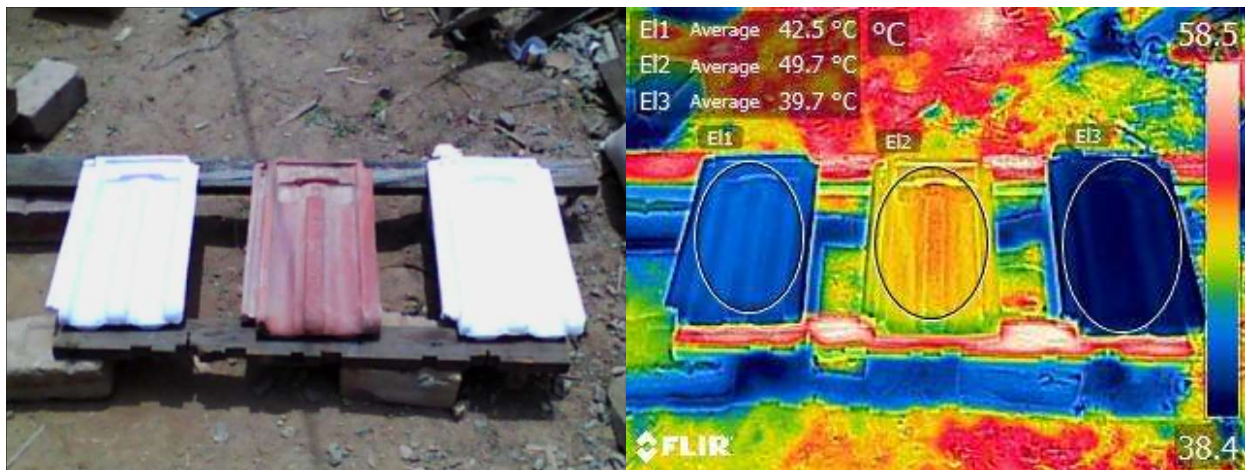
Figure 98: Surface temperatures of Mangalore clay tiles based on paint presence and type at an ambient temperature of 37.6°C and an assumed general emissivity of 0.90 (Left: Oil-based white paint, Center: Unpainted, Right: Water-based white paint)

Testing is currently underway in Bhuj to determine how the surface color changes the air temperature within the air cavity, as well as the impact it has on the chamber's internal air temperature. This data will serve as a method to determine the importance of the surface color on the overall performance of the system. If this proves to be a meaningful path, the team is investigating changing the aspect ratio, or the ratio between the top of the tile and the forward-facing lip of the tile. This aspect ratio can be decreased such that the forward-facing lip has more prominence and if this region is the only section visible from lower elevations, the sky-facing section of the tile can be painted or glazed white to reduce the overall heat absorption.

Improving the performance of the flat slab roof

Where many of the homeowners do not have the means of building a second level to their homes, further work should be spent looking at potential solutions that serve this market segment. Initial work is currently underway to look at the viability of using partially reflective shade nets on timers to shade the roof of the structure, limit the daytime heat reradiation to the roof below, while also making radiative cooling a possibility at night with the shade retracted. This idea can be extended to the courtyard in front of the home to help provide protection from the sun to the mother of the family, who is frequently in the courtyard as a homemaker.

Dissemination of the working knowledge to the region

All of the work produced to date has little significance if it cannot be employed by others. Using the connections and training arm of the Hunnarshala Foundation the team is working on means to distribute knowledge of the roofing system and the associated benefits, so that newly-trained artisans are equipped to produce a roof system and allow the roof method to spread organically. The team is also looking into producing roof schematics and publishing the designs in local newspapers such that a broader audience can be reached at such a critical time. A newspaper may reach the more educated populace, who have more access to funding to pursue this idea with minimal assistance from Hunnarshala.

Cross testing the approach in laboratory setups and different geographic environments

To help vigorously test the inclined roof systems with above-sheathing ventilation, the team will be pursuing laboratory testing to determine the importance of various aspects of the design. Using a climate-controlled chamber designed to mimic the solar and temperature profiles of the day, the team will be able to test the implication of roof angle, radiant barrier placement, surface absorptivity, air cavity spacing, and obstructions within the cavity on the overall performance. This research is paramount to application of this roofing design in other locales.

Additionally, the team recommends creating demonstration homes with this design in different regions to assess the cultural, societal, and technical factors that may change the overall viability of the roof designs. These designs have the potential to be beneficial outside of developing economies, and with appropriate documentation, may be eligible for custom energy efficiency/conservation grants.

As mentioned previously, the team is currently working to extend some of the passive design elements to housing in Nepal, where improvements in insulation, build quality, and airtightness can be beneficial to the living standards.

Active control of the air cavity

The team is also interested in pursuing active control of the air cavity to increase the performance of the system as a whole. These active controls may fall in three buckets: reduction of airflow when insulative properties are preferred, increase in airflow when heat extraction is preferred, and increase in operable areas to permit flow through the external layer to increase heat extraction.

Bibliography

Ahman, E., & Zupan, J. (2007). *Neonatal and Perinatal Mortality: Country, Regional and Global Estimates 2004.* Geneva: World Health Organization. Retrieved from http://apps.who.int/iris/bitstream/handle/10665/43800/9789241596145_eng.pdf;jsessionid=A3E9DF08F764F9801DCFEE358AD3813F?sequence=1

Ahmedabad Municipal Corporation. (2018, March 9). *Ahmedabad Heat Action Plan 2016.* Retrieved from National Resource Defense Council: https://www.nrdc.org/sites/default/files/ahmedabad-heat-action-plan-2016.pdf

Al-Homoud, M. S. (2005, March). Performance characteristics and practical applications of common building thermal insulation materials. *Building and Environment, 40*(3), 353-366. doi:10.1016/j.buildenv.2004.05.013

ANSI/ASHRAE. (2017). *Standard 55-2017 -- Thermal Environmental Conditions for Human Occupancy.* Atlanta, GA: ASHRAE.

Antony, A. P. (2018, May 14). Email: 'Nepal: Firewood Collection Numbers'. Cambridge, MA, USA.

Azhar, G. S., Mavalankar, D., Nori-Sarma, A., Rajiva, A., Dutta, P., Jaiswal, A., . . . Hess, J. (2014, March). Heat-Related Mortality in India: Excess All-Cause Mortality Associated with the 2010 Ahmedabad Heat Wave. *PLOS ONE, 9*(3), 1-8.

Balcomb, J. D. (1992). *Passive solar buildings.* Cambridge, MA: MIT Press.

Barakat, S. (1993). *Rebuilding and Resettlement, 9 Years Later: A case-study of the contractor built reconstruction in Yemen, following the 1982 Dhamar earthquake.* York, UK: University of York.

Barry, E. (2016, April 30). *A Year After Earthquake, Nepal's Recovery Is Just Beginning.* Retrieved from New York Times: https://www.nytimes.com/2016/05/01/world/asia/nepals-earthquake-recovery-remains-in-disarray-a-year-later.html

Bhalla, N. (2016, May 29). *Ahmedabad offers way to beat the heat as 1,786 killed in heat wave.* Retrieved from Reuters: https://in.reuters.com/article/india-heatwave-disasters/ahmedabad-offers-way-to-beat-the-heat-as-1786-killed-in-heat-wave-idINKBN0OD2GT20150529

Bowman, V. (2018, January 12). *Woman in Nepal dies after being exiled to outdoor hut during her period* . Retrieved from The Guardian: https://www.theguardian.com/global-development/2018/jan/12/woman-nepal-dies-exiled-outdoor-hut-period-menstruation

Burgess, R., Deschenes, O., Donaldson, D., & Greenstone, M. (2017, December 10). *Weather, Climate Change, and Death in India.* Retrieved from

http://www.lse.ac.uk/economics/Assets/Documents/personal-pages/robin-burgess/weather-climate-change-and-death.pdf

Chandramouli, C. (2013, 3 21). Housing Stock, Amenities & Assets in Slums - Census 2011. India. Retrieved from censusindia.gov.in/2011-Documents/On_Slums-2011Final.ppt

Dizhur, D., Dhakal, R. P., Bothara, J., & Ingham, J. M. (2016, May). Building Typologies and Failure Modes Observed in the 2015 Gorkha (Nepal) Earthquake. *Bulletion of the New Zealand Society for Earthquake Engineering, 49*(2), 211-232.

Dolma, T. (2016, February 11). *Nuns in Nepal Rebuild Sustainably*. Retrieved from GlacierHub: http://glacierhub.org/2016/02/11/in-nepals-mountains-rebuilding-sustainably/

European Environment Agency. (2016, Dec 20). *Extreme temperatures and health.* Retrieved from European Environment Agency: https://www.eea.europa.eu/data-and-maps/indicators/heat-and-health-2/assessment

Government of India Ministry of Housing and Urban Poverty Alleviation National Buildings Organization. (2015). *Slums in India: A Statistical Compendium.* New Delhi, India: Government of India. Retrieved from http://re.indiaenvironmentportal.org.in/files/file/SLUMS_IN_INDIA_Slum_Compendium_2015_English.pdf

Government of Nepal: National Planning Commission. (2015). *Nepal Earthquake 2015 Post Disaster Needs Assessment 2015 - Key Findings.* Kathmandu, Nepal: Government of Nepal. Retrieved from http://reliefweb.int/sites/reliefweb.int/files/resources/PDNA%20Volume%20A%20Final.pdf

Gradillas, M. S. (2015). *Analysis and design for thermally autonomous housing in resource-constrained communities: A Case Study in Bhuj, India.* Cambridge, MA: Massachusetts Institute of Technology. Retrieved from http://hdl.handle.net/1721.1/99245

Greiner, T. H. (1997, April). *Carbon Monoxide Poisoning: Dangers, Detection, Response, and Poisoning (AEN-193)*. Retrieved from Iowa State University: Department of Agricultural and Biosystems Engineeering: https://www.abe.iastate.edu/extension-and-outreach/carbon-monoxide-poisoning-dangers-detection-response-and-poisoning-aen-193/

Gutschow, N. (2011). *Architecture of the Newars: A History of Building Typologies and Details in Nepal - Volume 1: The Early Periods* (Vol. I). Chicago, Illinois: Serindia Publications. doi:10-1017/S0041977X13001195

Hottel, H. (1931). Radiant heat transmission between surfaces separated by non-absorbing media. *ASME Transactions. 53*, pp. 265-273. American Society of Mechanical Engineers.

Houghten, F. C., & Ingels, M. (1927). Infiltration Through Plastered and Unplastered Brick Walls. *ASHRAE Transactions*, 377-386. Retrieved from http://www.aivc.org/sites/default/files/members_area/medias/pdf/Airbase/airbase_00114.pdf

Incropera, F. P., Dewitt, D. P., Bergman, T. L., & Lavine, A. S. (2011). *Introduction to Heat Transfer* (Sixth ed.). Hoboken, NJ: John Wiley & Sons.

International Programme on Chemical Safety. (2002, June). *ICSC: 1440: Petrolatum (White)*. Retrieved from IPCS: INCHEM: http://www.inchem.org/documents/icsc/icsc/eics1440.htm

Jigyasu, R. (2002). *Reducing Disaster Vulnerability through Local Knowledge and Capacity. The Cace of Earthquake Prone Rural Communities in India and Nepals.* Trondheim: Norwegian University of Science and Technology.

Kreith, F., & Kreider, J. F. (1978). *Principles of Solar Engineering.* Washington, D.C.: Hemisphere Publishing Corporation.

Labsphere, A HALMAN Company. (2010, September 14). *Technical Guide: Reflectance Materials and Coatings.* Retrieved from A HALAMA Company: https://www.labsphere.com/site/assets/files/2553/a-guide-to-reflectance-materials-and-coatings.pdf

Labsphere, Inc. (2017). Optical-grade Spectralon® Reflectance Material. North Sutton, NH, USA. Retrieved from https://www.labsphere.com/site/assets/files/1827/pb-13021-000_rev_02_og_spectralon.pdf

Lawn, J. E. (2005, March 3). 4 million neonatal deaths: When? Where? Why? *Lancet, 365*, 891-900.

Lechner, N. (2001). *Heating, Cooling Lighting: Design Methods for Architects* (Second ed.). New Yrok, NY: John Wiley & Sons.

Lecompte, J. G. (1987). Airtightness of Masonry Walls. *Ventilation Technology - Research and Application* (pp. 1-12). Uberlingen: 8th AIVC Conference. Retrieved from http://www.inive.org/members_area/medias/pdf/Conf/1987/Lecompte.pdf

Lewcock, R. B. (1983). *Interim Report.*

Lucas Oil Products, Inc. (2018, March 14). Lucas Oil Products, Inc. Contact from Kongoletos #546597.

Lunze, K., & Hamer, D. (2012, March 1). Thermal protection of the newborn in resource-limited environments. *Journal of Perinatology, 32*, 317-324. doi:10.1038/jp.2012.11

Meir, I. A., & Roaf, S. (2002). Thermal Comfort -Thermal Mass: Housing in Hot Dry Climates. *9th International Conference on Indoor Air Quality and Climate*, (pp. 1050-1055). Monterey, Santa Cruz, US.

Modest, M. F. (2013). *Radiative Heat Transfer* (Third ed.). Oxford, UK: Academic Press.

Nelson, E. (2017). *Demonstration and Implementation of Thermally Passive Low-Income Housing: A Case Study in Bhuj.* Cambridge, MA: Massachusetts Institute of Technology.

NETZSCH-Gerätebau GmbH. (2014, January). Operating Instructions: HFM 436/3 Lambda. Selb, Germany.

NETZSCH-Gerätebau GmbH. (2014). Smart Solutions. Selb, Germany.

Neuberger, P., & Kic, P. (2017). Thermal Conductivity of Natural Materials Used for Thermal Insulation. *Engineering for Rural Development* (pp. 420-424). Jelgava: Latvia University of Life Sciences and Technologies. doi:10.22616/ERDev2017.16.N082

Office of the Prime Minister of India. (2015, June 17). *News Updates*. Retrieved from "Housing for All by 2022" Mission – National Mission for Urban Housing: http://www.pmindia.gov.in/en/news_updates/housing-for-all-by-2022-mission-national-mission-for-urban-housing/

Owens Corning Foam Insulation, LLC. (2011, September). FOAMULAR(R) Extruded Polystyrene (XPS) Insulation: SI and I-P Units for Selected Properties. Toledo, Ohio, USA. Retrieved from http://www.foamular.com/assets/0/144/172/174/1fb2fb08-5923-46de-b387-f4bdc3f68d50.pdf

Owens Corning Foam Insulation, LLC. (2015, February). FOAMULAR® Insulating Sheathing Extruded Polystyrene (XPS) Rigid Foam Insulation Product Data Sheet. Toledo, Ohio, USA. Retrieved from http://www.foamular.com/assets/0/144/172/174/1fb2fb08-5923-46de-b387-f4bdc3f68d50.pdf

Persky, M. J., & Szczesniak, M. (2008, April 1). Infrared, spectral, directional-hemispherical reflectance of fused silica, Teflon polytetrafluoroethylene polymer, chrome oxide ceramic particle surface, Pyromark 2500 paint, Krylon 1602 paint, and Duraflect coating. *Applied Optics*, 1389-1396.

Preiss, D. (2016, December 20). *15-Year-Old Girl Found Dead In A Menstrual Hut In Nepal*. Retrieved from National Public Radio: https://www.npr.org/sections/goatsandsoda/2016/12/20/506306964/15-year-old-girl-found-dead-in-a-menstrual-hut-in-nepal

Rohsenow, W. M., & Hartnett, J. P. (1973). *Handbook of Heat Transfer* (Third ed.). New York: McGraw-Hill Book Company.

Rutkowski, H. (1986). *Manual J: Residential Load Calculation.* Arlington, VA: Air Conditiong Contractors of America.

Sander, J., & McDaniel, E. (2007). Grease Characterization: Are All Greases Lithium Greases? *Lube Technologies* (pp. 431-437). Louisville, KY: Lubrication Technologies, Inc. Retrieved from http://www.lubetechnologies.com/assets/lube-excellence-07-paper-grease-(002).pdf

Santamouris, M. (2007). *Advances in Passive Cooling.* London, UK: Earthscan.

Santamouris, M., & Kolokosta, D. (2013). Passive cooling dissipation techniques for buildings and other structures: The state of the art. *Energy and Buildings, 57*, 74-94.

Sapkota, I., & Oden, P. C. (2008). Household characteristics and dependency on community forests in Terai of Nepal. *International Journal of Social Forestry, 1*(2), 123-144.

Simkhada, P., van Teijlingen, E., Rant, P. R., Sathian, B., & Tuladhar, G. (2015, June 29). Public Health, Prevention and Health Promotion in Post-Earthquake Nepal. *Nepal Journal of Epidemiology, 5*(2), 462-464. Retrieved from https://www.ncbi.nlm.nih.gov/pmc/articles/PMC4727543/pdf/nje-05-462.pdf

Son, K.-S., Pilakoutas, K., & Neocleous, K. (2006). Behaviour of concrete columns with drilled holes. *Magazine of Conrete Research, 58*(7), 411-419. doi:10.1680/macr.2006.58.7.411

St. Clair, P. C. (2016, March 31). Community forest management, gender and fuelwood collection in rural Nepal. *Journal of Forest Economics, 24*, 52-71. doi:10.1016/j.jfe.2016.03.002

Surface Optics Corporation. (2004, July 18). SOC 400T Field Use Protocol. (0.3). Rochester, NY, USA.

Surface Optics Corporation. (2008, June). SOC 400T User Guide. San Diego, CA, USA.

The American Society of Heating, Refrigerating and Air-Conditioning Engineers. (2018). *ASHRAE POCKET GUIDE for Air Conditioning, Heating, Ventilation, Refrigeration. SI* (Ninth ed.).

The Brick Industry Association. (2007, October). *Specifications for and Classification of Brick.* Retrieved from The Brick Industry Association: Technical Notes on Brick Construction:: http://www.gobrick.com/portals/25/docs/technical%20notes/tn9a.pdf

The Dow Chemical Company. (2018, February 8). TUFF-R™ and Super TUFF-R™ Polyisocyanurate Insulation. Midland, MI, USA. Retrieved from https://www.dow.com/webapps/lit/litorder.asp?filepath=styrofoam/pdfs/noreg/179-07932.pdf

The World Bank. (2017, December 15). *Press Release: World Bank Approves Additional Financing for Post-Earthquake Housing Reconstruction*. Retrieved from The World Bank: http://www.worldbank.org/en/news/press-release/2017/12/15/nepal-post-earthquake-housing-reconstruction-additional-financing

US Central Intelligence Agency. (2018, May 16). *India*. Retrieved from The World Factbook: https://www.cia.gov/library/publications/the-world-factbook/geos/in.html

Zarr, R. R., & Leigh, S. D. (2014, February 4). Standard Reference Material 1450d, Fibrous Glass Board, for Thermal Insulation Measurements. (T. K. Stovall, & T. Whitaker, Eds.) *ASTM Selected Technical Papers, STP1574*, 39-52. Retrieved from https://ws680.nist.gov/publication/get_pdf.cfm?pub_id=911463

Zarr, R. R., Harris, A. C., Roller, J. F., & Leigh, S. D. (2011, August 29). NIST Special Publication 260-173. Standard Reference Materials: SRM 1450d, Fibrous-Glass Board, for Thermal Conductivity from 280 K to 340 K. Gaithersburg, MD, USA. Retrieved from https://www.nist.gov/sites/default/files/documents/srm/SP260-173.pdf